WP2 - Deliverable 2.9

Report of geochemical results for 3 areas

Release Status: Public

Authors: Andrew Kilpatrick, Sylvain Stephant, Saeid Abad, Frédéric Mathurin,
Paula Afonso, Julio Carneiro, Manuel Ron Martin, Jose Mediato, Patricia Moita

Date: 26 March 2025

Filename and Version: PilotSTRATEGY D2.9 V4

Project ID Number: 101022664

Edited by Mark Wilkinson

PilotSTRATEGY (H2020- Topic LC-SC3-NZE-6-2020 - RIA)

1. Document History

1.1 Location

This document is stored in the following location:

Filename	PilotSTRATEGY D2.9 V4
Location	

1.2 Revision History

This document has been through the following revisions:

Version No.	Revision Date	Filename/Location stored:	Brief Summary of Changes
PilotSTRATEGY D2.9 V3	20/03/25	PilotSTRATEGY D2.9 V3	Final review by coordinator. Changes in authors list. Delete paragraph related to modelling strategy. Delete appendices section.

1.3 Authorisation

This document requires the following approvals:

AUTHORISATION	Name	Signature	Date
WP Leader	Mark Wilkinson	MW	20/03/25
Project Coordinator	Isaline Gravaud	IG	26/03/25

1.4 Distribution

This document has been distributed to:

Name	Title	Version Issued	Date of Issue
			26/03/2025

Kilpatrick A., Stephant S., Abad S., Mathurin F., Afonso P., Carneiro J., Martin M.R., Mediato J., Moita P., 2025. Report of geochemical results for 3 areas. Deliverable D2.9. EU H2020 PilotSTRATEGY project 101022664, report, pp93

Disclaimer

2. Executive summary

While much work has been carried out investigating the possible chemical reactions between reservoir rocks, cap-rocks, formation brines and injected CO_2, the nature of PilotSTRATEGY calls for a site-specific approach to assess the reactivity of the rocks present at each of the proposed pilot sites. Batch experiments were carried out by UEDIN and BRGM on samples from Spain and Portugal and from France, respectively. Flow through experiments were carried out by UEDIN on samples from France, Spain, and Portugal, with complementary flow-through experiments carried out by BRGM on samples from the French site.

In the Paris Basin, the Dogger reservoir has three main formations. The rocks are overwhelmingly calcite, and the proportions of most of the minor mineral phases are near or below the limit of quantification or the limit of detection at 1 to 6 weight %. Batch experiments were run in each of the three rock formations at reservoir pressure and temperatures. Unsurprisingly, the minerals most susceptible to dissolution in all experiments are calcite and gypsum / anhydrite. Changes in the apparent abundances of other minerals are difficult to quantify, as the detection limit and analytical precision of X-ray diffraction are too low to be confident that genuine changes are occurring. Based on changes in synthetic brine composition over the reaction time (up to 35 days), there is possible evidence of minor dissolution of ankerite/dolomite and quartz and minor precipitation of one or more aluminosilicates, such as kaolinite or illite, enhanced by the addition of CO_2 in the brine (pCO_2: 50, 180 bar). The reaction of the sulphate minerals gypsum/anhydrite appeared to follow the opposite pattern in the Dalle Nacrée Formation (dissolution) compared to the Comblanchian and Oolithe Blanche Formations (precipitation). For the Callovian mudstone (transitional caprock) the main reactions were the dissolution of calcite and gypsum, and possibly interstratified clays enhanced by the addition of CO_2. Plagioclase and quartz attained thermodynamical equilibrium, whereas dolomite precipitated. Potential slow precipitation of chlorite and/or kaolinite mineral were suspected, likely driven by the possible slow dissolution of Mg rich interstratified clays with higher pCO_2 conditions.

For the Ebro Basin (Spain) reservoir, an arkosic 'red bed' sandstone, data indicate some very minor dissolution of primary aluminosilicate phases following addition of CO_2 and subsequent acidification of the experimental brine. The primary phase dissolved is likely to be K-feldspar, along with some dissolution of or ion-exchange with some of the minor components present with only Fe reaching concentrations significantly above sub-ppm levels. There is no reason to suspect that this would interfere with the injection of CO_2 into the reservoir. There is no strong evidence for secondary precipitation (of carbonates, for example). Any precipitation which did occur is likely to be very minor and unlikely to be of concern at the reservoir scale.

For the Ebro Basin caprock (Spain) which contains more primary calcite than the reservoir, results reflective a system where reaction is dominated by dissolution of primary calcite, possibly with some minor secondary precipitation and minor dissolution of quartz and minor aluminosilicate phases. pH is buffered by calcite dissolution, likely making the dissolution of any silicate or aluminosilicate (which would only be present at concentrations <1%) phases present relatively slow. It is difficult to extrapolate this result to the scale of the storage site.

For the Lusitania Bain (Portugal) the reservoir mineral assemblage is of relatively low reactivity. Some initial desorption of Ca, or dissolution of minor Ca bearing phases occurred upon addition of CO_2, partially buffering the initial acidification of the fluid. After this there is evidence for slower dissolution of some aluminosilicate phases, but overall element concentrations remain low for the duration. There is no evidence for significant dissolution of the primary mineral assemblage, or secondary precipitation on the timescale of the experiment.

Flow-through experiments were carried out on a number of core plugs representative of the reservoir and caprock of interest. The tests were designed: (i) to test the gas and water relative permeability of the material during CO_2 / water flow, and (ii) characterize the rock reactivity in contact with supercritical CO_2 and/or CO_2-enriched fluid. Cyclic Flow Tests by UEDIN were specifically designed to determine the relative permeability of water and supercritical CO_2 in the reservoir, and, to some extent, characterise rock reactivity in supercritical conditions. These tests can be considered representative of the environmental conditions that would occur near the well. Percolation of a CO_2-enriched brine tests were performed by BRGM to simulate a continuous flow of brine equilibrated with CO_2 percolating through the reservoir rock and the caprock. These tests are representative of conditions prevailing at the outer edge of the CO_2 plume, far from the injection well.

For Spain, the samples supplied for relative permeability testing proved to be too unconsolidated for core plugs to be made, so one analogue reservoir sample (a sample from the Bunter Sandstone, cored in the Southern North Sea) was tested as an analogue. For both Portugal and Spain, relative permeability curves were successfully measured, with hysteresis between both gas and water relative permeability curves under the drainage and imbibition cycles. The hysteresis is more pronounced in the gas phase. The water relative permeability values during the imbibition process are higher compared to the drainage process. Conversely, the gas relative permeability values during the drainage process are higher than those during the imbibition process. Relative permeability curves are required for the digital modelling of CO_2 flow within a reservoir.

For Portugal, a caprock sample was tested for reactivity under flowing conditions along an induced fracture. Results indicate some enhanced dissolution of primary caprock material during exposure to CO_2. The results, however, are notably more subtle than those observed for the same material exposed to CO_2 in the batch experiments. This likely reflects the relative tightness of the intact sample used in the flow-through experiment, thereby limiting the surface area available for reactions (compared to the powdered material used in the batch experiment).

For both Portugal and Spain the caprocks contain significant calcite (13% of the sample in the Spanish case, 87% in the Portuguese case), which exhibited significant dissolution when exposed to CO_2 saturated brine. Calcite dissolution removed 6% of the original rock mass in the case of the Spanish sample and 11% in the Portuguese case. In both cases fluids likely became saturated with respect to calcium carbonate, leading to some secondary precipitation.

For the Paris Basin (France), flow through experiments with supercritical CO_2 used cyclic injection and withdrawal of gas/water, to measure the relative permeability of the Oolithe Blanche Formation. The tests recorded strong dissolution and a progressive increase of the porosity, intrinsic permeability, and gas-water relative permeability over the subsequent cycles. The flow through experiments with CO_2-enriched brine on an oolitic grainstone from the Oolithe Blanche Formation generated a so-called ‘worm-hole’, which is probably not representative of subsurface processes. The tests confirmed the high permeability of this formation and showed that carbonate minerals (mostly calcite) account for by far the largest part of system’s reactivity after the addition of CO_2. Minor dissolution of gypsum/anhydrite and quartz may contribute only to a minor part to the formation of the wormhole.

A sample of the caprock (a carbonate-rich mudstone) from the Paris Basin recorded no flow over 24 hours with 180 bar of pressure differential, despite the sample being cracked. The sample was sawn to produce an artificial 'fracture' to enable the experiment to proceed when almost total clogging of the porosity occurred during the experiment. The flow of the CO_2-enriched brine in the porous media induced substantial dissolution of carbonate (calcite, dolomite) and sulphate minerals (gypsum/anhydrite) in the core-plug, before reaching a geochemical steady state with respect to these mineral phases. Due to the large set of aluminosilicate minerals in the mineral assemblage, the interpretation of the reactive process involving clay mineral remains to be understood through geochemical modelling.

Overall, the results confirm that calcite-rich sediments are subject to (at least) some dissolution under the acidic conditions associated with CO_2 injection. Direct extrapolation of these results to the scale of a reservoir and/or caprock remains difficult. Calcite-poor sandstones undergo little reaction on laboratory time scales, as expected. The reaction trends, identified by the experiments, should be considered as first-order conceptual models for assessing geochemical reactions and understanding more generally the geochemical reactivity involved in both the reservoir and the caprock. The conceptual models remain to be validated or adjusted by the geochemical modelling exercise which aims to numerically simulate the experimental results within the framework of the project.

Table of Contents

The PilotSTRATEGY project has received funding from the European Union's Horizon 2020 research and innovation programme under grant agreement No. 101022664

3. Background & aims of work

3.1 Background

Much attention has been given to the reaction of CO_2 with formation brines and minerals over the past thirty years thanks to increasing interest in, and utilisation of geological carbon storage (GCS) with numerous studies investigating geochemical processes via experimental (Allan, Turner, and Yardley 2011; Bateman et al. 2011; Kaszuba, Yardley, and Andreani 2013; Rosenqvist, Kilpatrick, and Yardley 2012), and modelling (Celia and Nordbotten 2009; Gaus et al. 2008; Portier and Rochelle 2005) work, as well as collection and interpretation of data from natural analogues or operational GCS schemes.

Upon injection, depending on local hydrodynamics, CO_2 (likely in the supercritical phase) may remain as a static layer within the reservoir or, more likely, will migrate due to its relative buoyancy and the movement of formation groundwater. Around the edges of this plume formation fluid will evaporate into the CO_2 phase and CO_2 will dissolve into the formation fluid, initially pushing the rock-brine system away from its (assumed) initial equilibrium. A myriad of interlinked chemical interactions may thereafter act to bring the system to equilibrium. The reactions which take place may be highly site-specific (dependant on local pressure/temperature conditions, brine chemistry and primary mineralogy) and may continue over thousands of years before full equilibrium is reached (Baines and Worden 2004).

The initial interaction is the dissolution of supercritical CO_2 into the formation fluid. The extent of dissolution of a supercritical CO_2 plume will be partially controlled by fluid-rock interactions but, initially, the solubility of CO_2 in formation brine will be controlled primarily by local pressure, temperature and salinity (Rochelle, Czernichowski-Lauriol, and Milodowski 2004). Figure 3-1 demonstrates the dependence of CO_2 solubility on these parameters.

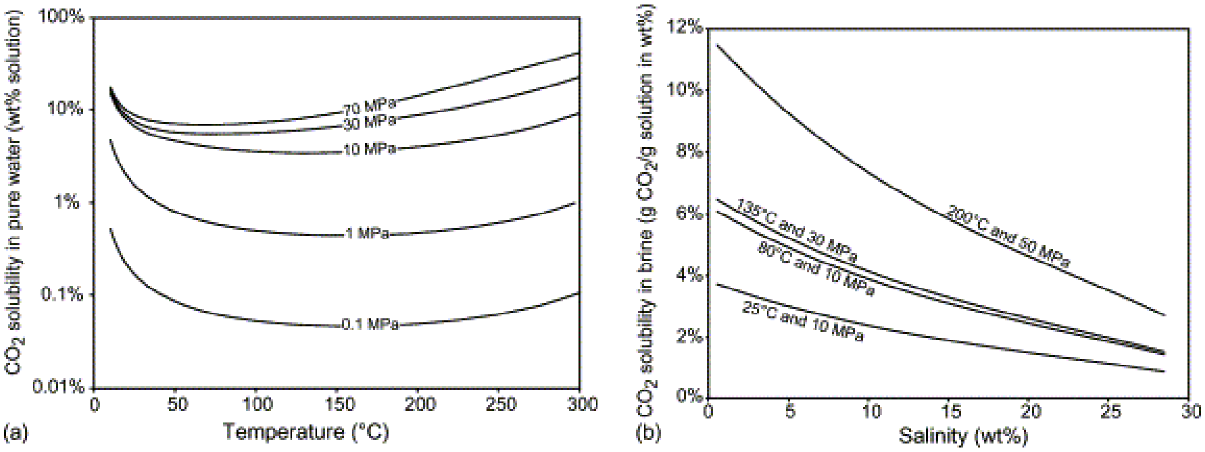

Figure 3-1: Variation in CO2 solubility with (a) pressure and temperature and (b) salinity (reproduced from Bachu & Adams 2003)

Note that at the pressures and temperatures of interest (around 50–100˚C and 5–10 MPa) increasing salinity acts to reduce CO_2 solubility (due to a salting out effect) and likewise increasing temperature decreases CO_2 solubility. Nevertheless dissolution of CO_2 into brines takes place rapidly at both laboratory and field scales (Rochelle, Czernichowski-Lauriol, and Milodowski 2004), but the extent to which this process will act to dissolve the CO_2 plume will depend on the surface contact area relative to the volume of CO_2. The process will slow as concentration gradients emerge around the plume as formation water becomes saturated with dissolved CO_2.

Equation 1 describes the dissolution of gaseous (or supercritical) CO_2 into water:

$$CO_{2(g)} \Leftrightarrow CO_{2(aq)} + H_2O \Leftrightarrow H_2CO_{3(aq)} (1)$$

Here dissolved CO_2 exists in equilibrium with relatively weak carbonic acid by reaction with the formation water. Assuming a static and unreactive system, dissolution of free-phase CO_2 is unlikely to occur after pore-fluid saturation (around 5–10 wt.% of solution). Additionally in its dissolved state CO_2 has the potential to degas from formation water if there is a drop in pressure, which may raise issues of storage security in some systems. In order to drive the dissolution of further CO_2 and to store it in a more secure form dissolved CO_2 must either be moved away from the free-phase plume, allowing contact with fresh unsaturated fluid or the dissolved CO_2 must be removed chemically. Movement of CO_2 saturated fluid away from the free-phase plume may occur by natural or induced groundwater flow, by diffusion (which is likely to be very slow), advection, or convection. Alternatively, dissolution of CO_2 into formation fluid may be driven by chemical effects.

Dissolved CO_2 will dissociate to form dissolved ionic species as illustrated by equations 2 and 3:

$$H_2CO_3^* \Leftrightarrow HCO_3^- + H^+ \quad (2)$$

$$HCO_3^- \Leftrightarrow CO_3^{2-} + H^+ \qquad (3)$$

This dissociation is controlled by pH (Gunter, Bachu, and Benson 2004) as illustrated by Figure 3-2. As can be seen the initial dissociation of dissolved CO_2 releases acidity (Equation 2), thus if there is a large supply of free-phase CO_2 available for dissolution that the system will be maintained at a relatively low pH.

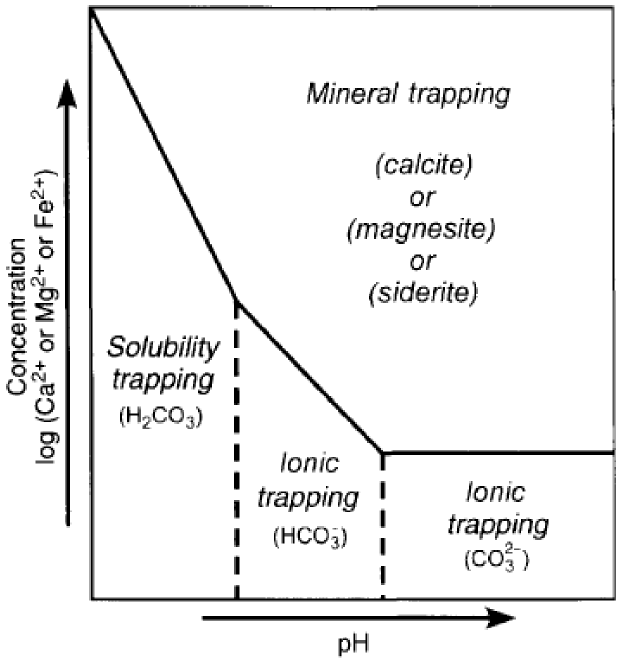

Figure 3-2: Dependence on CO2 trapping mechanisms on pH and divalent ion concentration (reproduced from Gunter et al. 2004).

From equations 1–3, further dissolution of CO_2 may occur if these reactions are pushed to the right, by neutralisation of acidity or by removal of carbonate species through mineral-fluid interactions. Initial reactions are likely to involve relatively rapid lowering of acidity by carbonate dissolution or ion exchange, whereby accessible cations held on mineral surfaces, such as clays, are exchanged for hydrogen ions in solution. While the availability of the cations may be limited in many rocks, this can provide a rapid process for the neutralisation of acidity. Additionally, the cations released may include Ca, Mg and/or Fe ions, which can then interact with bicarbonate in the formation fluid, causing carbonate mineral precipitation, as illustrated in general form by equation 4:

$$HCO_3^- + M_{(aq)}^{2+} \Leftrightarrow M^{(II)}CO_3 + H_{(aq)}^+ \qquad (4)$$

Here, the carbonate precipitate may be, for example, calcite ($CaCO_3$), magnesite ($MgCO_3$) or siderite ($FeCO_3$) depending on the cations supplied (Rochelle et al., 2004).

Further interactions of dissolved CO_2 with aquifer minerals involve the breakdown of aluminosilicate minerals, and may be similar, in some respects, to mineral weathering reactions at the Earth's surface. A general form for these reactions is illustrated by equation 5 (Baines and Worden, 2004):

$$CO_2 + H_2O + M^{(II)}Al_xSi_yO_z \rightarrow Al - Si\ mineral + M^{(II)}CO_3 \qquad (5)$$

Depending on aquifer mineralogy, they might include: reaction of anorthite to calcite and kaolinite; reaction of albite to Na-smectite, bicarbonate and quartz; and, in the presence of an NaCl brine, the reaction of K-feldspar to dawsonite and quartz (Rochelle et al., 2004).

The products of these reactions have been observed during laboratory scale experiments carried out under GCS conditions, as well as in systems which have contained CO_2 for geological time-scales (Baines and Worden, 2004; Rochelle et al., 2004). Examples include both formation of clays and carbonates and the dissolution of feldspars. Since the dissolution and/or fixation of CO_2 is desirable in terms maximising storage security and volume it is important to further understand these reactions in the context of industrial scale storage systems.

3.2 Aims

While, as outlined above, much work has been carried out investigating the reaction, or potential for reaction, between reservoir rocks, cap-rocks, formation brines and injected CO_2, the nature of PilotSTRATEGY project calls for a site specific approach in order to assess the reactivity of the rocks present at each of the proposed pilot sites. The experiments detailed herein were designed in order to provide an initial assessment of the reaction between samples of reservoir and caprock material and CO_2 in order to elucidate the potential impacts on the selected reservoirs of CO_2 injection.

Samples from target reservoirs (or nearest available analogues) were provided by project partners from Spain, Portugal and France and underwent testing either in non-flowing 'batch' type experiments, or in flow-through experiments. The batch experiments were carried out in order to identify reactions of interest and track these through time in order to gain an understanding of their relative magnitude and rates and, therefore, assess their potential impacts on reservoir and caprock materials (through, for example, dissolution of primary minerals, or secondary precipitation). The flow-through experiments were focussed less on detailed understanding of the geochemical systems involved and more on identifying if any gross changes to the reservoir materials, in terms of permeability variation, could be identified during exposure to CO_2 and CO_2 containing fluids.

The batch experiments were carried out by UEDIN and BRGM on samples from Spain and Portugal and from France, respectively. Flow through experiments with injection of supercritical CO_2 on samples from France, Spain, and Portugal were carried out by UEDIN. Reactive flow-through experiments, with injection of CO_2-enriched brine (dissolved CO_2) were carried out by BRGM on French samples.

4. Batch Experiments

4.1 Experiments on material from Spain and Portugal

4.1.1 Introduction

In order to assess the potential reaction between injected CO_2 and target reservoir and caprocks samples from both the Spanish and Portuguese target formations were selected and used in batch-type experiments carried out at UEDIN. Information on the selected samples can be found in Section 4.1.2 and the following sections will provide details on experimental methodologies and results.

4.1.2 Sample characterisation

Erreur ! Source du renvoi introuvable. presents the mineralogy of the samples used in the experiments as determined by XRD, while the below provides a more general background and geological context to the samples.

For Spain rock samples for geochemical characterization were obtained from two outcrops: Peñas Royas section and Torre de las Arcas section. Rocks were sampled on April 2002.
Both outcrops are located 55 km south of Lopin Structure. They are extensive outcrops where a complete stratigraphic sequence of reservoir (Units B1 and B2) and the seal rock formation (Röt facies) can be sampled. Even though rocks exposed in outcrops are affected by subaerial weathering processes and, consequently the geochemical reactions between CO_2, rocks and brine of reservoir and seals rocks can be slightly different than the burial materials.

TA-03 is a arkose, which appear in the stratigraphic sequence forming 1-1,5 m thick tabular layers with planar cross-bedding and groove cross-bedding of Unit B2. The rock is well-sorted, with the small grain sizes ranging from 100-120 microns in diameter. The porosity is around 10% predominantly intergranular in type. Mineralogically, skeletal grains consist of mono- and polycrystalline quartz, K-feldspar (25-30 %), metamorphic rock fragments (<5 %), together with Ti and Fe oxides-hydroxides, muscovite and zircon as accessories components (Table 1). The biding phase is an iron-rich matrix, likely composed of phyllosilicates (mica and kaolinite) and finely dispersed iron compounds (iron oxides/hydroxides). A small amount of siliceous cement (<5%) is also present.

The PR-11 sample is an anisotropic and heterogeneous marl Röt facies. Two varieties are distinguished according to the clay or carbonate predominance. Mineralogically, both varieties have carbonate contents between 30 and 50% and clay contents between 30 and 60%. The feldspar content is very constant, 5%. The marls is characterised by well-sorted, rounded carbonate (mostly dolomite) particles of 100-150 µm mean diameter and a grain-supported texture with low amounts of calcite cement and clay matrix. Both the grains and the matrix contain occasional Fe-oxides and/or hydroxides. The mineralogical composition contain calcite, dolomite, phyllosilicates (mica, kaolinite, smectite), quartz, and K-feldspar, although chlorite was only detected in a sample.

For Portugal, the rock samples were obtained from outcrops, as core samples were unavailable for both the caprock and the reservoir rock.

Sample CD-CRR-10 is representative of the Carrascal formation, part of the reservoir, that is composed primarily of fine- to coarse-grained sandstones. Although sample CD-CRR-10 has abundant quartz and K-feldspar, in the reservoir magnesian calcite, kaolinite, microcline, dolomite, and micas are also commonly found. The cement within the reservoir rocks are distributed heterogeneously, both laterally and vertically. Calcite cement is the most prevalent, but siliceous cements with kaolinite and iron oxyhydroxides are also frequently present.

Sample CD-DARN-15, also collected from at outcrop, represents a facies found in the upper section of the primary caprock. The facies in the lower section of the caprock, which is in contact with the reservoir, has a higher clay and marl content, as identified through offshore oil exploration wells. However, it was not possible to collect samples of those lower facies from outcrops.

Lab ID	*AGH0016*	*AGH0017*	*AGH0012*	*AGH0013*
ID as supplied	*TA-03*	*PR-11*	*CD-CRR-10*	*CD-DARN-15*
Description	*Sample of sandstone reservoir rock from the Ebro onshore reservoir, supplied as disagregated sample by Repsol*	*Sample of caprock from the Ebro onshore reservoir, supplied as disag. Sample by Repsol*	*Sample of reservoir rock from the Lusitania Basin Torres Vedras Group (offshore), supplied as disaggregated sample by University de Evora*	*Sample of caprock from the Lusitania Basin Torres Vedras Group (offshore), supplied as disaggregated sample by University de Evora*
	% Mineral Phase			
Quartz	*86.2*	*33.2*	*91.1*	*12.7*
K feldspar	*5.7*	*9.7*	*8.9*	*N.D.*
Chlorite	*N.D.*	*10.4*	*N.D.*	*N.D.*
Mica	*6.1*	*18.4*	*N.D.*	*N.D.*
calcite	*N.D.*	*13.2*	*N.D.*	*87.3*
Hematite	*0.2*	*N.D.*	*N.D.*	*N.D.*
Montmorillonite	*N.D.*	*15*	*N.D.*	*N.D.*
Clinochlore	*1.8*	*N.D.*	*N.D.*	*N.D.*

Table 4.1. XRD mineralogy for Spanish and Portuguese samples used in batch experiments

4.1.3 Methodology

Batch experiments were conducted in a stainless-steel reaction vessels, manufactured by Parr (*Figure 4-1* & *Figure 4-2*). The vessels are fitted with a PTFE liner, in which sit the experimental materials. The vessel is fitted with a dip-tube for sampling fluids during experimental runs, along with a rupture assembly and gas inlet. Once collected samples were immediately filtered and split: one sub-sample being preserved for ICP-OES analysis, another for anion analysis by ion chromatography, another for analysis of alkalinity and another being used benchtop measurement of pH and Eh, via a pre-calibrated Hanna benchtop pH/Eh meter and Mettler Toledo In-lab electrodes.

Solid samples were crushed using a steel jaw crusher and sieved to 125-250 µm. These sieved fractions were then rinsed with acetone until the supernatant ran clear in order to remove ultrafine material.

The fluids used in the experiments were prepared using laboratory reagent grade NaCl (purity >99.5%) supplied by Fisher Scientific, to make up initial brine solutions similar in strength to the formation fluids in the target reservoirs. To these were added crushed samples of the solids and the solid-liquid mixtures sealed in magnetically stirred vessels for several weeks in order for the contents to approach equilibrium. Following this equilibration process the resulting ‘equilibrated brine’ was withdrawn, filtered to remove any fine suspension, and used as the starting brine for the final experiments.

During each experimental set-up c. 5 g of the rinsed 125-250 µm solid sample was weighed into a Teflon liner, along with 150–200 ml of the pre-equilibrated, filtered brine solution and a magnetic stirring bead. At this point a sample of the starting fluid was collected and preserved for ICP-OES analysis. The Teflon liner was then placed in a pressure vessel, which was then sealed and placed on a magnetic stirring plate, housed in an oven. Initially, a gas line was connected to the sampling valve and nitrogen gas was passed through the vessel’s dip-tube and bubbled through the brine in order to remove oxygen from the solution and from the vessel headspace. This was continued for one hour, after which the gas line was connected to the gas inlet and the vessel pressurised to some point below

The PilotSTRATEGY project has received funding from the European Union’s Horizon 2020 research and innovation programme under grant agreement No. 101022664

the actual run pressure with nitrogen (this pressure rose to the actual run pressure as the temperature increased). The oven was then switched on, set to the desired run temperature, the stirrer was set to stir for one minute every few hours and the vessel left overnight. The next day a second sample was taken and again the vessel left overnight. The vessels were then left for several days, under nitrogen pressure alone to, again, allow some equilibration between the solids and liquids prior to addition of CO_2. Following this procedure the appropriate runs (those run with CO_2 rather than nitrogen) were depressurised, and flushed and repressurised with CO_2. Following addition of CO_2 experiments were sampled regularly for the duration of the runs (1–2 months). Sample splits taken were as detailed above.

Figure 4-1 (below). Parr reaction vessel used for stirred batch experiment

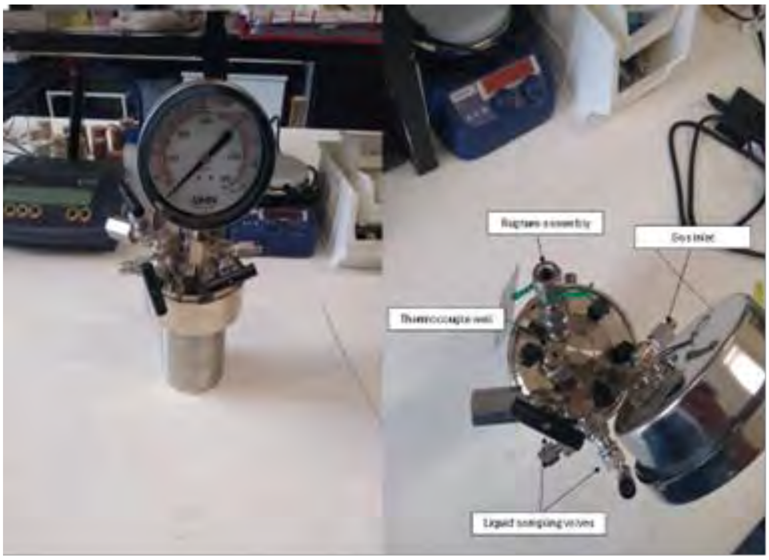

Figure 4-2 (below). Parr reaction vessels in oven, with magnetic stirrers and gas lines attached

At the end of each experimental run a final sample was taken while the vessel remained pressurised, after which as much fluid as possible was expelled via the dip tube after which the vessel was fully depressurised and removed from the oven. Solid samples were then retrieved from the vessels. One half of this solid was gently rinsed with IPA to remove residual brine, dried in an oven at 30°C, and preserved for possible optical analysis.

4.1.4 Results (Spain)

Four experiments were carried out using samples from the Spanish target region (Ebro, Spain). One sample of reservoir rock and one sample of caprock were selected and prepared as described in Section 4.1.2. Each sample was reacted under both carbon dioxide and nitrogen pressures, such that reactions due to CO_2 alone (rather than due to reaction between the starting brine and solid) could be distinguished. The experimental conditions are summarised in *Table 4.1*. Measured values of pH, Eh and select elemental concentrations are shown in *Figure 4-3 & Figure 4-4*.

Run ID	**Gas**	**Temp. (°C)**	**Solid Wgt (g)**	**Liquid vol. (ml)**	**Pressure (bar)**	**Fluid/solid together**	**CO2 added**	**Experiment off**	**Run Time, days**	**Solid used**	**Original Solid ID**	**Brine used**
1164	*CO2*	*65*	*5.024*	*150*	*150*	*05/06/2024*	*19/06/2024*	*24/07/2024*	*34*	*AGH0016*	*TA-03*	*200 g/l NaCl pre-equilibrated with solid*
1165	*N2*	*65*	*5.008*	*150*	*150*	*05/06/2024*	*N/A*	*24/07/2024*	*34*	*AGH0016*	*TA-03*	*200 g/l NaCl pre-equilibrated with solid*
1166	*CO2*	*65*	*4.985*	*150*	*150*	*05/06/2024*	*19/06/2024*	*24/07/2024*	*35*	*AGH0017*	*PR-11*	*200 g/l NaCl pre-equilibrated with solid*
1167	*N2*	*65*	*4.998*	*150*	*150*	*05/06/2024*	*N/A*	*24/07/2024*	*35*	*AGH0017*	*PR-11*	*200 g/l NaCl pre-equilibrated with solid*

Table 4.1. Run summary for batch experiments on Spanish samples

During the run using the reservoir sample (AGH0016/TA-03) pH was observed to drop sharply upon addition of CO_2 from an initial pH of around 7 to around pH 5, after which pH remained relatively constant for the remainder of the run. The nitrogen control run, on the other hand, shows a slight increase in pH over the course of the run. Calcium concentrations show a sharp increase upon addition of CO_2 after which they remain relatively steady. The source of the calcium is ambiguous: but it is possibly sourced from minor calcite or anorthite, present in concentrations below the XRD detection limit (c. 1%). The steep initial rise in concentrations, however, may suggest an ion-exchange process, likely from the surface of the micas present. Silicon, magnesium, manganese and iron all show a steady initial rise in concentration upon addition of CO_2, before flattening after around 10 days. The rise in silica concentrations are likely due to dissolution of primary K-feldspar and the concomitant rise in Mg, Mn and Fe likely due to dissolution of primary hematite, clinochlore and mica. Potassium concentrations are initially high, likely due to potassium impurities in the NaCl used to make the initial brine. Over the course of the CO_2 run potassium concentrations increase slightly, likely reflecting some minor dissolution of the potassium feldspar within the sample.

The data from these runs indicate some very minor dissolution of primary aluminosilicate phases following addition of CO_2 and subsequent acidification of the experimental brine. The primary phase dissolved is likely to be K-feldspar, releasing Si and K to solution, along with some dissolution of or ion-exchange with some of the minor components present. The dissolution of these components is limited, with only Fe reaching concentrations significantly above sub-ppm levels. As would be expected the quartz, making up the bulk of the sample, does not appear to undergo significant dissolution: Si concentrations reach around 20 ppm, likely close to saturation with respect to silica. There is no strong evidence for secondary precipitation (of carbonates, for example), either from the concentration data or from calculated saturation indices (made using PHREEQC). Ideally SEM analysis would have been undertaken to confirm this, but due to equipment availability this was not possible prior to the preparation of this report. Given the low elemental concentrations, however, any precipitation which did occur is likely to have been very minor and unlikely to be of concern at the reservoir scale.

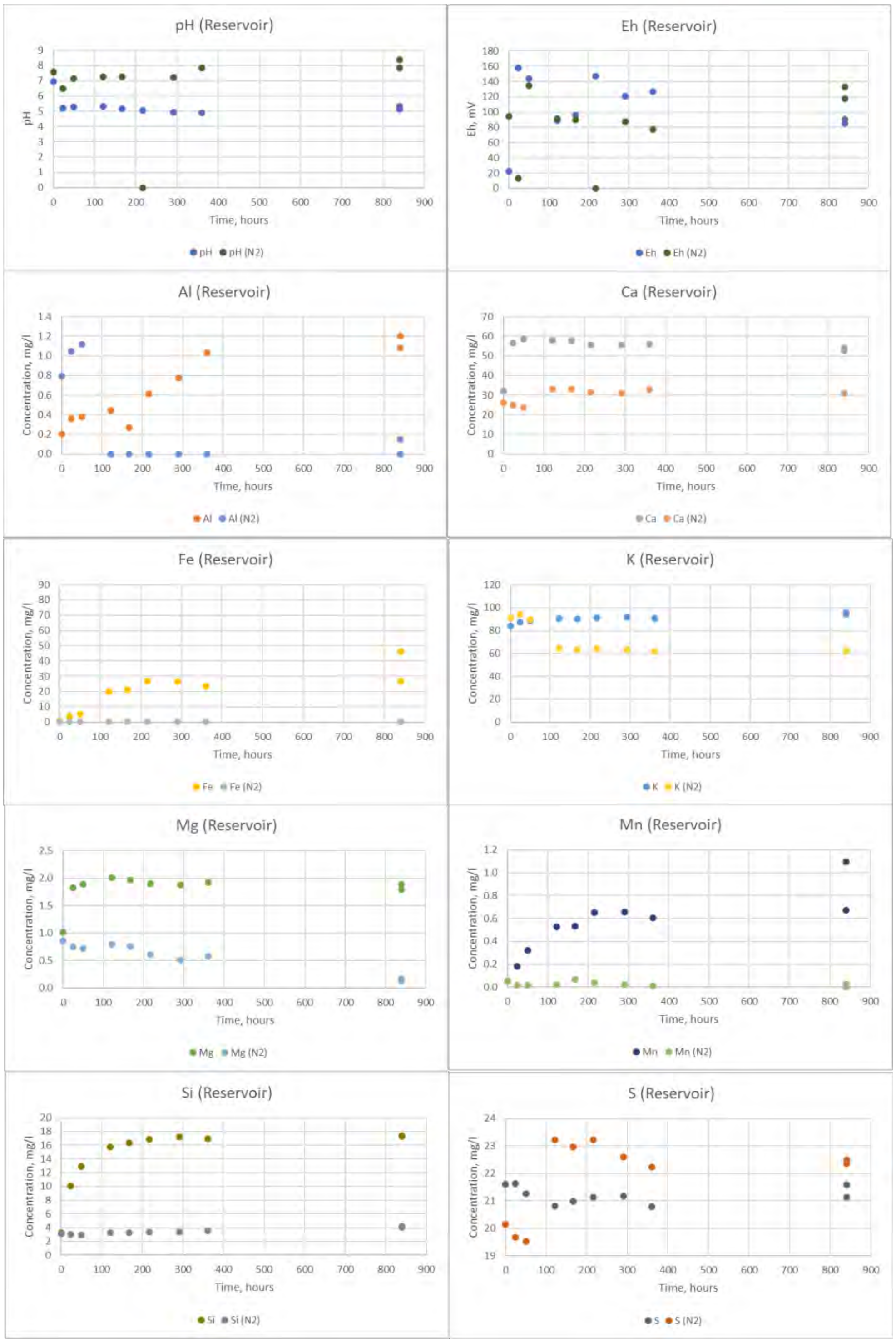

Figure 4-3. Selected elemental concentrations from CO2 and N2 runs using Spanish reservoir material

The PilotSTRATEGY project has received funding from the European Union's Horizon 2020 research and innovation programme under grant agreement No. 101022664

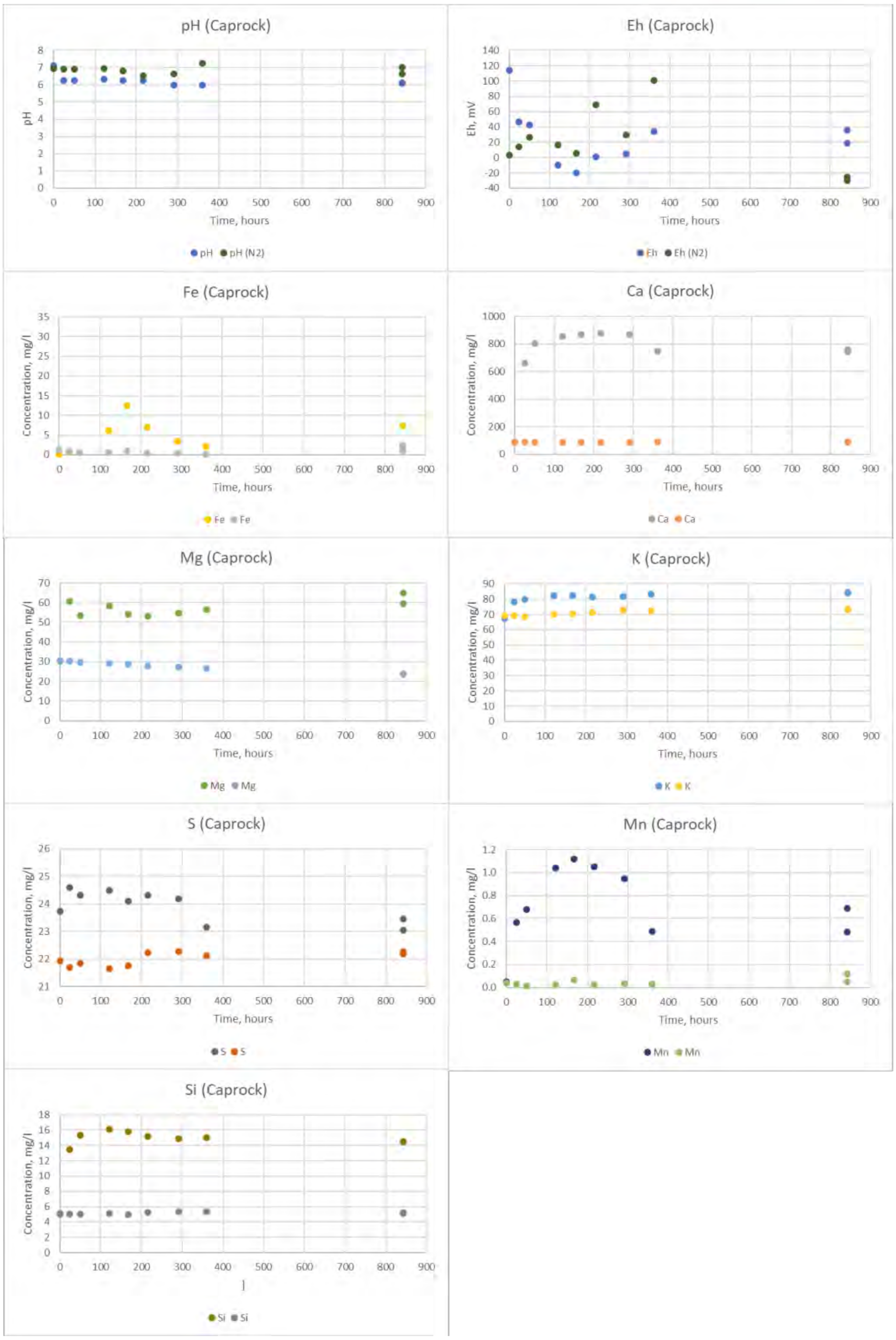

Figure 4-4. Selected elemental concentrations from CO2 and N2 runs using Spanish caprock material

The caprock sample (PR-11/AGH0017) varies considerably from the reservoir sample containing significant carbonate in the form of calcite and significant clay content (see *Table 4.1*) and this is reflected in the chemical changes and elevated concentrations of several elements observed.

Measured pH during the CO_2 run drops from a value of around pH 7 to pH 6 upon addition of CO_2, whereupon it remains relatively stable for the remainder of the run. The drop is less substantial than that observed for the run using the reservoir material, likely due to the availability of calcite for dissolution and subsequent buffering of acidity generated via CO_2 dissolution. This is also reflected in the Ca concentrations which rise substantially, from c. 90 mg/l to c. 650 mg/l within a few hours of CO_2 addition. Concentrations peak at between 200–300 hours at c. 850 mg/l Ca. By 300 hours Ca concentrations have flattened and then drop slightly, stabilising at around 750 mg/l. This concentration profile suggests notable dissolution of the primary calcite. The peak value of 850 mg/l Ca would require the dissolution of around 0.3 g Calcite, c. 6% of the original sample mass used in the experiment, or c. 48% of the original calcite content in the experiment (based on the XRD derived mineralogy). The slight drop in concentrations at later times is suggestive of some secondary precipitation. Modelling of the fluid compositions using PHREEQC, however, does not indicate that the fluids are supersaturated with respect to any Ca bearing phases phases, though it should be noted that the modelling of fluids with such high salinities can be problematic. The ion activity coefficients for such high ionic strength solutions are poorly defined (where they have been measured at all) and so results from such modelling should be treated with caution. In this case, from the Ca concentration profile, it seems likely that saturation with respect to a Ca bearing phase (likely $CaCO_3$) was reached and some, limited, secondary precipitation did occur, although follow up SEM analysis would be needed to confirm this. It is also possible that Na-Ca exchange on clay surfaces may have had an influence on these concentrations, given the relatively high montmorillonite content detected by XRD.

Concentrations of other elements are generally low. As for the experiment carried out using the reservoir material Si concentrations in the CO_2 run rise quickly to the level of silica saturation (c. 16 ppm), indicating some enhanced dissolution of the primary aluminosilicate mineral in these conditions. Mg concentrations in the CO_2 run are around double those in the N_2 run, possibly reflecting impurities within the primary calcite and the enhanced dissolution of this mineral under these conditions. K concentrations are relatively elevated at the start of both the CO_2 and the N_2 runs, likely reflecting some impurity of the NaCl used to make the initial solution, but K concentrations do rise slightly over the course of the CO_2 run, possibly indicating some minor dissolution of the primary K-feldspar present.

These results are reflective of a system where reaction is dominated by dissolution of primary calcite (likely achieving saturation with respect to calcite), possibly with some minor secondary precipitation and minor dissolution of quartz and minor aluminosilicate phases. pH is relatively efficiently buffered by this calcite dissolution, likely making the dissolution of any silicate or aluminosilicate (which would only be present at concentrations <1%) phases present relatively slow.

Similar results were obtained by Ordõnez et al. (2024) who studied the effects of exposure to CO_2-rich brine on sandstones and marls as potential deep storage reservoir and seal in the Ebro Basin.

4.1.5 Results (Portugal)

Four experiments were carried out using samples equivalent to those from the Portuguese target region (Lusitania Basin, offshore Portugal). One sample of reservoir rock and one sample of caprock were selected and prepared as described in Section 4.1.2. Each sample was reacted under both carbon dioxide and nitrogen pressures, such that reactions due to CO_2 alone (rather than due to reaction between the starting brine and solid) could be distinguished. The experimental conditions are summarised in *Table 4.2*.

Run ID	Gas	Temp. (°C)	Solid Wgt (g)	Liquid vol. (ml)	Pressure (bar)	Fluid/solid together	CO2 added	Experiment off	Run Time, days	Solid used	Original Solid ID	Brine used
1160	*CO2*	*40*	*5*	*150*	*100*	*04/04/2024*	*22/04/2024*	*31/05/2024*	*38*	*AGH0012*	*CD-CRR-10*	*55.6 g/l NaCl pre-equilibrated with solid*
1161	*N2*	*40*	*5*	*150*	*100*	*04/04/2024*	*N/A*	*31/05/2024*	*38*	*AGH0012*	*CD-CRR-10*	*55.6 g/l NaCl pre-equilibrated with solid*
1162	*CO2*	*40*	*5*	*150*	*100*	*04/04/2024*	*22/04/2024*	*31/05/2024*	*38*	*AGH0013*	*CD-DARN-15*	*55.6 g/l NaCl pre-equilibrated with solid*
1163	*N2*	*40*	*5*	*150*	*100*	*04/04/2024*	*N/A*	*31/05/2024*	*38*	*AGH0013*	*CD-DARN-15*	*55.6 g/l NaCl pre-equilibrated with solid*

Table 4.2. Run summary for batch experiments on Portuguese samples

Measured values of pH, Eh and select elemental concentrations are shown in *Figure 4-5* & *Figure 4-6*.

For the reservoir sample tested, pH shows an initial drop upon addition of CO_2 from pH 7.4 to 4.8. This corresponds to a sharp initial rise calcium concentrations, which peak at around 75 ppm at around 100 hours. Ca concentrations fall thereafter, steadying at around 20 ppm at around 400 hours. This concentration is similar to that observed in the nitrogen control experiment in which Ca concentrations remain essentially unchanged for the duration. This behaviour likely corresponds to some initial dissolution of a calcium bearing mineral (no calcium carbonate or calcium feldspar was detected during XRD analysis, but these may have been present at levels below detection) or of desorption of Ca^{2+} from mineral surfaces. The later drop in Ca concentrations after a rise pH levels rise, possibly reflecting some minor dissolution of carbonate and buffering of pH. Modelling does not, however, indicate the supersaturation of any Ca bearing phases under these conditions and at these concentrations (bearing in mind the difficulties in modelling such high salinity solutions described in the previous section).

Concentrations of other elements are generally low, or similar to those observed in the corresponding nitrogen control experiment. Si and Al in the CO_2 experiment have elevated concentrations compared to the nitrogen counterpart and show a gradual rise for the duration of the experiment, likely reflecting relatively slow dissolution of k-feldspar or other aluminosilicates present below detection. This also would correspond with initial rises in Mg and Fe observed. Mg concentrations rise until around 300 hours when, as for Ca, concentrations drop to levels similar to those observed in the nitrogen control run. As for Ca, there is no indication from modelling that any Mg bearing phases were supersaturated under these conditions and this may, again, represent some adsorption of cations from solution.

The evidence presented here reflects a mineral assemblage relatively low in reactivity. Some initial desorption of Ca, or dissolution of minor Ca bearing phases, occurs upon addition of CO_2, partially buffering the initial acidification of the fluid. After this there is evidence for slower dissolution of some aluminosilicate phases, but overall element concentrations remain low for the duration. There is no evidence for significant dissolution of the primary mineral assemblage, or secondary precipitation on the timescale of the experiment.

Fluid samples from the experiment carried out using the caprock samples with CO_2 are characterised by notably elevated Ca levels, while concentrations of other elements remain low or similar to those observed in the corresponding nitrogen control experiment. Upon addition of CO_2 observed pH levels drop slightly, from c. pH 6.9 to c. 6.4. This drop is low relative to the c 2.5 unit drop in pH observed in the experiment using the reservoir sample and indicates a significantly higher capacity for buffering pH for the caprock material. This is primarily due to the availability of calcite in this sample (around

87%) compared to the reservoir material. Ca concentrations rise for the initial 200 hours of the experimental run, after which they flatten out, remaining largely stable, maybe with a very slight decrease, for the remainder of the experiment. Modelling indicates that in this case supersaturation with respect to $CaCO_3$ was reached during the run and the slight drop in Ca concentrations at later times likely represents some minor secondary precipitation of a calcium carbonate phase. The peak Ca concentration reached was c. 1400 ppm. Assuming all of this was derived from primary calcite, this would equate to the dissolution of around 0.5 g calcite or 12% of all calcite originally present in the sample used.

Concentrations of other elements remain very low and/or similar to those observed in the nitrogen control experiments. Mg concentrations rise to around 10 ppm following a release curve similar to that observed for Ca indicating that this is also likely derived from primary calcite dissolution. Si and Al concentrations are elevated in the CO_2 run, relative to the N_2 control, but reach concentrations of only 2.5 and 0.5 ppm, respectively, indicating some enhanced, but very minor, dissolution of aluminosilicate phases in the CO_2 experiment.

The results presented here indicate large scale dissolution of the calcite present in the caprock sample induced by addition of CO_2. The Ca release is efficient at buffering the pH to much higher values than those observed in the experiment carried out using the reservoir material and this is reflected in more limited dissolution of aluminosilicate phases and (other than for Ca) lower elemental release than observed in the experiment carried out using the reservoir material.

Figure 4-5. Selected elemental concentrations from CO2 and N2 runs using Portuguese reservoir material

The PilotSTRATEGY project has received funding from the European Union's Horizon 2020 research and innovation programme under grant agreement No. 101022664

Figure 4-6. Selected elemental concentrations from CO2 and N2 runs using Portuguese caprock material

4.1.6 Discussion and Conclusions

The results from the two sets of experiments on samples from Spain and from Portugal are largely consistent in terms of the broad findings. In both cases the reservoir materials, lacking minerals particularly prone to dissolution under CO_2 conditions (i.e., carbonates), show relatively low reactivity. Primary silicate and aluminosilicate minerals are dissolved, or leached, to a limited extent (Si is released from quartz or feldspars to levels consistent with saturation with respect to silica, for example) but overall concentrations remain relatively low, as the dissolution rates for these minerals are relatively low, even under the acidic conditions created by addition of CO_2.

The story for the caprock materials is, however, very different. In the case of both the Spanish and Portuguese caprock samples reactivity in the rock-brine-CO_2 systems is driven by initial acidification of the starting brine followed by dissolution of primary calcite, which is present in both caprock samples but absent from their reservoir counterparts. In both cases the dissolution is significant. In the case of the caprock from Spain, primary calcite made up around 13% of the initial sample. Of this, around 48% dissolved, representing around 6% of the original sample mass. In the Portuguese case, calcite constituted around 87% of the original rock mass, of which around 12% dissolved, representing around 11% of the original sample mass.

In both cases, judging by the flattening of, and drops in, the Ca concentration curves, it is assumed that saturation with respect to $CaCO_3$ was reached, likely resulting in some secondary precipitation. No SEM data was available to confirm this, but modelling carried out using PHREEQC did indicate that the samples taken during the experiment carried out using the Portuguese caprock sample did become saturated with respect to calcite, likely resulting in precipitation of amorphous calcium carbonate. This was not the case for the modelling carried out for samples from the experiment carried out using the Spanish caprock sample, but given the high salinities involved (particularly in the Spanish cases) this may have been due to issues around the modelling of very high activity solutions.

While considering the implications of these results for reservoir scale systems some features of the experiments should be borne in mind:

- The experiments represent very high water: rock ratio systems. While surface area has been enhanced, through powdering of the samples, the fluid available for contact with, for example, a given area of calcite, is likely far in excess that available in a natural reservoir system.
- The experimental systems are relatively well mixed, such that one can assume that all available mineral surface area can contact the entire volume of fluid present and that there are no significant concentration gradients within the system on the timescales that samples were collected.

In the real system water:rock ratios will be considerably lower. Where CO_2 saturated fluids contact calcite dissolution will occur, but given an excess of available calcite, fluids will become saturated with respect to calcite much more rapidly (since there is, relative to the amount of rock available, lower volumes of fluids to saturate). Hence, in a static system, at least, the percentage of the bulk rock dissolved in this manner is unlikely to approach the levels observed here (i.e., 5–10%).

A more useful way to present the results may be to present them as mass of calcite dissolved per litre of CO_2 saturated brine contacting the rock surface area. In this case we arrive at values of 2.1 g calcite dissolved per litre of fluid in the Spanish case and 3.5 g in the Portuguese case. Note that these would represent minimum masses, as they do not take into account any secondary precipitation occurring alongside dissolution. Ideally these values would be normalised to available surface area, but in this case a reactive (i.e., BET) surface area measurement was not available. At this grainsize, however, reactive surface area would likely be on the order of 1–10 m^2/g. For 1 m^2 of available surface area of rock this would yield values of between 0.07–0.7 g/l calcite dissolved in the Spanish case and 0.04–0.4 g/l in the Portuguese case.

An assessment of the impact of this level of dissolution should be made in the context of the hydrodynamics of the full-scale reservoir system. In a system where there is large areal contact between CO_2 saturated water and the caprock materials and fresh CO_2 saturated fluid is constantly moving in to replace fluids carrying dissolved calcite, then levels of dissolution may be significant. Where the system is more static fluids would generally become saturated with respect to calcite after dissolving a small amount of mineral and dissolution would slow significantly or cease altogether until more, fresh, fluid becomes available. Other factors, such as the distribution of calcite within the caprocks, may also play a role in dictating overall dissolution rates and magnitudes.

The results of this work indicates that, while the selected reservoir samples have proven relatively unreactive, contact between CO_2 saturated fluids and the caprock materials in the Spanish and Portuguese cases would lead to dissolution of the primary calcite present in both samples. The extent of this dissolution and its impact in terms of opening fresh porosity and fluid-migration pathways within the caprocks should be assessed in the context of the hydrodynamics of the full system, i.e., utilising reactive transport modelling.

4.2 Experiments on Material from France

The French area of interest is located near the centre of the Paris sedimentary Basin, 55 km southwest of Paris city (Grandpuits-Bailly-Carrois county). The (onshore) area was studied for oil exploration during the second half of the 20th century (*Figure 4-7*). The target reservoir is in the Dogger platform at a depth between 1500 and 2000 m.

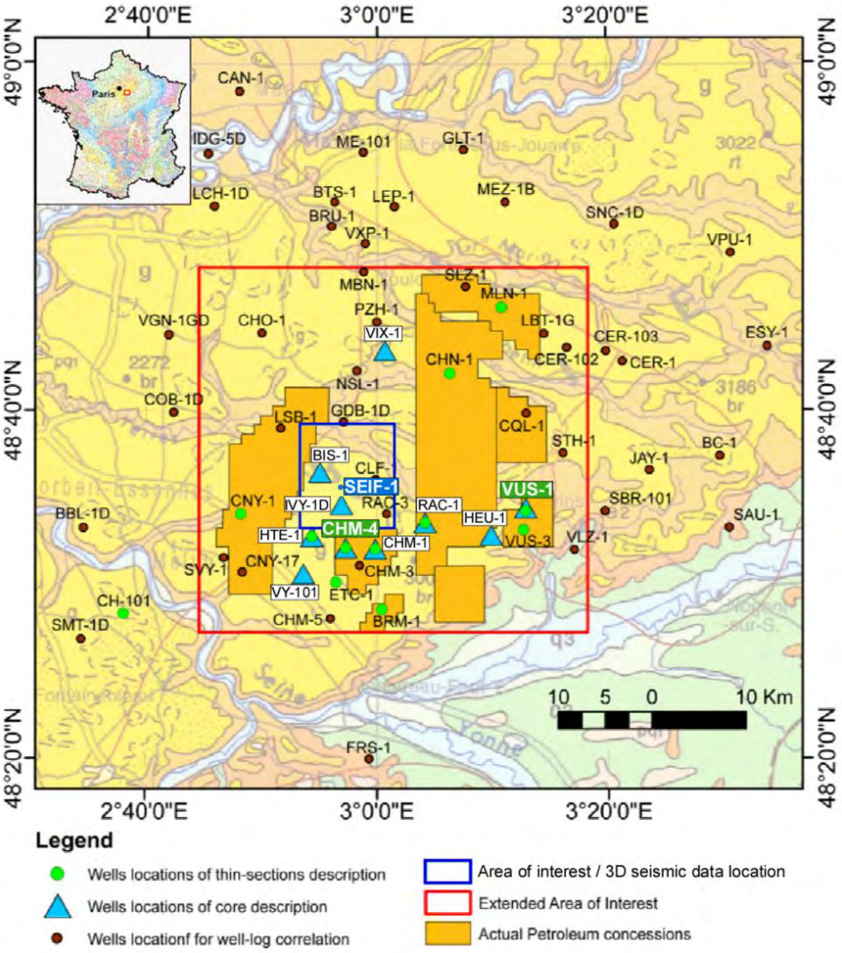

Figure 4-7. Map of the French area of interest with location of the oil concessions and available wells with drilled cores used for the geochemical characterisation in the PilotSTRATEGY project.

The Dogger platform is present over the whole Paris basin and is a sequence of middle Jurassic limestones. Well correlation in the study area has revealed that the lateral facies variations are small compared to the vertical facies variations (Bordenave and Issautier, 2023). Accordingly, the vertical facies distribution defines the framework of the complex lithostratigraphic platform, with six main geological formations (

Figure 4-8), the *Dalle Nacrée* (Early Callovian); the Comblanchian limestones (Late Bathonian); the *Oolithe Blanche* (Late Bathonian); the limestones with Pholadomya fossils (marly limestones; Late Bathonien to Late Bajocian); the marls with Ostrea acuminata fossils (Late to Early Bajocian) and the crinoidal limestones (Early Bajocian). Although the *Oolithe Blanche* formation is the main target reservoir for CO_2 injection and storage, the storage reservoir includes also the overlying Comblanchian limestones and *Dalle Nacrée* formations as the injected CO_2 would tends to move upward toward the caprock. The Callovian marls are the bottom of the caprock to the storage reservoir (*Figure 4-8*).

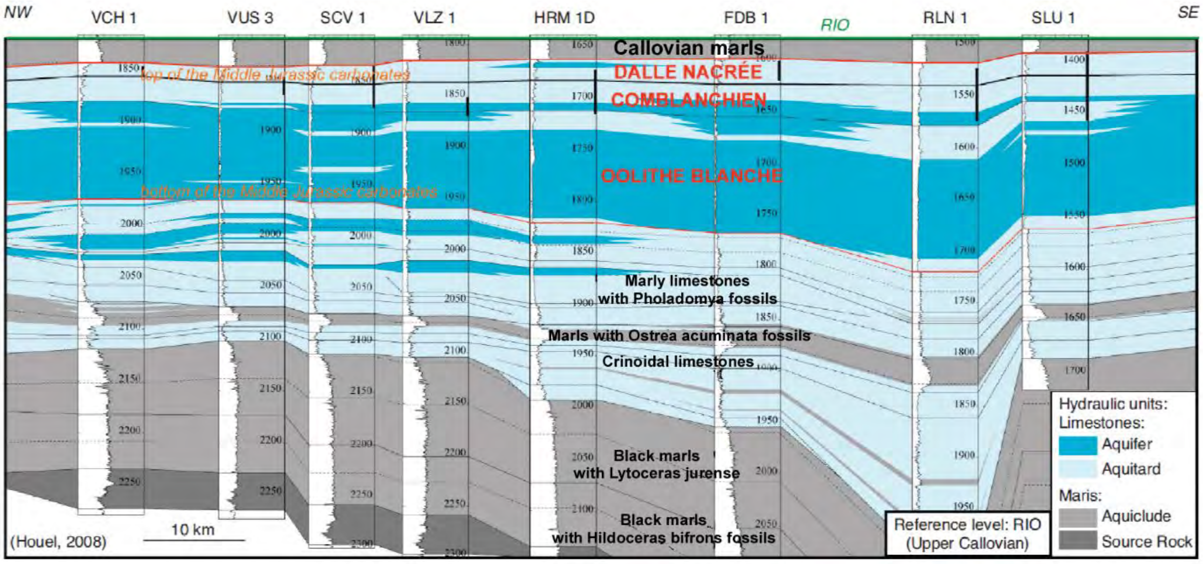

Figure 4-8. Example of distribution of the main formations and potential aquifer, aquitard and aquiclude units based on well correlation profiles and relative porosity of the Dogger carbonates in the PICOREF study area, located 5 – 10 km South-East from the PilotSTRATEGY study area (adapted from Houel (2008)).

4.2.1 Reservoir and caprock geochemical characterization

4.2.1.1 Core and rock sample selection

Among the numerous wells and available drilled cores of the broad area, the French team described the core from deep wells in and surrounding the area of interest (Figure 4-7), to better understand the target reservoir in the Dogger platform and the overlying caprock before selecting representative rock samples. The geochemical characterization for the area of interest focused on the three uppermost Dogger formations (i.e. *Dalle Nacrée, Comblanchian* and *Oolithe Blanche* formations) for the reservoir and the overlying Callovian-Oxfordian argillites-to-marls for the caprock. The selection of rock samples was completed in two stages, based first on the core material available in 2022 from oil exploration in the surrounding area, before considering newly available cores from a private industrial well within the area of interest in 2024.

Most of the geochemical characterisation of the reservoir and caprock was performed on rock samples collected in 2022. As coring was only conducted on the Callovian transgressive deposits during oil exploration, the cores available covered mainly the topmost part of the targeted storage reservoir. The sampling strategy has been conducted with the objective of having a better understanding of the reservoir property variations related to sedimentary facies, using existing well log data. Following the core description through 10 wells by the BRGM team (Figure 4-7), two wells with cores reaching the deepest part of the *Oolithe Blanche* Formation and well log showing important reservoir properties variations through the same sedimentary facies were selected for sampling and geochemical characterisation: Vulaines-1 (VUS1) and Charmottes 4 (CHM4).

Drilled in 1978, the Vulaines-1 well is located at 11 km east to the Area of Interest (Figure 4-7). The Vulaines-1 cores intersect from depth -1819 to -1919 m (TVD) the *Dalle Nacrée*, *Comblanchian* and the upper *Oolithe Blanche* Formations as well as the lowermost part of the *Marnes de Messengis* Formation, also considered as the transitional Callovian caprock. More detailed facies description and stratigraphic interval in the Early Callovian to Late Bathonian limestones were addressed in the PilotSTRATEGY Deliverable 2.7 – Conceptual Geological Models Report (Bordenave and Issautier, 2023) and the PilotSTRATEGY Deliverable 2.6 – Petrophysics Report (Fleury et al., 2023). Among the 100 meters of the cored section only 57 m of cores were recovered. A total of 13 samples (mostly cuttings or core plugs) were selected along the Vulaines 1 cores for the geochemical rock characterisation.

The Charmottes 4 well, located at 2 km south of the Area of Interest (Figure 4-7), was drilled and cored from depth - 1790 to -1826m (TVD), with 95% recovery. The 34 meters of cored sedimentary section are mainly the *Dalle Nacrée*, *Comblanchian* and the upper *Oolithe Blanche* Formations. A total of 8 samples (mostly cuttings or core plugs) were selected along the Charmottes 4 cores for the geochemical rock characterisation.

From regional studies, it is known that the topmost part of the targeted storage reservoir has poor reservoir properties compared to rest of the formation. Following discussion with a local industrial, the BRGM team managed to get access, in 2024, to additional cores drilled (i) along the entire *Oolithe Blanche* Formation and (ii) within in the area of interest: well SEIF-1 (*Figure 4-7*). In addition to core description and petrophysical characterisation, a few rock samples were collected from the intermediate to deep part of the *Oolithe Blanche* Formation and the Callovian-Oxfordian caprock to complete the geochemical characterisation of the reservoir and apply experiments on representative core plug samples.

4.2.1.2 Pristine brine selection

The significant variation of the salinity of the pristine groundwater, according to the geographical position and depth in the Dogger aquifer was decribed in the PilotSTRATEGY Deliverable 2.11 – Regional Hydrogeology Report (Mathurin et al., 2023). The pore water composition in the Dogger aquifer was characterised, both in the centre of the Paris basin (regional scale; Rojas et al., 1989) and in the vicinity of the prospective area (local scale). Investigation on a local scale, more appropriate for the selection a representative composition of the brine, was based on a database belonging to the Vermilion Energy Company, owner of the productive oil wells from the surrounding petroleum concessions.

Based on the Piper and Schoeller-Berkaloof diagram (Figure 4-9; Figure 4-10), which are charts used in hydrogeology to visualize the chemical composition of water based on the concentrations of dissolved major elements, the mineralization of the groundwater is of sodium-chloride type with a salinity ranging 6 – 37 g/L (median : 20 g/L). The synthetic brine composition used in the reactive batch and flow through experiments was selected to be representative of the Dogger aquifer nearby the target area. A groundwater sample collected in the Charmottes 3 well, located at c.a. 5 km south of the Area of Interest (Figure 4-7), is thought to be representative of mineral content, with an intermediate salinity (19.2 g/L) which is close to the median groundwater salinity in the local Dogger aquifer.

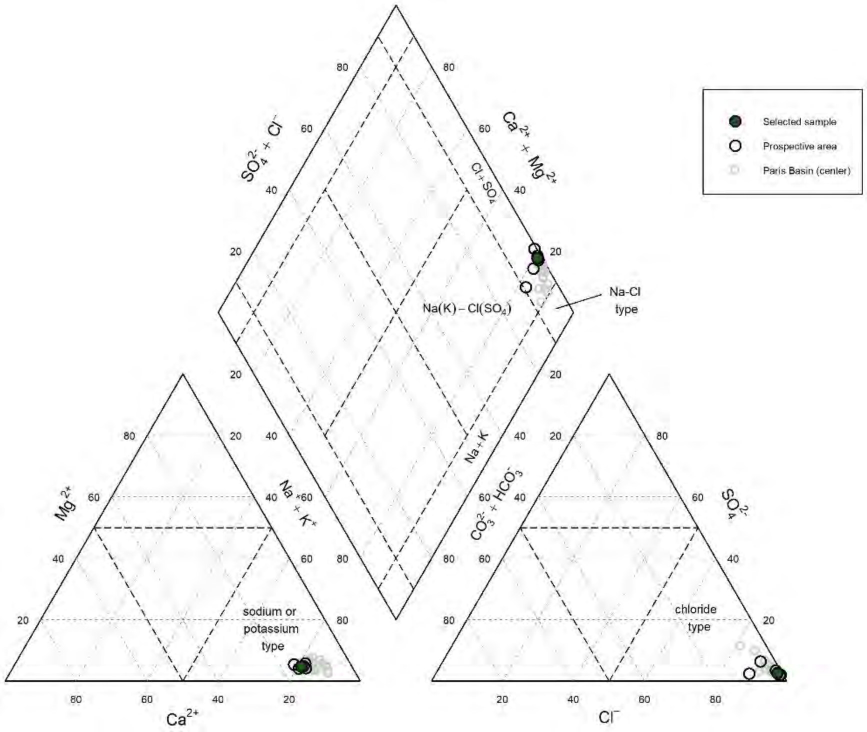

Figure 4-9. Piper diagram of the groundwater in the Dogger aquifer in the centre of the Paris Basin and in the immediate vicinity of the prospective area.

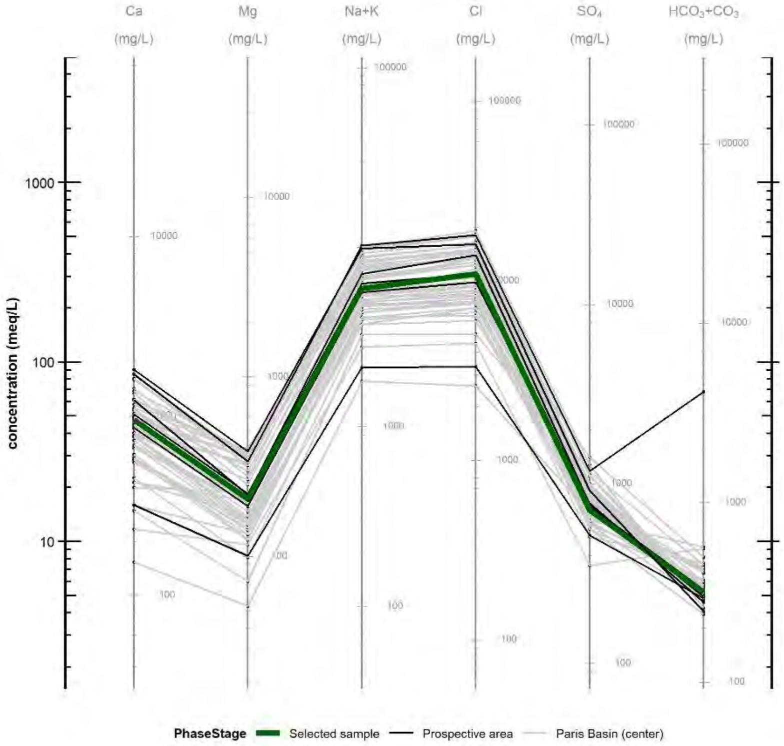

Figure 4-10. Schoeller-Berkaloof diagram of the groundwater in the Dogger aquifer in the centre of the Paris Basin and in the immediate vicinity of the prospective area: concentrations of major elements.

4.2.1.3 Methodology for rock analyses

The mineralogical and geochemical characterisation of the reservoir and caprock samples relies on results of a combination of several analytical methods, summarised in Table 4.3, applied at the BRGM laboratories.

Table 4.3. List of analytical methods applied for the characterisation of the rock samples.

Analytical method	Analytical outcomes
X-ray diffraction (XRD) & Rietveld refinement	Semi-quantitative mineralogical composition of crystalline phases
Optical cathodoluminescence (CL)	Internal structure of the rock sample and first overview of the rock chemical variation
Scanning Electron Microscopy (SEM) with BackScattered Electron (BSE) detector	High resolution of surface topography and characterisation of the relative mineral density
SEM coupled with Energy Dispersive X-Ray (EDS)	Qualitative identification of trace mineral phases

All collected rock samples were analysed and compared by X-ray diffraction, scanning electron microscope and cathodoluminescence techniques, to check potential changes in mineral composition, crystalline phase and chemical composition within the reservoir and the caprock.

Crystalline phases were identified by X-ray diffraction and (semi-)quantified by the Rietveld refinement on powdered rock with a Bruker D8 Advance diffractometer in a θ-θ configuration, employing Cu Kα radiation (λ=1.541 Å) with a rotating sample stage. The samples were scanned between 4 and 75°. Data were collected with a time of 556.8 seconds and a scan speed of 0.03° 2θ/second. X-ray diffraction patterns were qualitatively analyzed with the Diffrac SuiteTM software. Rietveld refinement was subsequently performed on the X-ray powder pattern using the SiroQuant V.4 program from Sietronics.

The mineralogical organization and microstructure were determined using optical cathodoluminescence, complemented by Scanning Electron Microscopy (SEM) observations coupled with a BackScattered Electron (BSE) detector. An Energy Dispersive X-Ray (EDS) detector was also used to complete XRD observations and identify mineral phases with very low concentrations.

4.2.1.4 Reservoir characterisation

The 21 samples collected from the Charmottes 4 (Figure 4-11) and Vulaines 1 (Figure 4-12) cores, revesled a reservoir mostly composed of calcite (≥ 95 weight %), with an overall increasing percentage of calcite with depth (up to 99 wt.%). The results of the XRD analyses, coupled with Rietveld refinement, revealed that the remaining percentage of the mineral phases were mainly composed, in descending order, of ankerite/dolomite, quartz, pyrite, gypsum, kaolinite and illite and/or mica, although the proportion varies spatially. Comparatively, the Charmottes 4 samples were relatively rich in pyrite, whereas the Vulaines 1 samples were more rich in gypsum.

Whether calcium sulphate crystallize as gypsum or anhydrite depends primarily upon temperature and to a lesser extent on pressure and chemistry. In low temperatures (< 42 °C; Hill 1937) and the presence of available water, anhydrite can hydrate (or rehydrate) and convert to gypsum. With the groundwater temperature in the Dogger aquifer ranging locally between 55 and 70°C (measurements taken in 2012), the occurrence of gypsum as primarily precipitate can be questioned in the reservoir (depth >1800 m), where pressure and temperature conditions are more favorable to the occurrence of anhydrite. It cannot be ruled out that the gypsum identified by XRD analysis results from the reprecipitation of anhydrite into gypsum within the cores during or after the drilling. Accordingly, the wording “gypsum/anhydrite”, instead of “gypsum”, is used hereafter.

With respect to depth, the presence of illite and/or mica (< 1.5 wt.%), kaolinite (< 0.8 wt.%) and gypsum/anhydrite (< 0.5 wt.%), occured mainly in the upper part of the analyzed Charmottes 4 section (Figure 4-11), associated with rock samples collected from the Dalle nacrée formation and possibly a transition level located at 1812.5 m (Figure 4-11). Ankerite/dolomite in fluctuating proportions (0.1 - 1.6 wt.%), was present over a large interval of the profile, alongside quartz (0.1 - 0.9 wt.%), whose proportion overall tended to decrease with depth.

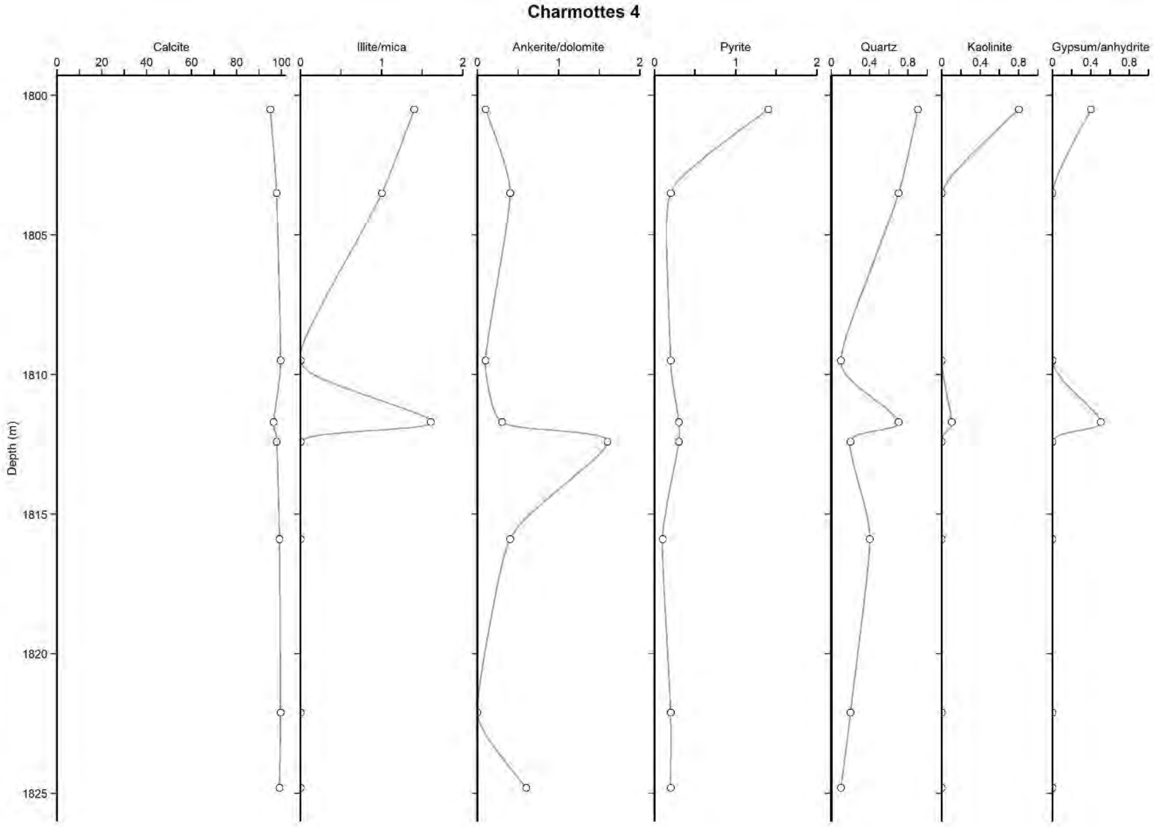

Figure 4-11. Semi-quantitative proportion of mineral phases (weight %) in the Dogger reservoir along the vertical profile of the Charmottes 4 well (estimation determined by XRD-Rietveld analyses).

For Vulaines 1 samples, pyrite (< 2 wt.%), illite and/or mica (< 1.6 wt.%), gypsum/anhydrite (0.9 wt.%), and kaolinite (< 0.5 wt.%) occurred mainly in the upper part, associated to samples collected from the Dalle nacrée Formation and along transition level located at 1895 m (Figure 4-12). The gypsum/anhydrite and ankerite/dolomite mineral were present over a large interval of the profile, with a general enrichment from the top to the bottom of the Comblanchian Formation, and in the upper part Oolithe Blanche Formation (only for gypsum/anhydrite). In comparison of the Comblanchian Formation, the upper part Oolithe Blanche Formation displayed relatively higher proportion of kaolinite (< 0.4 wt.%).

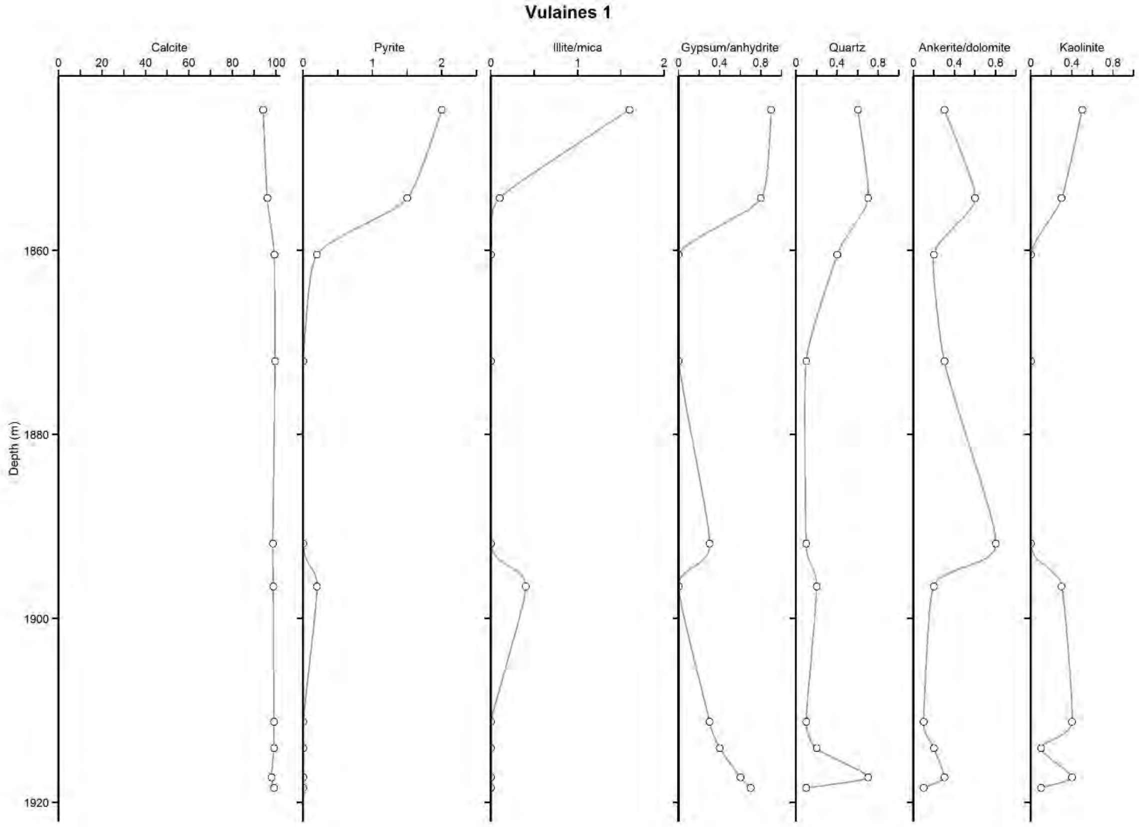

Figure 4-12. Semi-quantitative proportion of mineral phases (weight %) in the Dogger reservoir along the vertical profile of the Vulaines 1 well (estimation determined by XRD-Rietveld analyses).

The characterisation of the intermediate to deep Oolithe Blanche Formation relied on only a few samples from the SEIF 1 well, preventing study of the change in the mineral proportions with depth. However, comparison of the mineral proportion between the upper part (Vulaines 1 cores) and the intermediate to deep (SEIF 1 core samples) Oolithe Blanche Formation confirmed relative constant calcite, kaolinite and quartz proportions within the oolitic reservoir (Figure 4-13). The absence of gypsum and a relative enrichment of ankerite are the main notable features in the intermediate to deep levels of the Oolithe Blanche Formation.

The ankerite and dolomite minerals could not be differentiated from each other by XRD analysis applied on the reservoir samples, preventing to confirm the occurrence of both mineral phases. SEM-EDS analyses were applied to further investigate the nature of the Mg rich carbonates on a limited number of samples, which covered the Comblanchian and the Oolithe Blanche Formations.

The SEM-EDS analyses of crushed rock (mineral powder) from the Comblanchian Formation could barely confirm the occurrence of dolomite or ankerite, as Mg-rich phases were poorly represented among the studied sample Vulaines 1 – 1872 m (Figure 4-14). Most of the minor mineral phases (pyrite, quartz or kaolinite) could be identified as individual minerals, apart for gypsum/anhydrite which were mainly identified as coprecipitated or coated on several calcite minerals. Similar analyses were performed on sample Vulaines 1 – 1917 m, representative of the upper part of the Oolithe Blanche Formation (Figure 4-15). If pyrite, gypsum/anhydrite, quartz and dolomite were identified as independent mineral phases, no occurrence of ankerite mineral could be detected from EDS analyses.

The observation of calcite mineral with Mg enrichment might indicate either coprecipitation and/or coating of dolomite with calcite minerals or Mg impurities in the calcite minerals.

As a result of the higher proportions of Mg-rich carbonate within the intermediate to deep part of the Oolithe Blanche Formation (Figure 4-13), ankerite and dolomite minerals were both observed on the consolidated rock samples from SEIF 1 (

Figure *4-16*). Ankerite was coprecipitation with dolomite in the cemented sample, in between the calcitic oolite grains, likely from a diagenesis process. The same was also observed on samples from SEIF 1 – 1852 m (Figure 4-17). The spatial distribution of the Mg-rich carbonate and pyrite minerals gives a limited effective surface area to these minerals, restricting the interaction with the pore fluid. Calcite was the mineralogical phase with the largest specific surface area in contact with the porosity, by far.

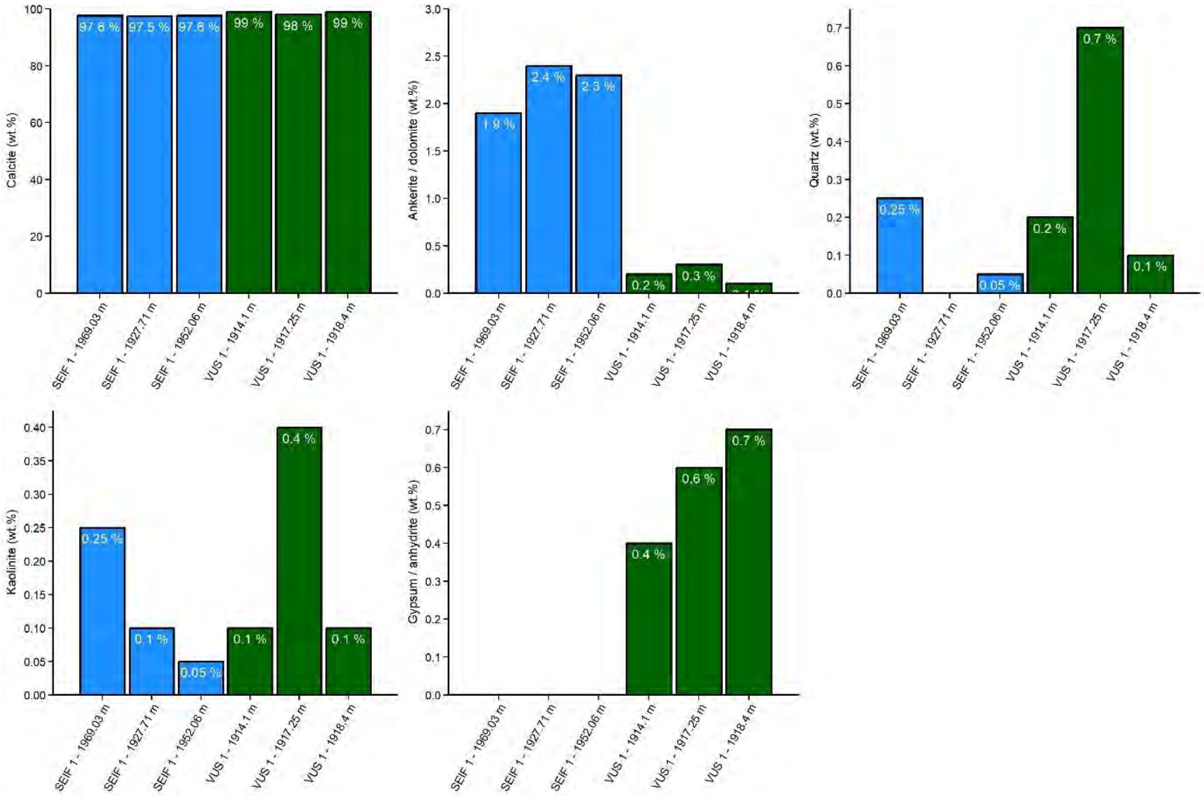

Figure 4-13. Semi-quantitative proportion of mineral phases (weight %) in the upper part (Vulaines 1 well – green) and intermediate to deep part (SEIF 1 well - blue) of the Oolithe Blanche Formation. Estimation determined by XRD-Rietveld analyses.

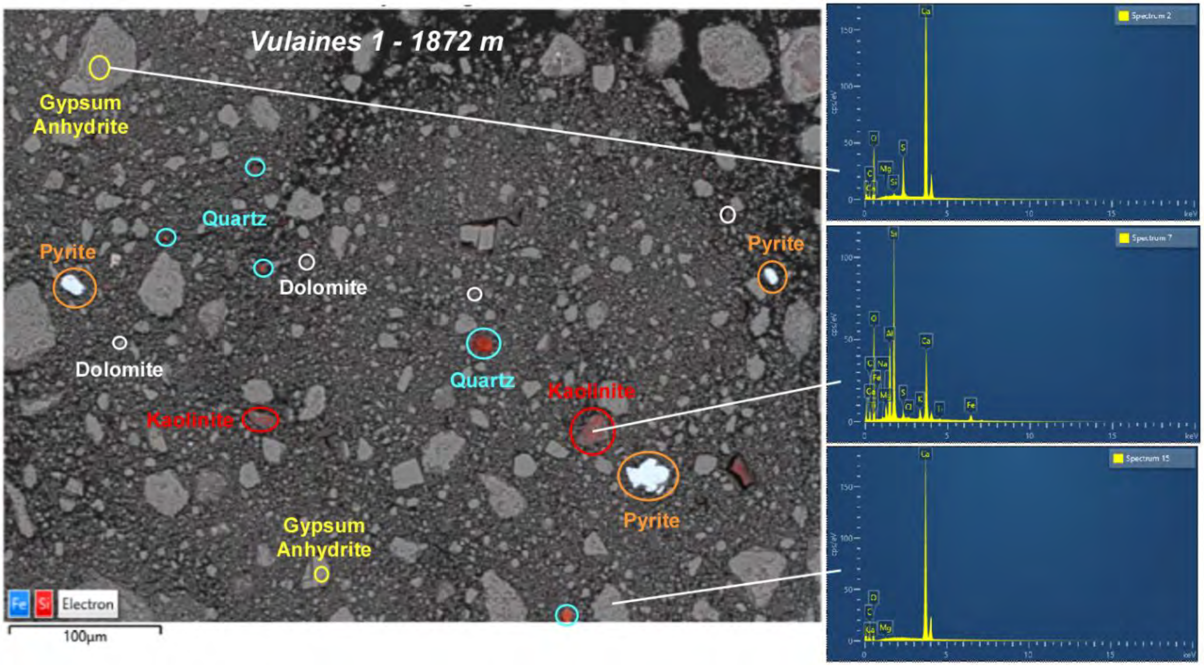

Figure 4-14. SEM-BSE-EDS analyses of the crushed Vulaines 1 – 1872 sample (fine mineral powder): BSE image (left) and EDS elemental analyses (right) for various mineral phases.

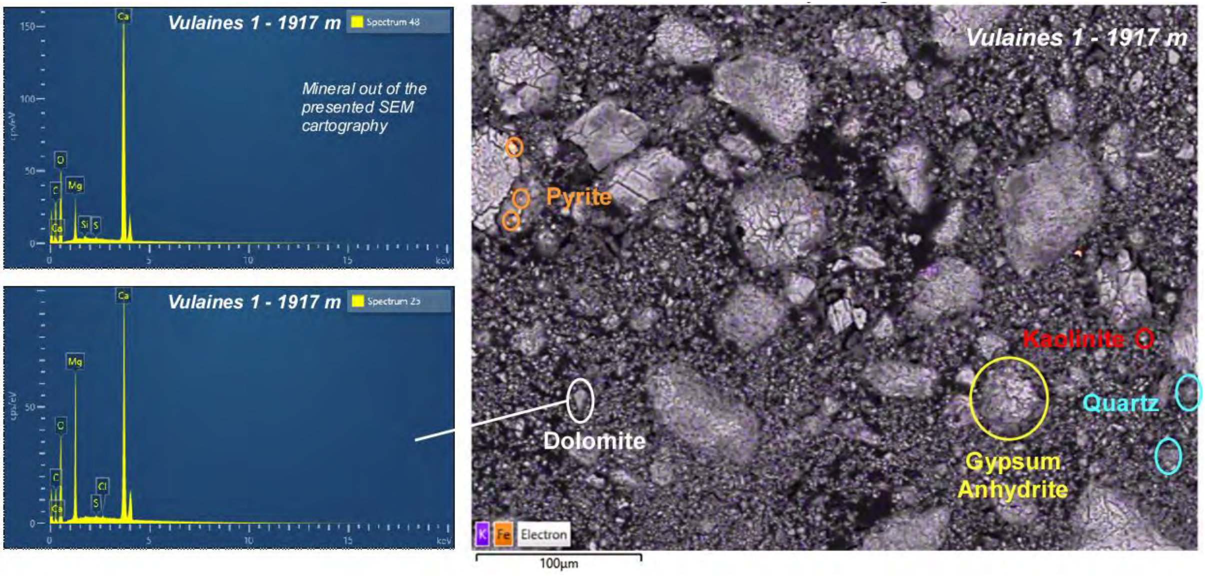

Figure 4-15. SEM-BSE-EDS analyses of the crushed Vulaines 1 – 1917 sample (fine mineral powder): BSE image (left) and EDS elemental analyses (right) for various mineral phases.

The PilotSTRATEGY project has received funding from the European Union's Horizon 2020 research and innovation programme under grant agreement No. 101022664

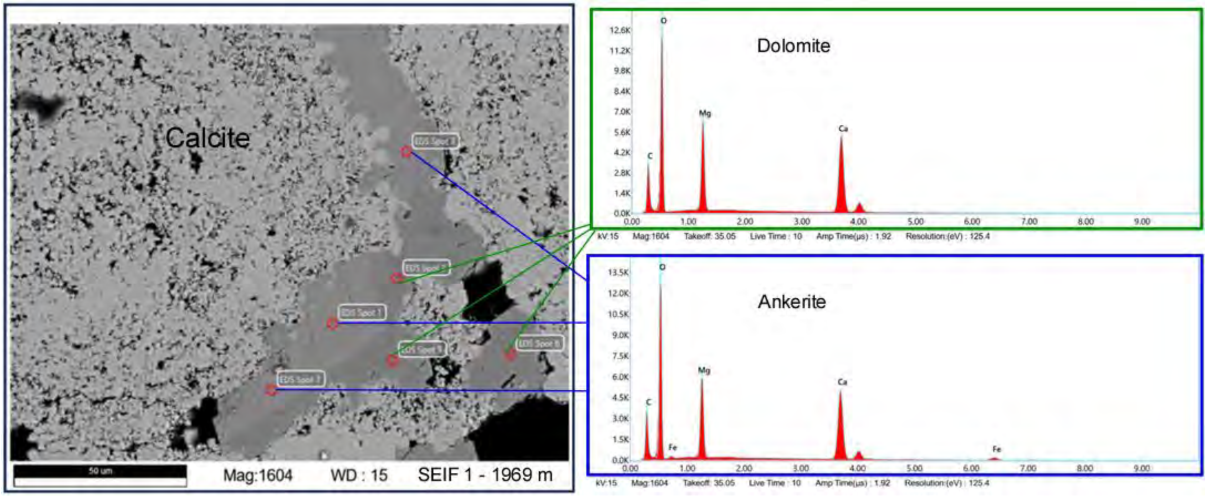

Figure 4-16. SEM-BSE-EDS analyses of the rock sample from SEIF 1 – 1969 m (consolidate rock): BSE image (left) combined with EDS elemental microanalyses (right) of dolomite and ankerite.

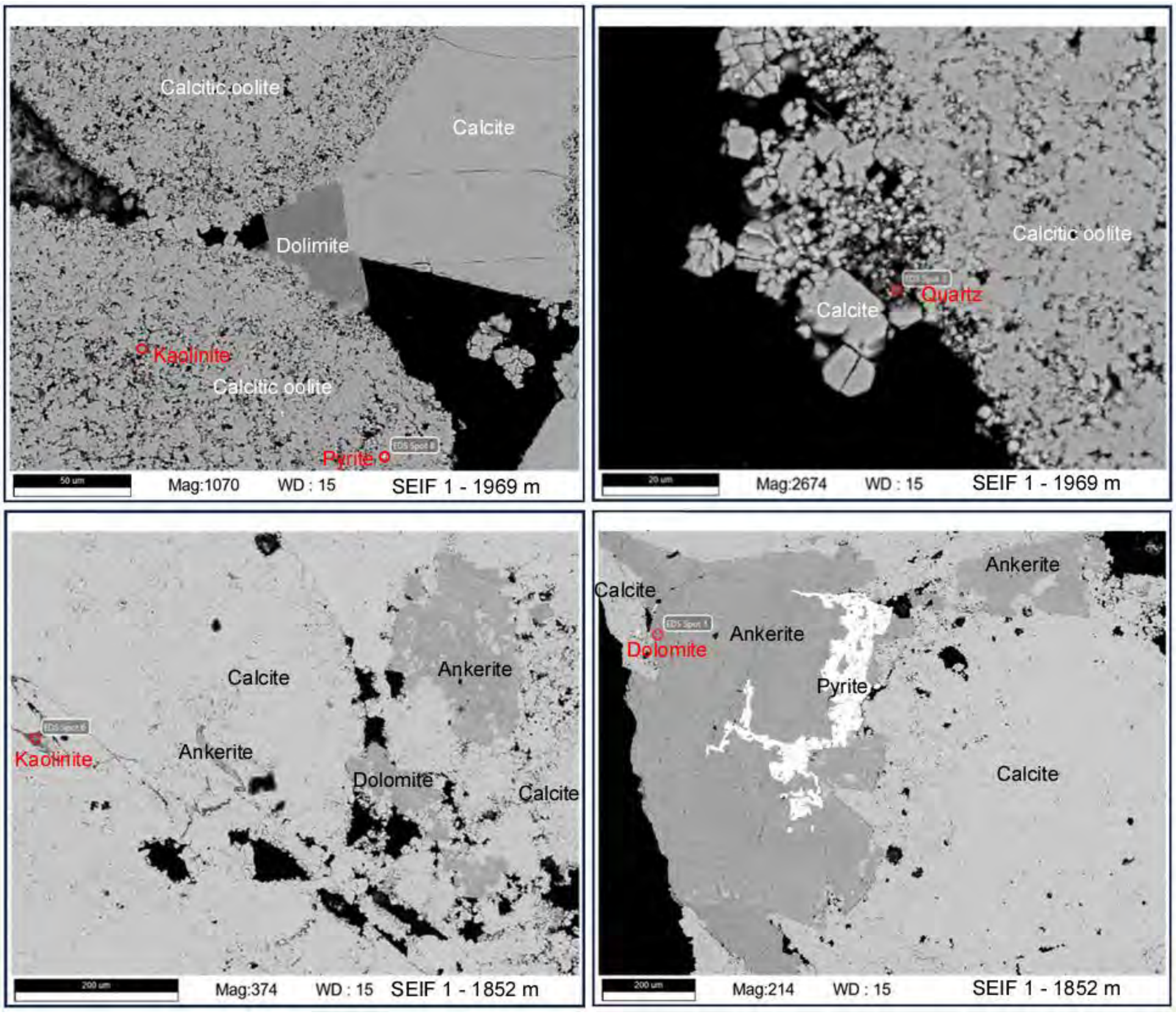

Figure 4-17. SEM-BSE cartography of the rock samples SEIF 1 – 1969 m (top) and SEIF 1 – 1852 m (bottom): illustration of the mineral assemblage of consolidate rock from the Oolithe Blanche Formation.

4.2.1.5 Caprock characterisation

The mineralogical characterisation of the caprock relied mostly on three rock samples collected along the Vulaines 1 core – bottom of the caprock (transitional mudstone) – and a duplicate sample from SEIF 1 – 1840 m – 1.5 m above the top of the transitional caprock (Callovian mudstone). The XRD-Rietveld results emphasised a large set of mineral phases, up to 13, composing the caprock (Figure 4-18). The mudstone is primarily composed of illite and/or mica (25 wt.%), clay minerals (25 wt.%) – including smectite and/or interstratified illite/smectite (20 wt.%), kaolinite and chlorite –, quartz (22 wt.%) and calcite (16 wt.%). The remaining percentage of the mineral phases were mainly composed, in descending order, of ankerite, pyrite, plagioclase, dolomite, K-feldspar, gypsum/anhydrite and anatase.

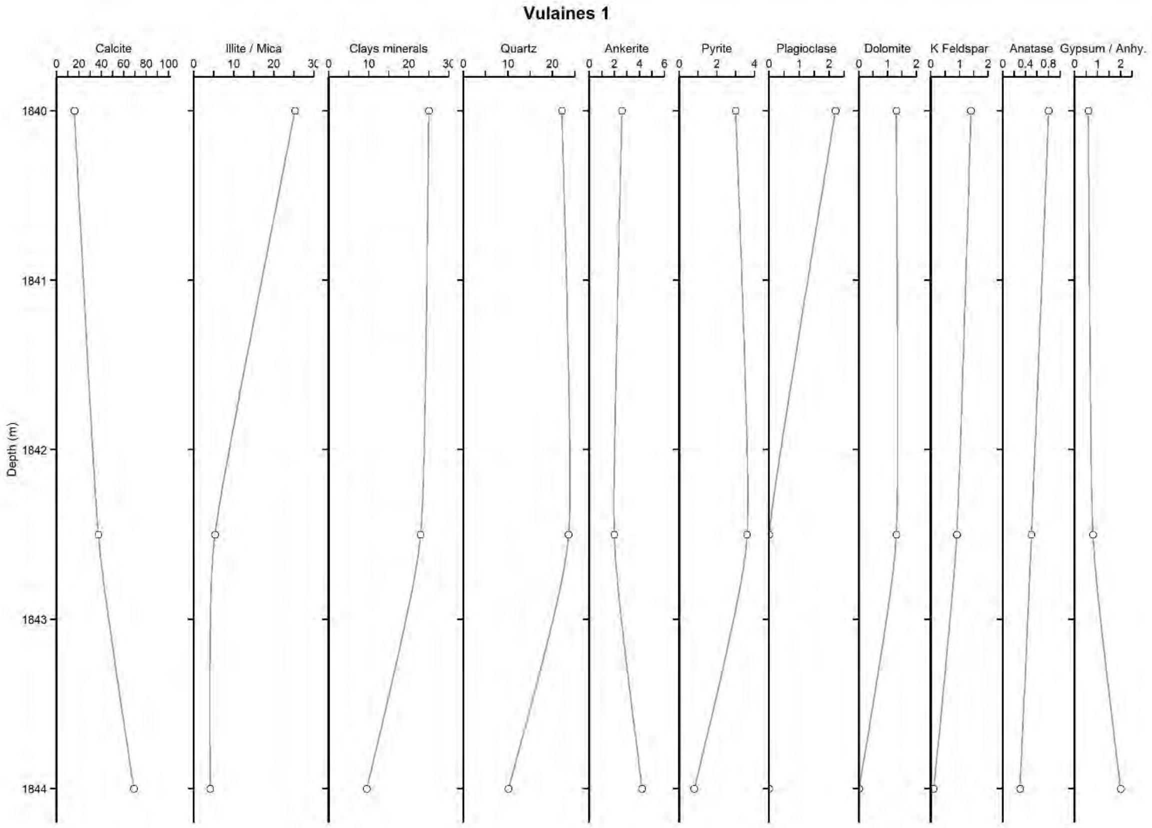

Figure 4-18. Semi-quantitative proportion of mineral phases (weight %) in the transitional Callovian mudstone along the vertical profile of the Vulaines 1 well (estimation determined by XRD-Rietveld analyses).

Within the transitional Callovian mudstone, the proportions of calcite, ankerite and gypsum/anhydrite increased with depth, until to reach the top of the Dalle Nacrée Formation. Inversely, the proportion of all the other identified mineral phases tended to decrease with depth (*Figure 4-18*).

Comparison of the mineralogical composition of the Callovian mudstone cored drilled along the Vulaines 1 and SEIF 1 wells showed relative stability in the proportion of calcite, quartz, illite and/or mica, chlorite, ankerite/dolomite and plagioclase within the upper part of the mudstone (Figure *4-19*). The absence of detected dolomite mineral and a change in the proportion of clay mineral – i.e. slightly lower proportion of smectite and/or interstratified illite/smectite compensated by higher proportion of kaolinite – in SEIF 1 samples represented the main discrepancies observed between the mudstone and the transitional mudstone.

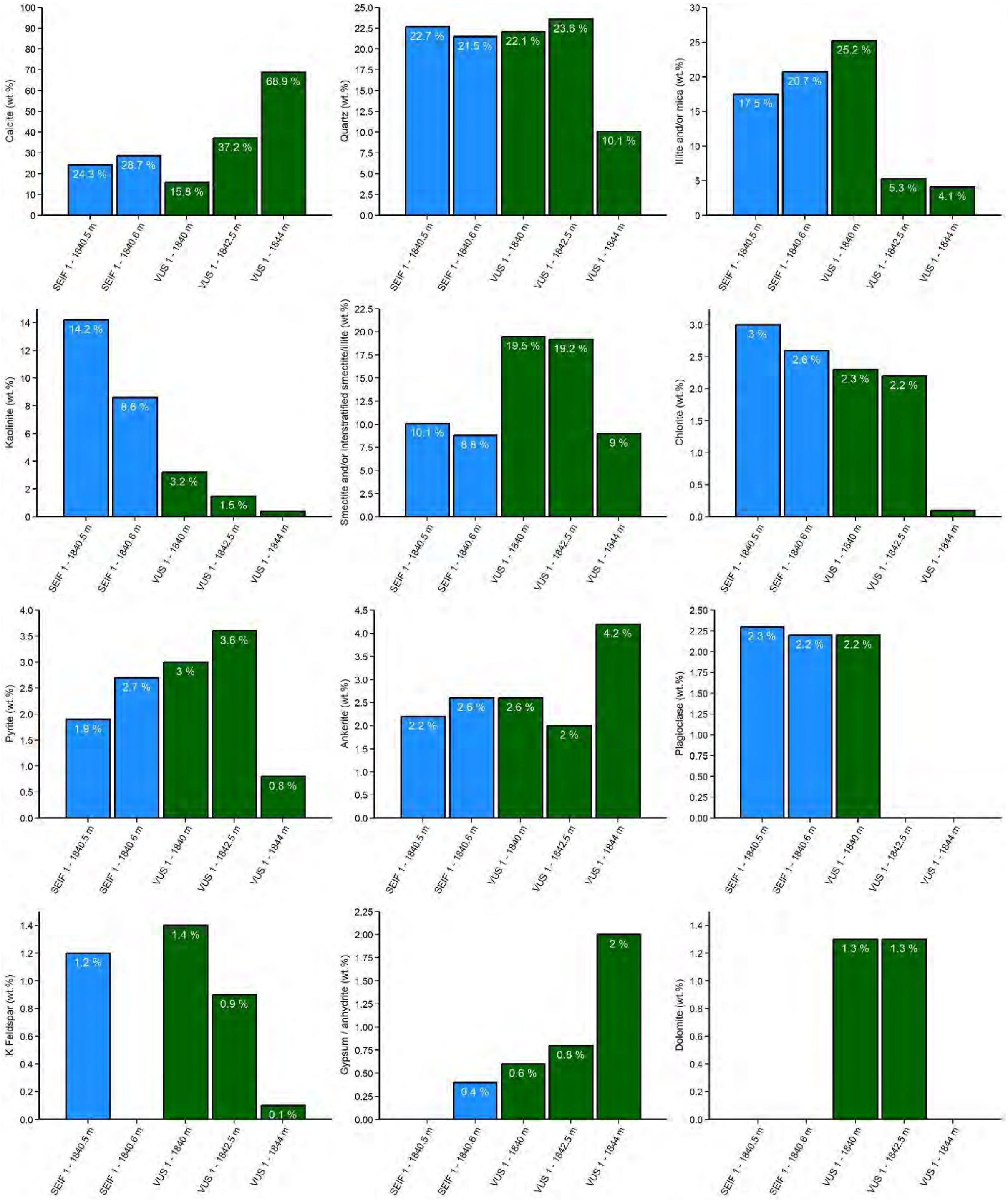

The PilotSTRATEGY project has received funding from the European Union's Horizon 2020 research and innovation programme under grant agreement No. 101022664

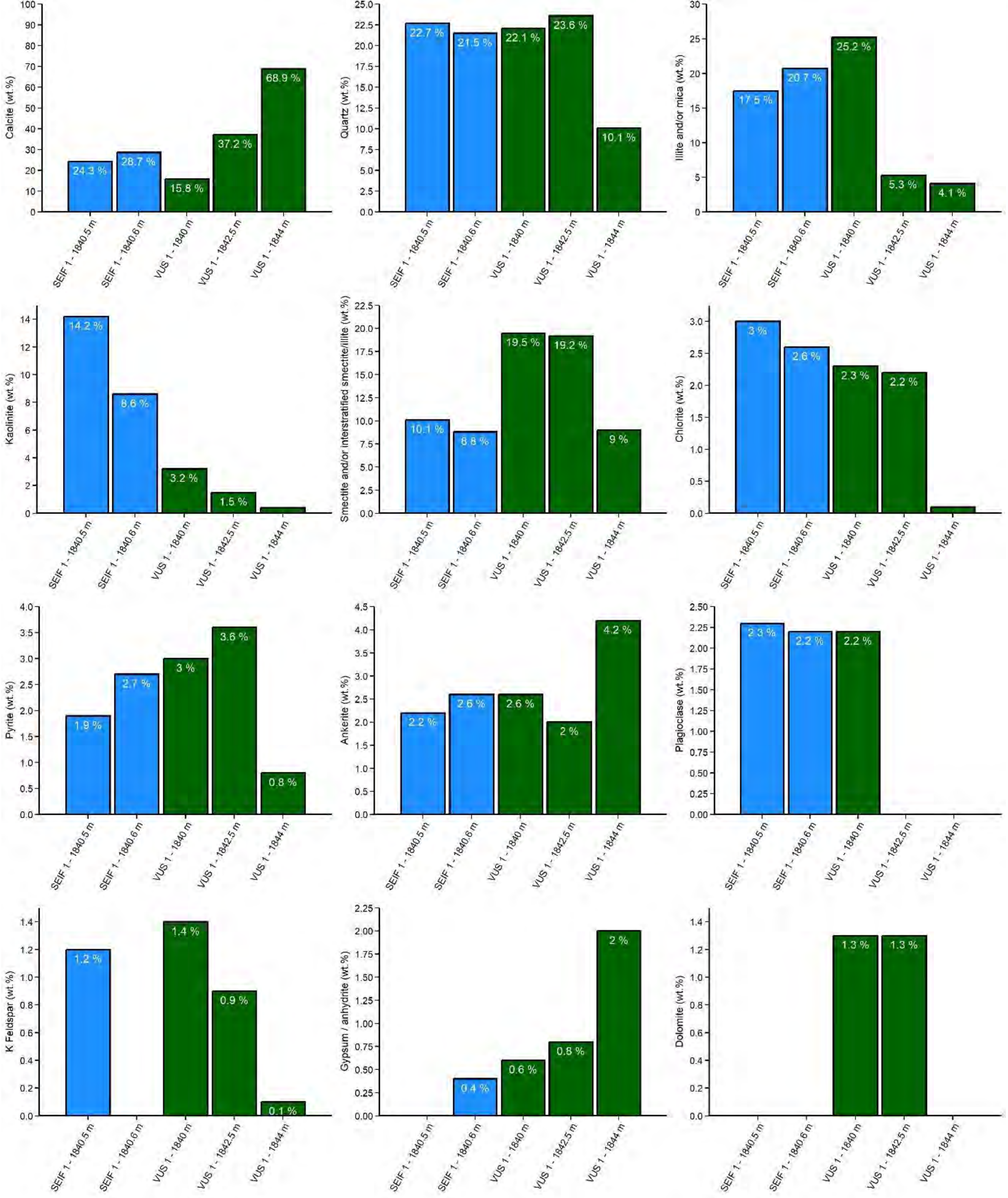

Figure 4-19. Semi-quantitative proportion of mineral phases (weight %) in the Callovian mudstone: Vulaines 1 – transitional caprock (green) and SEIF 1 (blue) – representative caprock. Estimation determined by XRD-Rietveld analyses.

The SEM petrography of the mineral assemblage and the texture of the consolidated Callovian mudstone illustrates the dominant proportions of clay and mica minerals (Figure 4-20). Most of the minor mineral phases are embedded in clay mineral fractions.

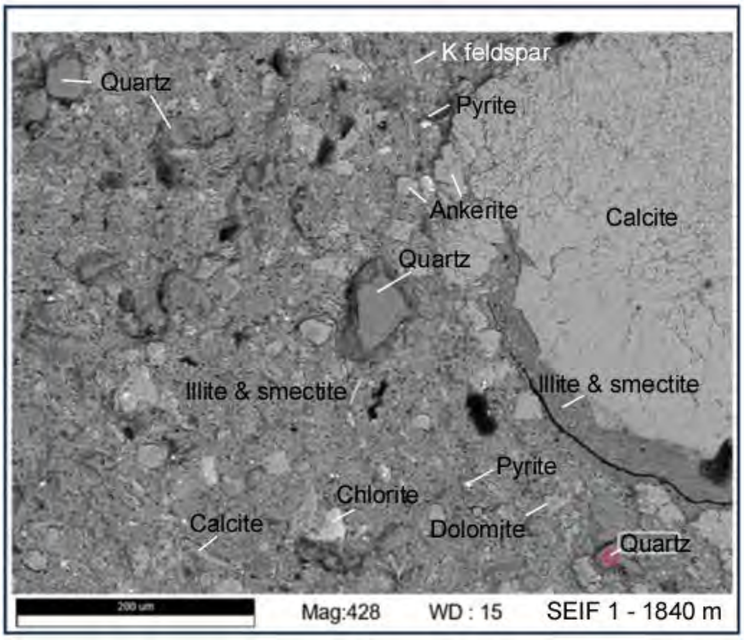

Figure 4-20. SEM-BSE image of the rock samples SEIF 1 – 1840 m with the identified mineral phases.

4.2.2 Experimental methodology

4.2.2.1 Experimental facility

The rock mineral reaction rate of the prospective reservoir and caprock were quantified with the BioREP facility. BioREP (BioReactors for the Deep Environment) is an experimental platform for studying deep environments and characterising the natural biogeochemical processes and/or industrial processes. Part of the network of European Research Infrastructure ECCSEL platforms designed for the capture, transport, use and geological storage such as CO_2, the BioREP facility is located in the BRGM research centre in Orléans, France.

The experimental devices can be used to perform static and/or dynamic tests (batch experiment, percolation through rocks, fluid transfer, etc.) using various matrices (cores, cuttings, crushed rocks, synthetic materials) and work at up to 500 bar and up to 250°C, to study the interactions between water, rocks, gases.

For the PilotSTRATEGY project the BioREP platform was used to mimic geochemical processes associated with fluid-rock interactions during CO_2 injection under a range of CO_2 partial pressures at high pressure and temperature (i.e. at conditions prevailing in the reservoir), while continuously monitoring geochemical and evolution during the experiment. BioREP consists of several reactors, transfer columns and other tools (pumps, sensors, etc.) that can be modulated and combined *ad infinitum* to perform customized tests. TransREP, which is one of the four setups of the platform, was used to take advantage of the multiple reactors (500 ml) and run several batch experiments simultaneously (Figure 4-21).

The PilotSTRATEGY project has received funding from the European Union's Horizon 2020 research and innovation programme under grant agreement No. 101022664

Figure 4-21. Picture of the TransREP experimental setup, part of the BioREP platform.

4.2.2.2 Rock sample selection

Samples from reservoir and caprock were selected based on the results of the reservoir and caprock geochemical characterisation. Only the Charmottes 4 and Vulaines 1 cores were available when the batch experiments were designed and run. The rock sample selection aimed to integrate the geological knowledge from the reservoir and the associated minor variations in mineral composition between the different formations. Accordingly, the estimate of rock reactivity was undertaken on three limestone samples from the reservoir, each representative of (i) the Dalle Nacrée, (ii) the Camblanchian and (iii) the Oolithes Blanches Formations, and one mudstone sample, representative of the (iv) caprock. As only the Vulaines 1 cores covered each of the four-targeted formation, the rock samples selected for the batch experiment were solely collected from this cored well. Each of the four rock samples were selected based on the relative composition of the mineral assemblage (Figure 4-22).

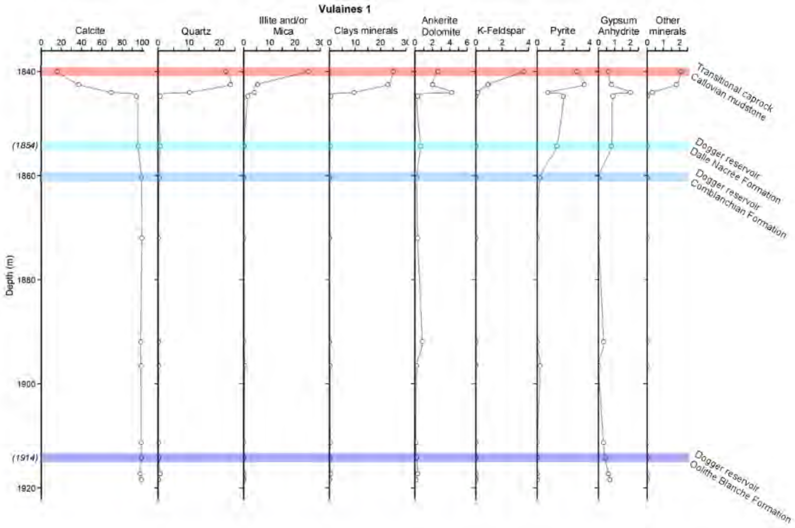

Figure 4-22. Selected samples for the batch experiments all collected along the Vulaines 1 cores, to cover the three main formations composing the Dogger reservoir and the Callovian mudstone.

4.2.2.3 Synthetic brine

For the French site, the batch experiments focused mostly on the assessment of the reactivity of the different rock type of the storage complex exposed to CO_2 injection. The impact of water composition on geochemical processes was considered out of scoop within this experimental task. Accordingly, a synthetic brine solution was made, based on the selected brine sample from Charmottes 3 well (see section 4.2.1.2; Figure 4-10) collected in the Dogger aquifer, most likely in the Dalle Nacrée Formation, without testing any other chemical composition of the brine within the experiments. Due to a lack of reference water for the pore water in the Callovian mudstone, the same synthetic brine was used in all batch experiments, for the geochemical assessment of both the reservoir samples and the caprock samples.

The components of the simplified brine solution are presented in Table 4.4. To ensure a constant water composition, a large volume of synthetic brine was prepared prior the beginning of the batch tests. The solution was initially concentrated 10 times and divided in 2 sub-solutions to avoid precipitation during storage (i.e. before use). Iron and fluorine were not included in the simplified brine since addition of a minor amount of associated salts (e.g. $FeSO_4.7H_2O$) would cause artificial formation of iron and fluorite precipitates when mixing the two sub-solutions before use. Lithium, strontium and barium were not included due to lack of information in the reference sample. The synthetic brine composition was analysed frequently to ensure there was no change.

Table 4.4. Components used to set the composition of the synthetic brine (concentrated 10 times)

Salt components	mass for 1 liter (g)
NaCl	139.26
$CaCl_2.2H_2O$	34.99
$MgCl_2$	8.19
KOH	1.26
Na_2SO_4	10.58
Na_2SiO_3	0.78

4.2.2.4 Experimental design

The batch experiment consisted of homogenised crushed rock (<80 µm), synthetic brine (with a water/rock ratio of 10) and a gas mixture (Figure 4-23) placed in a 500 ml reactor. The gas-water-rock system interacted for defined period within the reactor at a monitored pressure (180 bar) and temperature (70°C), both representative of the Dogger reservoir conditions. The use of a magnetic stirrer, and the circular flow generated in the liquid phase, optimised gas-liquid exchanges and the thermodynamic equilibrium between the resulting solution and the mineral assemblage.

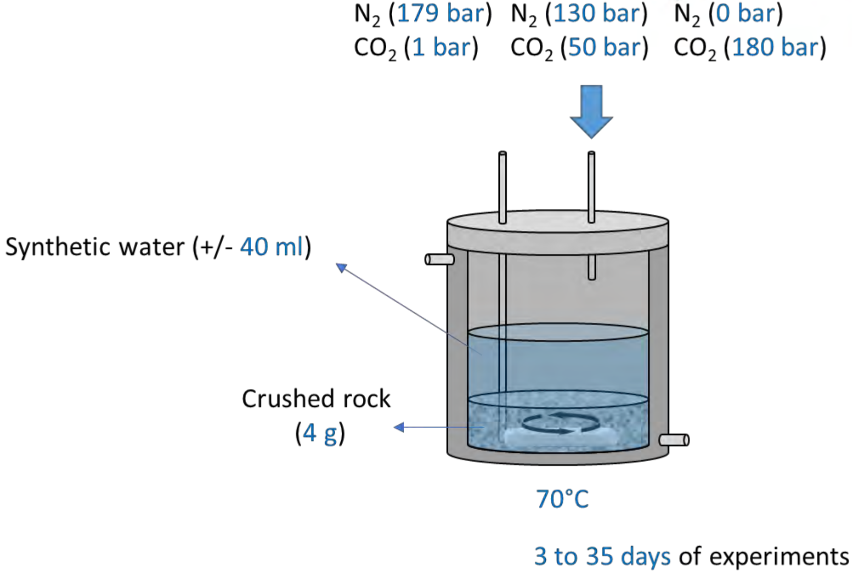

Figure 4-23. Illustration of the batch experiments performed in the BioREP plateform.

Four different types of rock were used during the set of experimental tests designed to assess reactivity within the reservoir and the caprock formations (Figure 4-22). The rock samples (cuttings) were crushed (< 80 µm) with an Agat motor grinder for each formation in order to homogenize the powdered sample and enhance the specific surface area likely to react with the fluid (Figure 4-23).

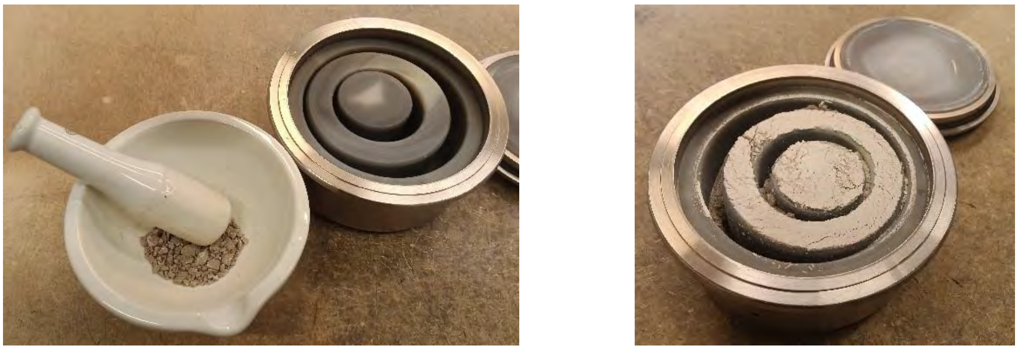

Figure 4-24: rock samples before and after crushing (< 80 µm): rock cuttings (left), powdered sample (right)

Three different CO_2 partial pressures were tested to reproduce (i) the natural conditions within the reservoir (pre-injection; $P_{CO2} = 1$ bar) and to characterize the impact of a CO_2 injection on geochemical processes, including (ii) CO_2 under supercritical state (i.e. $P_{CO2} = 180$ bar) and (iii) dissolved CO_2 (i.e. $P_{CO2} = 50$ bar). Experiments with P_{CO2} at 1 bar and 50 bar were run with the addition of nitrogen gas (an inert gas) at partial pressures of 179 and 130 bar, respectively, to ensure a total pressure of 180 bar in the reactor.

Prior to each experiment, all components of the BioREP platform (e.g. reactors, tubes, valves, pumps) were cleaned, by immersion in nitric acid (10%) for 24 hours, before to be rinsed with ultrapure water (MilliQ water) and dried by injection of nitrogen gas within the experimental setup.

Crushed rock and synthetic brine were placed into a Teflon beaker, inside the reactor. After closure, air was removed from the reactor by gently increasing the N_2 pressure within the experimental setup to achieve an oxygen partial pressure of 0.5 ppm (estimated). CO_2 and potentially N_2 (according to the CO_2 partial pressure) were injected at the target pressure.

The tests were run and stopped definitively after each time step to perform water and rock analysis, as no intermediary samplings were made. This method aimed (i) to keep the same water/rock ratio for all the test, and (ii) to minimise a potential removal of the fine fraction (i.e. clay particles) induced by the water sampling. Each intermediary sampling would have modified the mineral assemblage and geochemical equilibrium. Accordingly, a total of 31 individual experimental runs were performed to study the ongoing geochemical processes in the reservoir formations and the caprock (Table 4.5).

Table 4.5. Summary of the batch experiments performed for the geochemical assessment of the French storage complex

Formation	rock sample	time step	P_{CO2}
Dalle nacrée	VUS 1 - 1854.5 m	7 days	1 bar
Dalle nacrée	VUS 1 - 1854.5 m	20 days	1 bar
Dalle nacrée	VUS 1 - 1854.5 m	3 days	50 bar
Dalle nacrée	VUS 1 - 1854.5 m	7 days	50 bar
Dalle nacrée	VUS 1 - 1854.5 m	3 days	180 bar
Dalle nacrée	VUS 1 - 1854.5 m	7 days	180 bar
Dalle nacrée	VUS 1 - 1854.5 m	20 days	180 bar
Comblanchian	VUS 1 - 1860.45 m	3 days	1 bar
Comblanchian	VUS 1 - 1860.45 m	7 days	1 bar
Comblanchian	VUS 1 - 1860.45 m	20 days	1 bar
Comblanchian	VUS 1 - 1860.45 m	3 days	50 bar
Comblanchian	VUS 1 - 1860.45 m	7 days	50 bar
Comblanchian	VUS 1 - 1860.45 m	3 days	180 bar
Comblanchian	VUS 1 - 1860.45 m	7 days	180 bar
Oolithe Blanche	VUS 1 - 1914.1 m	7 days	1 bar
Oolithe Blanche	VUS 1 - 1914.1 m	20 days	1 bar
Oolithe Blanche	VUS 1 - 1914.1 m	3 days	50 bar
Oolithe Blanche	VUS 1 - 1914.1 m	7 days	50 bar
Oolithe Blanche	VUS 1 - 1914.1 m	20 days	50 bar
Oolithe Blanche	VUS 1 - 1914.1 m	7 days	180 bar
Oolithe Blanche	VUS 1 - 1914.1 m	20 days	180 bar
Oolithe Blanche	VUS 1 - 1914.1 m	35 days	180 bar
Transitional caprock	VUS 1 - 1840 m	3 days	1 bar
Transitional caprock	VUS 1 - 1840 m	7 days	1 bar
Transitional caprock	VUS 1 - 1840 m	20 days	1 bar
Transitional caprock	VUS 1 - 1840 m	3 days	50 bar
Transitional caprock	VUS 1 - 1840 m	7 days	50 bar
Transitional caprock	VUS 1 - 1840 m	20 days	50 bar
Transitional caprock	VUS 1 - 1840 m	7 days	180 bar
Transitional caprock	VUS 1 - 1840 m	20 days	180 bar
Transitional caprock	VUS 1 - 1840 m	35 days	180 bar

At the end of each experiment, water was sampled and the electrical conductivity, pH and Eh values were measured immediately. Water samples were collected, filtered (<0.45 µm) and properly conditioned to ensure the quality of the chemical analyse – i.e. dilution and acidification (for cations only) and storage at 4°C (see section 4.2.2.5). After water sampling, the reactor was depressurized and the solution was filtrated at 0.2 µm to recover the rock particles (fine mineral fraction). The filtration was finalized by adding 5 mL of ethanol (70%) to avoid the precipitation of minerals due to rock drying. Rock samples were stored at ambient temperature until analysed.

4.2.2.5 Rock and water analyses

The mineralogical and geochemical characterisation of the powdered rock samples, both prior and after batch experiments, relied on a combination of several analytical methods, previously presented in section 4.2.1.3, and summarised in Table 4.3. Additionally, the elemental composition of the brine solution (dissolved concentrations) was determined before and after each batch test to monitor the chemical evolution of aqueous phases over the experimental reaction time.

The water sampling was optimised to limited the volume of aqueous solution and the 4 subsamples required to cover all analyses for the geochemical characterisation. pH, Eh and conductivity measurements were determined from a first water subsample. The second subsample was filtrated (<0.45 µm), before storage and acidic titration (ISO 9963 – LQ = 10 mg/L) for quantification of the dissolved inorganic carbon (DIC). The third subsample was filtrated (<0.2 µm) and acidified with HNO_3 (to achieve pH < 2) for the quantification of major elements by ICP-AES (ISO 1185 – OPTIMA 5300 DV - Perkin Elmer), and trace metals by ICP-MS (ISO 17294 – NEXION 350 X - Perkin Elmer). The final subsample resulted from filtration (<0.2 µm) and dilution (c.a. x 10) to prevent precipitation, before analyses of major anions concentrations using ion chromatography (ISO 10304 – Thermo-Dionex ICS3000). All analyses were performed at the BRGM laboratory.

4.2.3 Geochemical reactivity assessment

4.2.3.1 Reservoir

The semi-quantitative evolution of the mineralogy over different reaction time steps for pCO_2 of 1 bar, 50 bar and 180 bar was analysed for the Dalle Nacrée (Figure 4-25), the Comblanchian (Figure 4-26) and the Oolithe Blanche Formations (Figure 4-27).

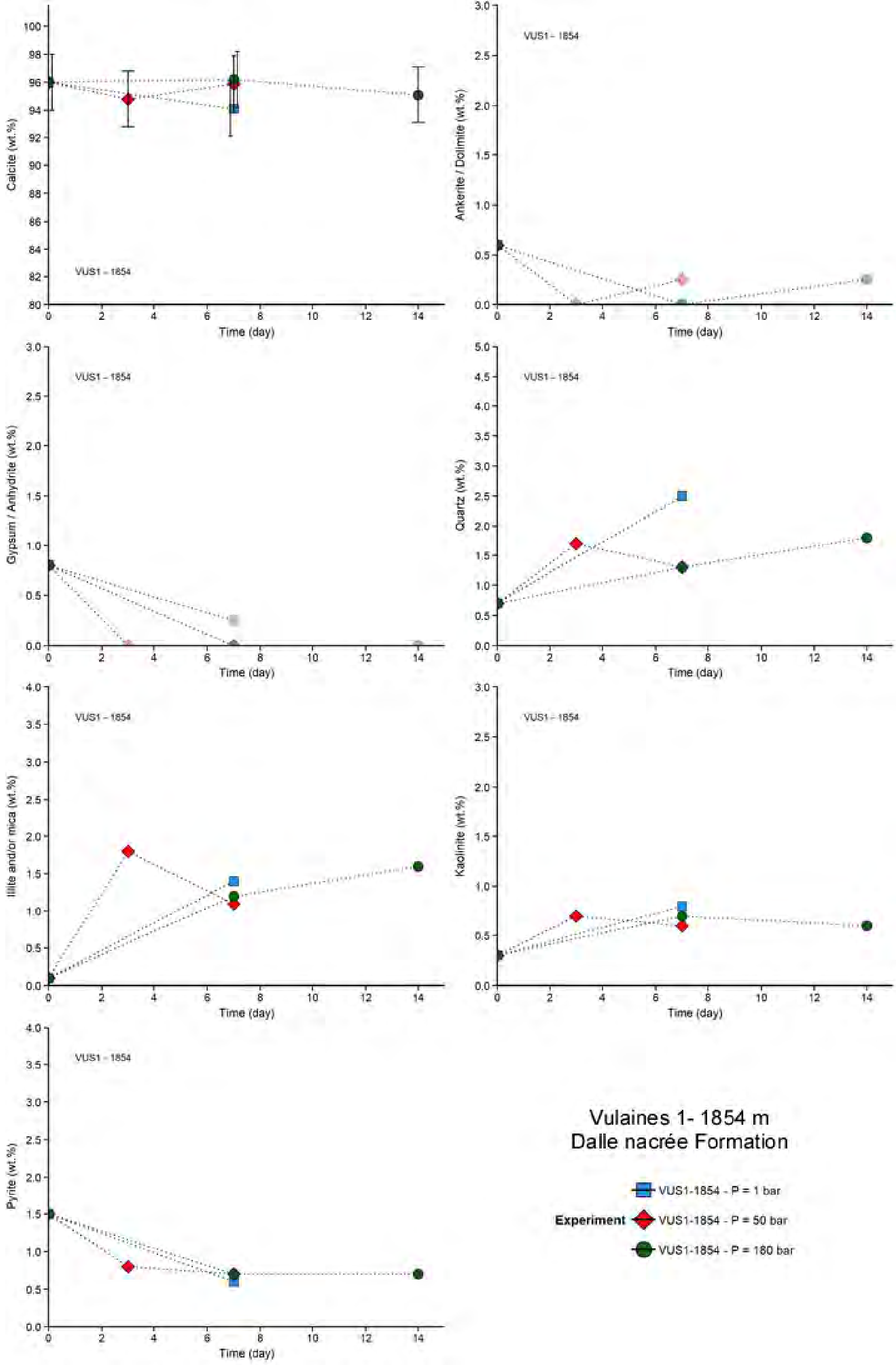

Figure 4-25: XRD-Rietveld results for the whole rock analyses (batch experiment – powdered rock) of the Dalle Nacrée Formation over different time steps of reaction with different CO2 gas partial pressure. Experimental runs occurred at a total pressure of 180 bar and 70 °C. Transparent symbols are mineral phase below the limit of quantification or, when plotted as 0, below the limit of detection in the sample. Analytical uncertainty (+/- 2%).

The PilotSTRATEGY project has received funding from the European Union's Horizon 2020 research and innovation programme under grant agreement No. 101022664

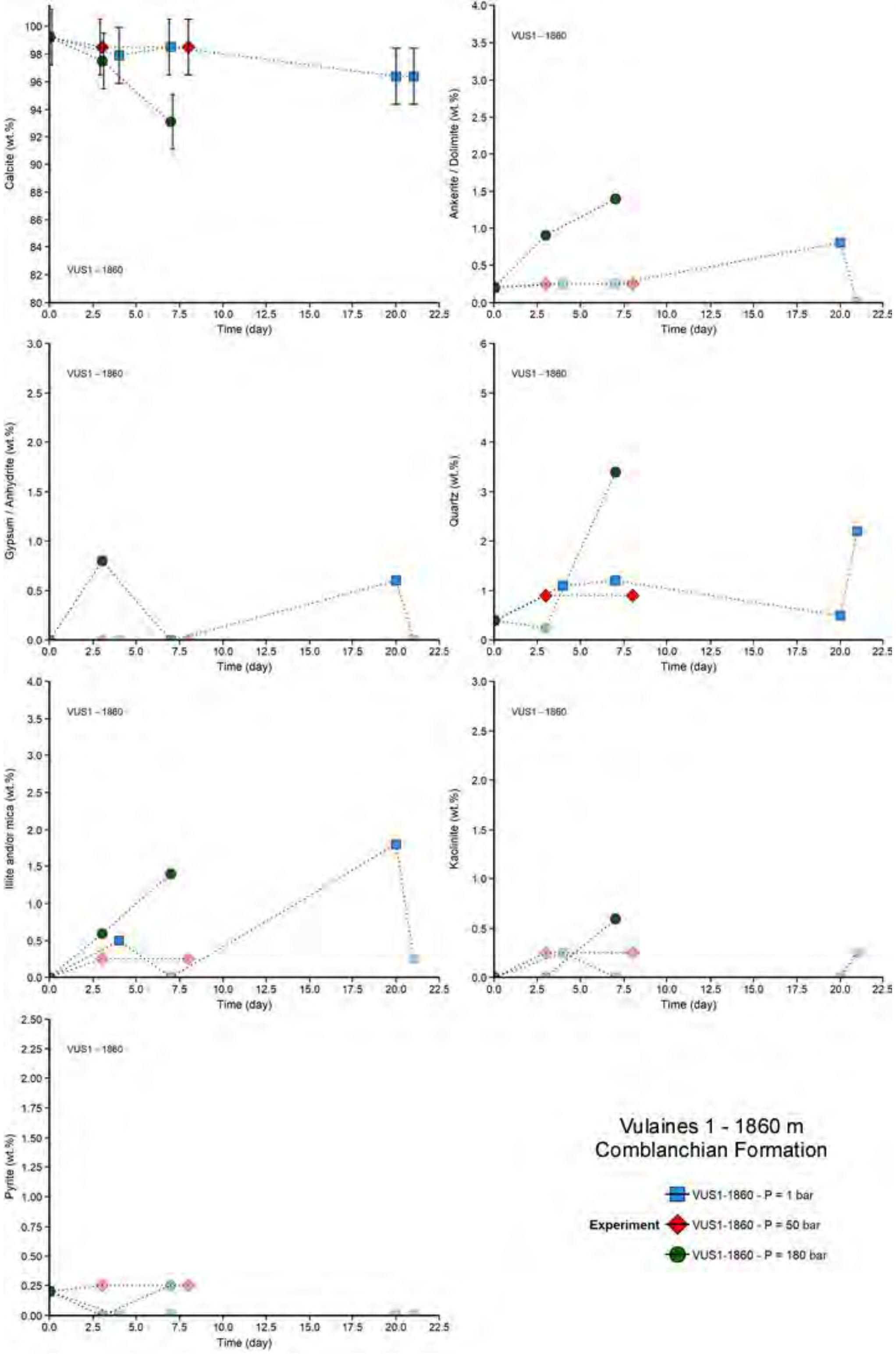

Figure 4-26: XRD-Rietveld results for the whole rock analyses (batch experiment – powdered rock) of the Comblanchian Formation over different time steps of reaction with different CO2 gas partial pressure. Experimental runs occurred at a total pressure of 180 bar and 70 °C. The transparency of the symbols reflects mineral phase below the limit of quantification or, when plotted as 0, below the limit of detection in the sample. Analytical uncertainty (+/- 2%).

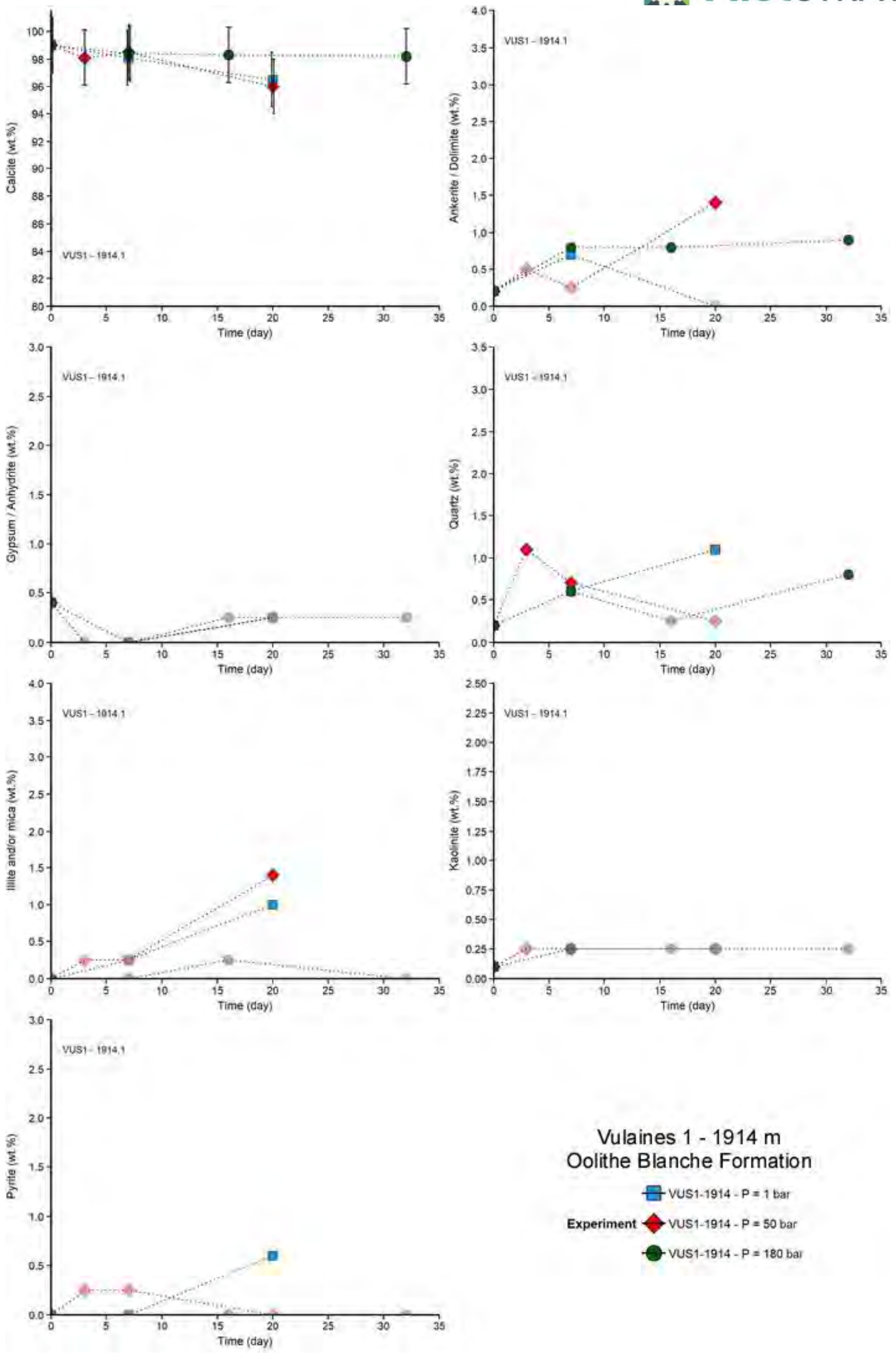

Figure 4-27: XRD-Rietveld results for the whole rock analyses (batch experiment – powdered rock) of the Oolithe Blanche Formation over different time steps of reaction with different CO2 gas partial pressure. Experimental runs occurred at a total pressure of 180 bar and 70 °C. The transparency of the symbols reflects mineral phase below the limit of quantification or, when plotted as 0, below the limit of detection in the sample. Analytical uncertainty (+/- 2%).

The PilotSTRATEGY project has received funding from the European Union's Horizon 2020 research and innovation programme under grant agreement No. 101022664

The whole rock mineralogy of the reservoir consists mainly of carbonate minerals, with a predominance of calcite ($CaCO_3$ > wt.95 %) which is, like any carbonate mineral, is highly sensitive to the concentration of dissolved CO_2. The proportion of calcite tends to decrease over time in the Comblanchian formation at pCO_2 of 1 bar (within the uncertainty range) and 180 bar (significant trend; Figure 4-26) and in the Oolithe Blanche Formation at pCO_2 of 1 and 50 bar (within the uncertainty range; Figure 4-27). These trends emphasis the occurrence of calcite dissolution in the reactor over the experimental time in both the Comblanchian and the Oolithe Blanche Formations (i.e. Bathonian Formations). The variation of pCO_2 in the reactor did not change significantly the calcite proportion over time in the Dalle Nacrée Formation, suggesting too limited dissolution to be detected by XRD-Rietveld analyses (Figure 4-25). The higher proportion of calcite in the Dalle Nacrée Formation (98 wt.%) compare to in the Comblanchian and Oolithe Blanche (96 wt.%) may partly explain the lack of trend, as the results are only semi-quantitative (weight %).

The proportions of most of the minor mineral phases are near or below the limit of quantification or the limit of detection, which prevents a clear evolution over the reaction time. For instance, the evolution of the proportion of gypsum/anhydrite remained unclear in any of the reservoir formations, as initially quantified in the unreacted samples but poorly detected over the experimental time steps. Also observed for the ankerite/dolomite in the Dalle Nacrée Formation (Figure 4-25), this case suggest a potential dissolution of the minerals – i.e. if the mineral composition of the powder sample is fully homogeneous. In the Bathonian Formations (Figure 4-26; Figure 4-27) a slight rise of the ankerite /dolomite proportion was observed over time in the samples mainly for pCO_2 scenarios for which calcite dissolution tended to occur. The increase in ankerite/dolomite must be taken with caution, as it may be induced by the dissolution of dominant calcite mineral phase rather than by precipitation.

For other minor minerals, the proportion of the mineral phase evolved rather similarly in the Comblanchian and the Oolithe Blanche Formations (Figure 4-26; Figure 4-27) – due to overall low proportion – with no clear trend of changes in the proportion of kaolinite, quartz and pyrite minerals over time, but a possible increase of illite and/or mica over the reaction time. Due to slightly lower calcite proportion in the Dalle Nacrée Formation, an overall increase in the proportion of kaolinite, quartz or illite and/or mica minerals could be observed over reaction time, combined to a decrease in pyrite proportion (Figure 4-25). Apart from pyrite, all these phases are silicate or aluminosilicate minerals, which involve slow kinetic rate (e.g. kaolinite) and specific pressure-temperature conditions to precipitate (e.g. quartz). It is therefore likely that the extent of the rise of mineral proportion is more associated to the dissolution of calcite – i.e. decrease of the total mass of calcite in the mineral assemblage – than significant precipitation of quartz or clay minerals over the experimental reaction time in the Dalle Nacrée.

To quantify the reactivity of the reservoir formation and further validate the presumed geochemical reactions of carbonate minerals, the main patterns of the XRD-Rietveld results shall be related to the evolution of the brine composition reacting with the Dalle Nacrée (Figure 4-28), the Comblanchian (Figure 4-29) and the Oolithe Blanche (Figure 4-30) formations at different pCO_2. The saturation index (S.I.) for the mineral phases identified by XRD-Rietveld analyses were calculated, relative to the brine, over the experimental time. S.I. calculation were made with the PhreeqC software, a speciation program, using the Thermoddem database (Blanc et al., 2012; Parkhurst and Appelo, 2013).

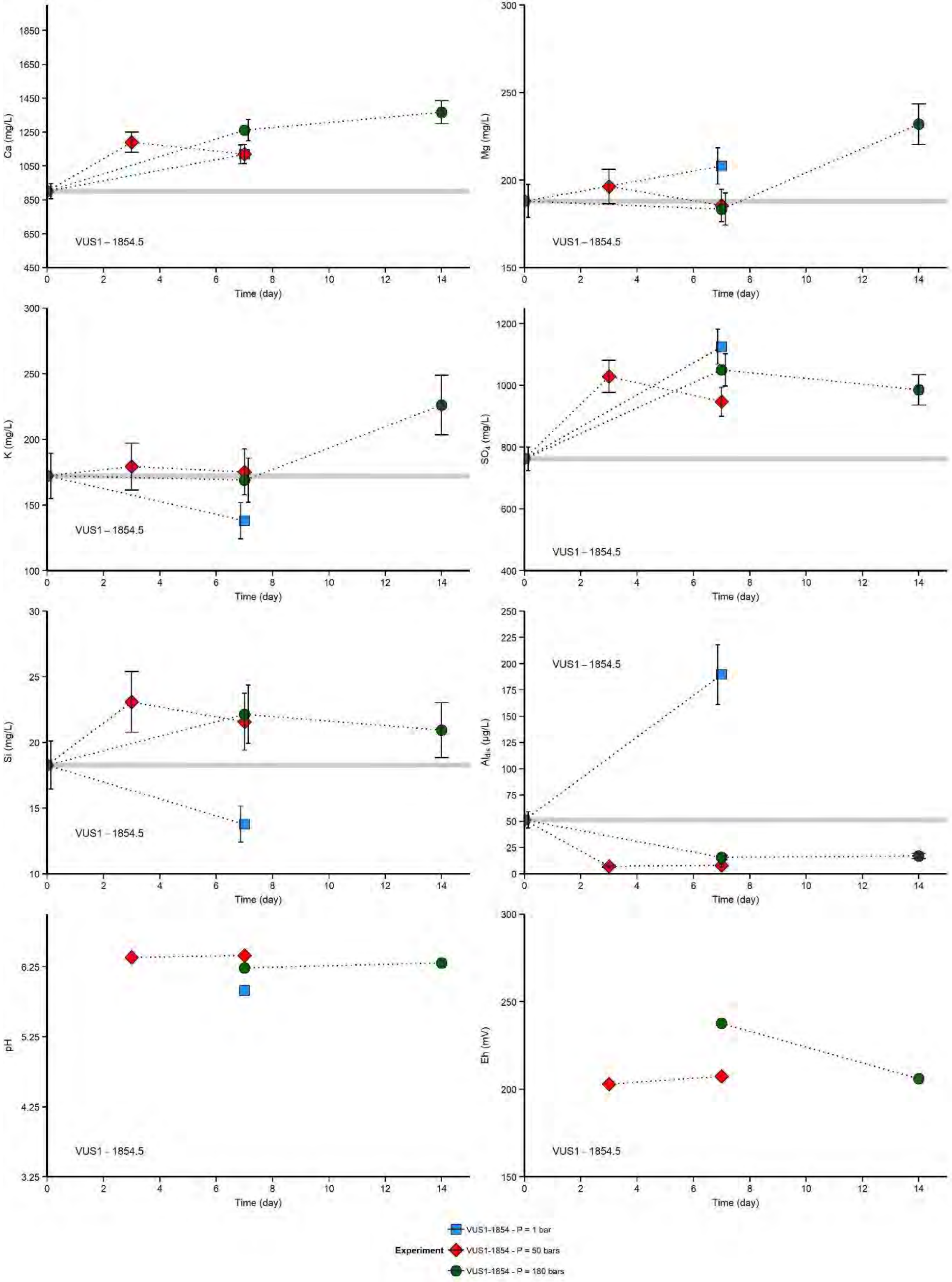

Figure 4-28. Concentration of selected dissolved elements, pH and Eh of the solution in contact with powder samples of the Dalle Nacrée Formation (batch experiment) over different time steps of reaction with different CO2 gas partial pressure. Experimental runs occurred at a total pressure of 180 bar and 70 °C. Only fluid samples with coherent composition are plotted. The grey horizontal bar corresponds to the composition of the synthetic brine.

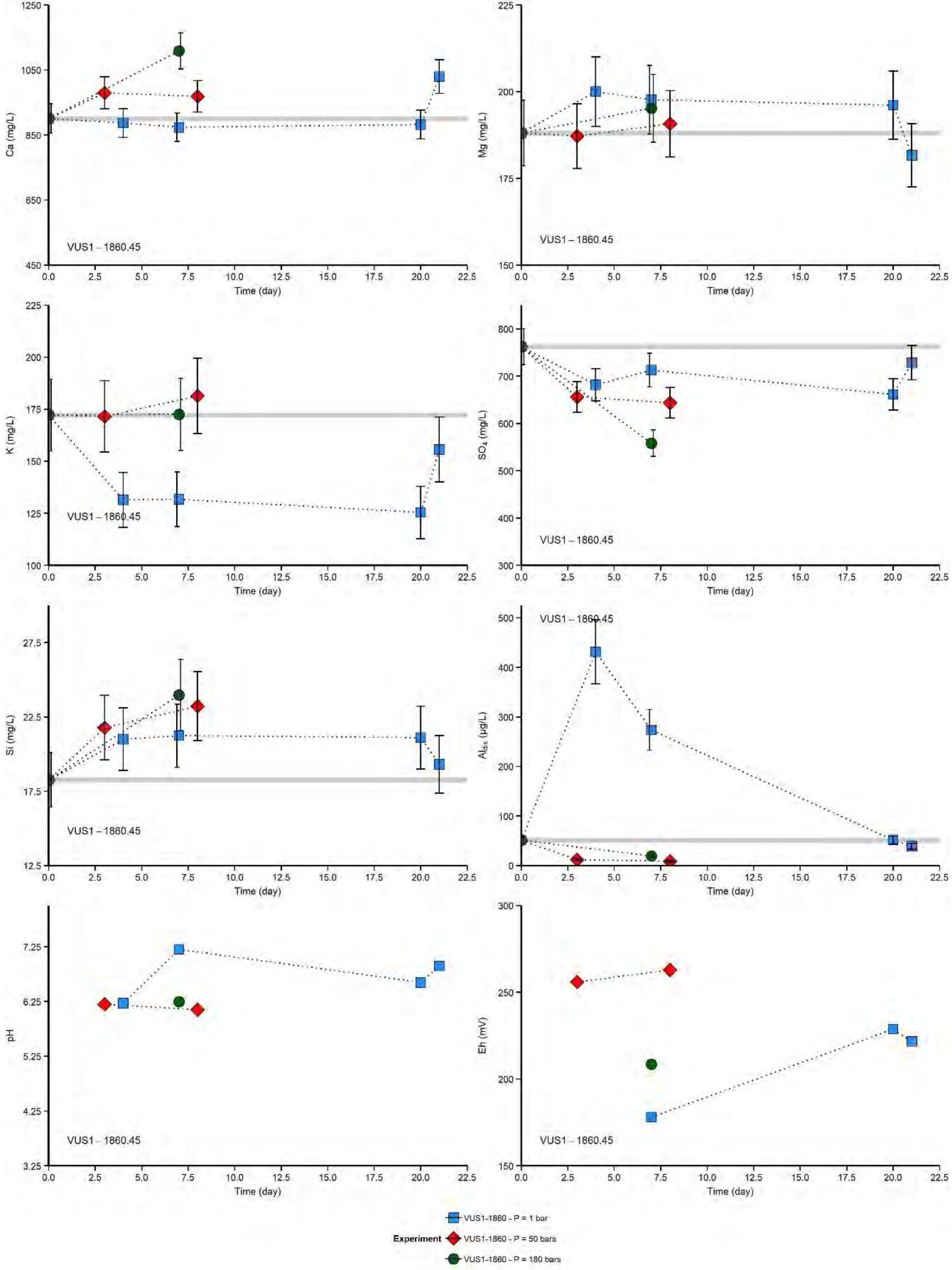

Figure 4-29. Concentration of selected dissolved elements, pH and Eh of the solution in contact with powder samples of the Comblanchian Formation (batch experiment) over different time steps of reaction with different CO2 gas partial pressure. Experimental runs occurred at a total pressure of 180 bar and 70 °C. Only fluid samples with coherent composition are plotted. The grey horizontal bar corresponds to the composition of the synthetic brine.

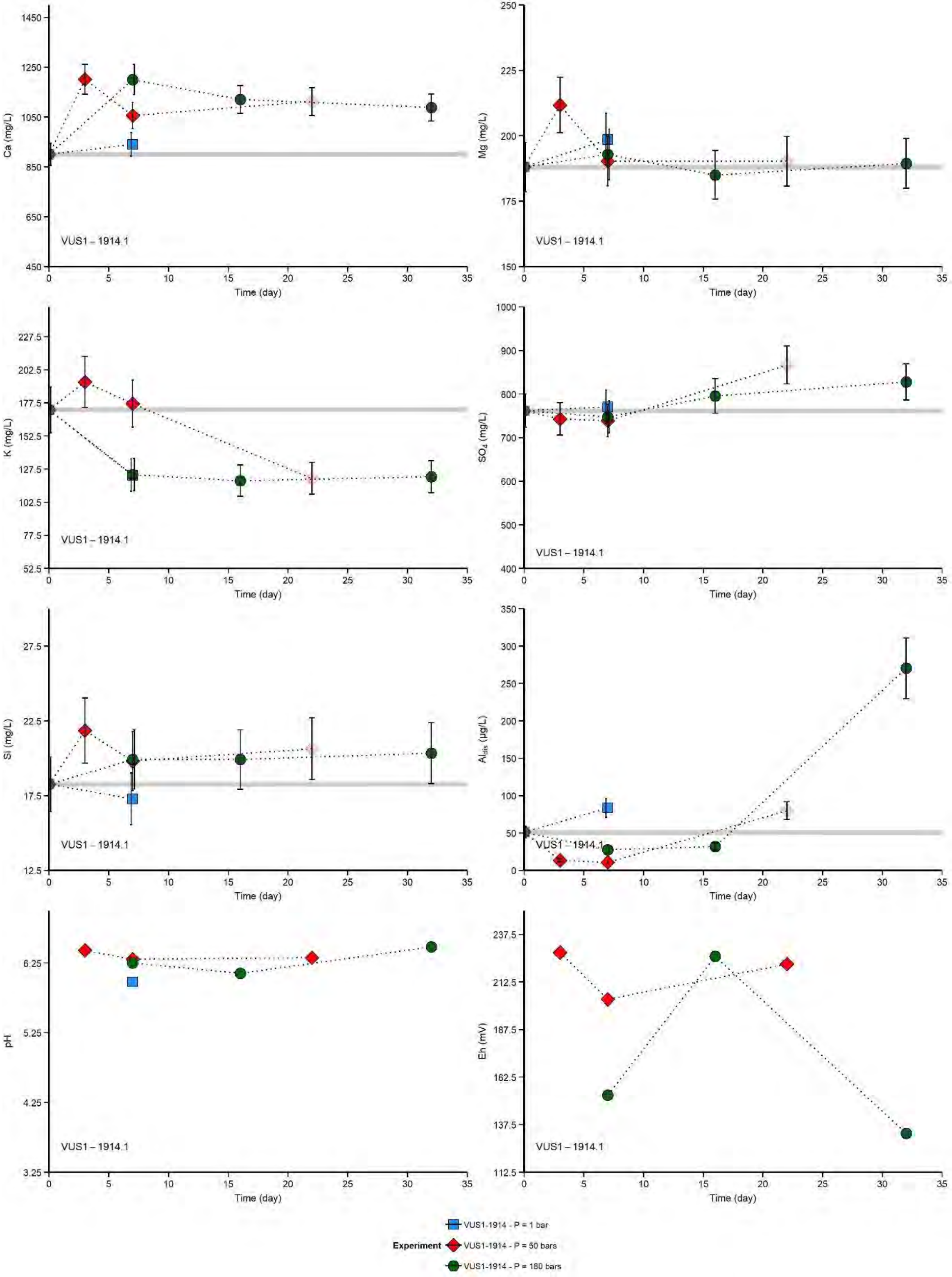

Figure 4-30. Concentration of selected dissolved elements, pH and Eh of the solution in contact with powder samples of the Oolithe Blanche Formation (batch experiment) over different time steps of reaction with different CO2 gas partial pressure. Experimental runs occurred at a total pressure of 180 bar and 70 °C. Only fluid samples with coherent composition are plotted. The grey horizontal bar corresponds to the composition of the synthetic brine.

The progressive dissolution of CO_2 in the aqueous solution led to a decrease in pH, which is partly-to-mostly buffered by the dissolution of carbonates minerals (rapid dissolution) and aluminosilicate (intermediate to slow dissolution). Considering the short-to-intermediate duration of the experimental scenarios (14 to 32 days), carbonate dissolution must be the main buffering reaction in the reservoir (pH = 6.25 for most scenarios).

In the Dalle Nacrée Formation (Figure 4-28), the joint increase of Ca, Mg and SO_4 concentrations in the brine points to dissolution of both ankerite/dolomite (Mg-Ca carbonates) and gypsum/anhydrite ($CaSO_4$), which both contribute to the rise of dissolved Ca. The saturation indices of the aqueous solution with respect to calcite, dolomite and anhydrite suggest an equilibrium of the brine with these mineral phases, regardless of the pCO_2. Dissolution of calcite, gypsum/anhydrite and dolomite occurred until equilibrium was reached with the aqueous solution. Potential re-precipitation of calcite or any other secondary Ca-carbonate mineral remain challenging to determine as the evolution of dissolved Ca concentration is driven by several mineral phase. Although the limited number of samples prevents the drawing of firm conclusions, the increase of Mg and SO_4 concentration in the aqueous solution appears to be less significant for pCO_2 at 50 bar and 180 bar than for pCO_2 at 1 bar. This pattern suggests that possible minor re-precipitation of anhydrite and ankerite/dolomite may occur over the experimental period.

In the Comblanchian Formation (Figure 4-29), the evolution of Ca, Mg and SO_4 concentrations was (i) highly sensitive to the pCO_2 and (ii) highly variable depending on the element. For all pCO_2 scenario cases, the Mg concentration slightly increased, whereas the SO_4 concentrations decreased over time. The saturation indices of calcite, dolomite, ankerite and anhydrite relative to the brine all indicate the attainment of thermodynamic equilibrium over the reaction period. Dissolution of ankerite /dolomite and calcite to various extents – depending on pCO_2 – tend to release Ca in solution, which promotes precipitation of anhydrite. The source of Ca in the brine seems to derive from the dissolution of ankerite / dolomite in the scenario case with pCO_2 at 1 bar. Calcite dissolution may drive the dissolved Ca concentrations at higher pCO_2 (50, 180 bar), for which the rise of Mg concentration remained more moderate.

In the Oolithe Blanche Formation (Figure 4-30), the trend of Ca concentration was fairly similar to those observed in the Comblanchian Formation, with a significant concentration rise (i.e. with respect to the analytical uncertainty) for pCO_2 at 50 and 180 bar. The Mg concentrations tended to rise rapidly for pCO_2 at 50 bar, more moderately for pCO_2 at 1 bar and remained fairly stable before decreasing for pCO_2 at 180 bar. Throughout the reaction time the aqueous solution was at or near equilibrium with respect to calcite, ankerite and dolomite, suggesting moderate-to-rapid calcite and ankerite/dolomite dissolution with pCO_2 at 1 and 50 bar. The SO_4 concentration tended to remain stable (within the analytical uncertainty) over the first 10 days before increasing over time for pCO_2 at 50 and 180 bar. With a saturation index near equilibrium, anhydrite may have precipitated until reaching equilibrium over the first 10 days. Minor calcite or dolomite re-precipitation may involve partial (re-)dissolution of anhydrite, which drove the rise of SO_4 concentration. The influence of the calcite dissolution and (ankerite/dolomite) on a potential re-dissolution of gypsum/anhydrite remains to confirm (e.g. with geochemical modelling), although the reactional process might be rather limited.

With respect to silicate (quartz) and aluminosilicate minerals (kaolinite and illite and/or mica), the brine interacting with samples from the Dalle Nacrée (Figure 4-28) for pCO_2 at 50 bar and 180 bar displayed rather stable K concentrations, an increase in Si concentration and a decrease in Al concentration over the reaction time. With respect to saturation indices, the aqueous solution was supersaturated with respect to kaolinite and illite and at equilibrium with respect to quartz. Accordingly, the addition of CO_2 (pCO_2: 50 & 180 bar) and the resulting acidification of the aqueous solution caused the dissolution of silicate minerals until equilibrium was reached by the solution with respect to quartz, and the possible precipitation of aluminosilicate minerals (e.g. illite, mica and/or partially kaolinite).

The patterns of the K, Si and Al concentrations in the brine reacting with the Comblanchian Formation (Figure 4-29) were similar to those observed in the Dalle Nacrée. These patterns suggest similar reaction processes involving quartz dissolution and the possible precipitation of minor aluminosilicate minerals.

In the brine reacting with the Oolithe Blanche Formation, the evolution of the Al concentrations differed slightly from the other reservoir formations for pCO_2 at 50 and 180 bar, with first a progressive decrease followed by a slow increase of the concentration (Figure 4-30). Such a pattern, identified at a longer reaction time than in the experiment with the samples from the Dalle Nacrée and the Comblanchian Formation, involves co-reactions of aluminosilicate minerals. As the brine is supersaturated with respect to both kaolinite and illite and/or mica throughout the experimental period, the precipitation of at least one of these minerals contributes to the early decrease of dissolved Al concentration. However, the dissolving aluminosilicate mineral contributing to the rise of the Al concentration remains unidentified. The trend of the Si concentration was similar to those observed with the Dalle Nacrée and the Comblanchian Formation. The aqueous solution being in equilibrium with respect to quartz, the latter trend certainly results from quartz dissolution.

In general terms, the experimental batch results enable the identification of a number of potential geochemical reactions when CO_2 is injected in the reservoir, either as supercritical or dissolved phase. Similar changes are observed in the three formations in the Dogger reservoir. Dissolution of calcite, ankerite/dolomite and quartz and precipitation of aluminosilicate, such as kaolinite and/or illite, are the main reactive process to consider for the assessment of the reactivity in the Dogger reservoir. However, the reactivity of the sulphate minerals (gypsum/anhydrite) appeared to follow an opposite pattern in the Dalle Nacrée Formation (dissolution), compared to the Comblanchian and Oolithe Blanche Formation (precipitation). Moreover, potentially more complex fluid-rock interaction involving aluminosilicate minerals might occur in the Oolithe Blanche Formation.

Thermodynamic equilibrium of the brine appears to constrain the nature of the mineral phases initially present in the reservoir. In other words, the partial dissolution of carbonate mineral – minerals particularly prone to dissolution under CO_2 conditions – drive the (re-)precipitation of carbonates and/or sulphate minerals already occurring in the pristine reservoir formations. Any additional mineral(s) (if any) may remain as (very) minor phase(s), as none was identified neither by XRD-Rietveld nor by SEM-EDS analyses over the simulated experimental reaction time. Ca concentrations are most notably elevated above the levels in the initial synthetic brine, suggesting that the carbonate minerals (mostly calcite, ankerite, dolomite) account, by far, the largest part of system's reactivity after the addition of CO_2 in the native underground environment. An assessment of the impact of the dissolution level is further clarified with a reactive flow-through experiment presented in section **Erreur ! Source du renvoi introuvable.**.

4.2.3.2 Caprock

The Callovian mudstone, also regarded as the transitional caprock, varies substantially from the reservoir formations in term of mineral composition, due not only to a larger number of mineral phases but also to a significantly lower proportion of calcite and higher proportion of quartz and clay minerals (Figure 4-31). Because only a limited amount of cuttings were available (these are rock powder and chips from drilling), the set of batch experiments required the use of different transitional caprock samples – i.e. from depth 1840 and 1842 m – to cover the entire set of scenario cases considered for the geochemical assessment.

Because of the mineralogical variability within the transitional caprock (Figure 4-18), the results of the batch experiment on the transitional caprock can display a large discrepancy in the proportion of the mineral phases from a sample to another, between the cuttings from different core section/depth and possibly within the powder material of a single sample. The former case is illustrated in the XRD-Rietveld of the batch experiments applied for pCO_2 at 180 bar, for which both samples VUS 1 – 1840 m and VUS 1 – 1842 m were used. For instance, the proportion of illite and/or mica was originally different within the two samples, which influenced the resulting trend of reaction after exposure to pCO_2 at 180 bar (Figure 4-31). The latter case concerns mostly minerals found in low proportions (e.g. pyrite or plagioclase) – which disrupts any trends within the results – and minerals with either low-reactivity or slow kinetics (e.g. quartz). A further complication is that substantial dissolution of any minerals results in an increase in the proportion of the other minerals, if no another additional mineral phase precipitates. The impact of this third phenomena remains difficult to assess, especially when the most reactive minerals occur in intermediate-to-low proportions (weight %) of the total assemblage.

Taking all these aspects into account, only the main, most reliable patterns can be considered in an attempt to establish the dominant geochemical processes. Focusing on trends after the start of exposure of the water-rock phases to the gas phase, many minerals remained stable in terms of proportion (weight %). Regardless of the pCO_2 conditions, smectite/mixed clays, ankerite/dolomite, K feldspar and anatase reached rather stable proportions through the experimental time, suggesting either thermodynamical equilibrium between the aqueous solution and the mineral assemblage, or low-reactivity (precipitation occurring only under high pressure and temperature conditions) or slow-kinetics of these minerals. Thermodynamical equilibrium might be reached after partial dissolution (smectite) or precipitation (ankerite) of the mineral phase following water-rock interaction at an early stage of the experiment. The measured proportions of anatase are all within experimental error of each other, making the detection of any reaction impossible.

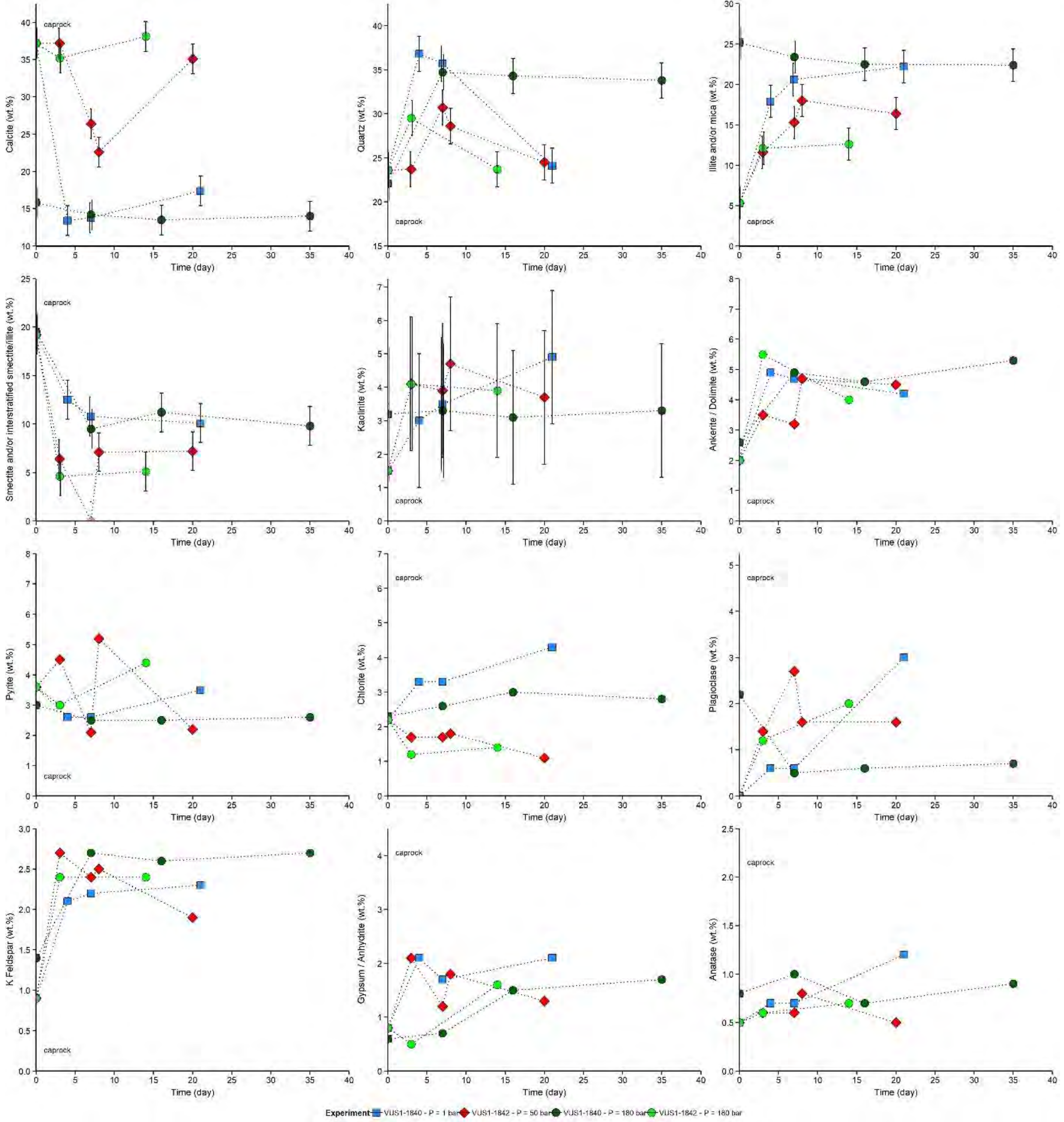

Figure 4-31: XRD-Rietveld results for the whole rock analyses (batch experiment – powdered rock) of the Callovian mudstone (transitional caprock) over different time steps of reaction with different CO2 gas partial pressure. Experimental runs occurred at a total pressure of 180 bar and 70 °C. Transparent symbols are mineral phase below the limit of quantification or the limit of detection in the sample. Analytical uncertainty (+/- 2%).

A number of minerals appeared to be more sensitive to the applied pCO_2 conditions. Gypsum / anhydrite shows more rapid dissolution for pCO_2 at 1 bar (reservoir conditions) and 50 bar (CO_2 dissolved) than at 180 bar (supercritical CO_2), whereas kaolinite reached stable proportion (thermodynamical equilibrium) faster for pCO_2 at 50 and 180 bars than at 1 bar. Although the trend is not totally straightforward, calcite dissolution and illite precipitation were more rapid for pCO_2 at 1 bar and 50 bar. Comparatively the calcite and illite proportion remained relatively stable for pCO_2 at

180 bar. The chlorite proportion stayed among the most stable minerals within the mineral assemblage. Although the variation remained within the analytical uncertainty, minor precipitation of chlorite might occur for pCO_2 at 1bar, whereas dissolution is suggested for pCO_2 at 50 bar. The trends for plagioclase and Quartz remained unclear.

The number of mineral phases in the transitional caprock assemblage is far larger than in the reservoir rock (Figure 4-31). Understanding the evolution of synthetic brine composition over reaction time is therefore far more complex (Figure 4-32), as an individual ion is generally carried by several different mineral phases. The evolution of the aqueous solutions are therefore discussed together with the results of the XRD-Rietveld and the calculation of the saturation index made by using PhreeqC software with the Thermoddem database (Blanc et al., 2012; Parkhurst and Appelo, 2013).

For carbonate minerals (calcite, ankerite/dolomite), the XRD-Rietveld results suggest partial calcite dissolution and partial ankerite and/or dolomite precipitation before stabilization (Figure 4-31). However, Mg enrichment of the water revealed the likely dissolution of ankerite/dolomite before reaching stable concentrations (Figure 4-32). Calculation of water saturation indices confirms thermodynamic equilibrium with calcite for all experimental pCO_2 conditions, and with dolomite only for pCO_2 conditions at 1 and 50 bar. For a pCO_2 of 180 bar, the aqueous solution remained supersaturated with respect to dolomite, potentially due to ankerite precipitation. This hypothesis cannot be verified by calculating saturation indices, as dissolved Fe concentrations were below the limit of quantification. The downward trend in Ca and Mg concentrations over the reaction time in the 180-bar experiment, associated with a drop in Eh favorable to the presence of Fe in reduced form (Fe^{2+}), suggest favorable conditions for thermodynamical equilibrium of the aqueous solution with respect to ankerite (Figure 4-32). The Ca concentration of the aqueous solution illustrates a more significant calcite dissolution for pCO_2 at 1 bar (natural condition).

Gypsum / anhydrite are the main sulfate minerals identified in the transitional caprock. The XRD-Rietveld results suggest partial dissolution of these minerals, faster for pCO_2 at 1 and 50 bar than for pCO_2 at 180 bar (Figure 4-31). The concentrations of SO_4 in the aqueous phase further confirm the trends identified by XRD-Rietveld analyses, at an early stage of the experimental period (Figure 4-32). However, SO_4 concentration drop over the experimental period for pCO_2 at 1 and 50 bar. This evolution might be related to a partial re-precipitation of anhydrite, as the aqueous solutions are in equilibrium with respect to both gypsum and anhydrite over the entire experimental period. The extent of the gypsum dissolution seems more extensive for pCO_2 at 50 bars (higher rise in SO_4 concentration; Figure 4-32), conditions simulating significant enrichment of dissolved CO_2 in the aqueous solutions.

There are many silicate and aluminosilicate minerals in the transitional caprock, also meaning that the evolution of the Si and Al concentrations in the brine depends on the reactivity of these minerals.

Plagioclase, for which XRD-Rietveld result were unclear, are the main sodium-aluminosilicate mineral. The Na concentration in the aqueous phase were relatively stable over the experimental time, with minor deviation from the pristine composition within the analytical uncertainty range (Figure 4-32). The brine was in equilibrium with respect to albite (plagioclase) over the entire experimental time for pCO_2 at 50 bars and at or near equilibrium for pCO_2 at 1 and 180 bar. These results suggest that plagioclase regulates the aluminium and silicon concentrations of the brine. The relatively stable sodium concentration of the brine suggests only minor dissolution of plagioclase compared to the initial sodium content of the brine., i.e. too low to confidently quantify

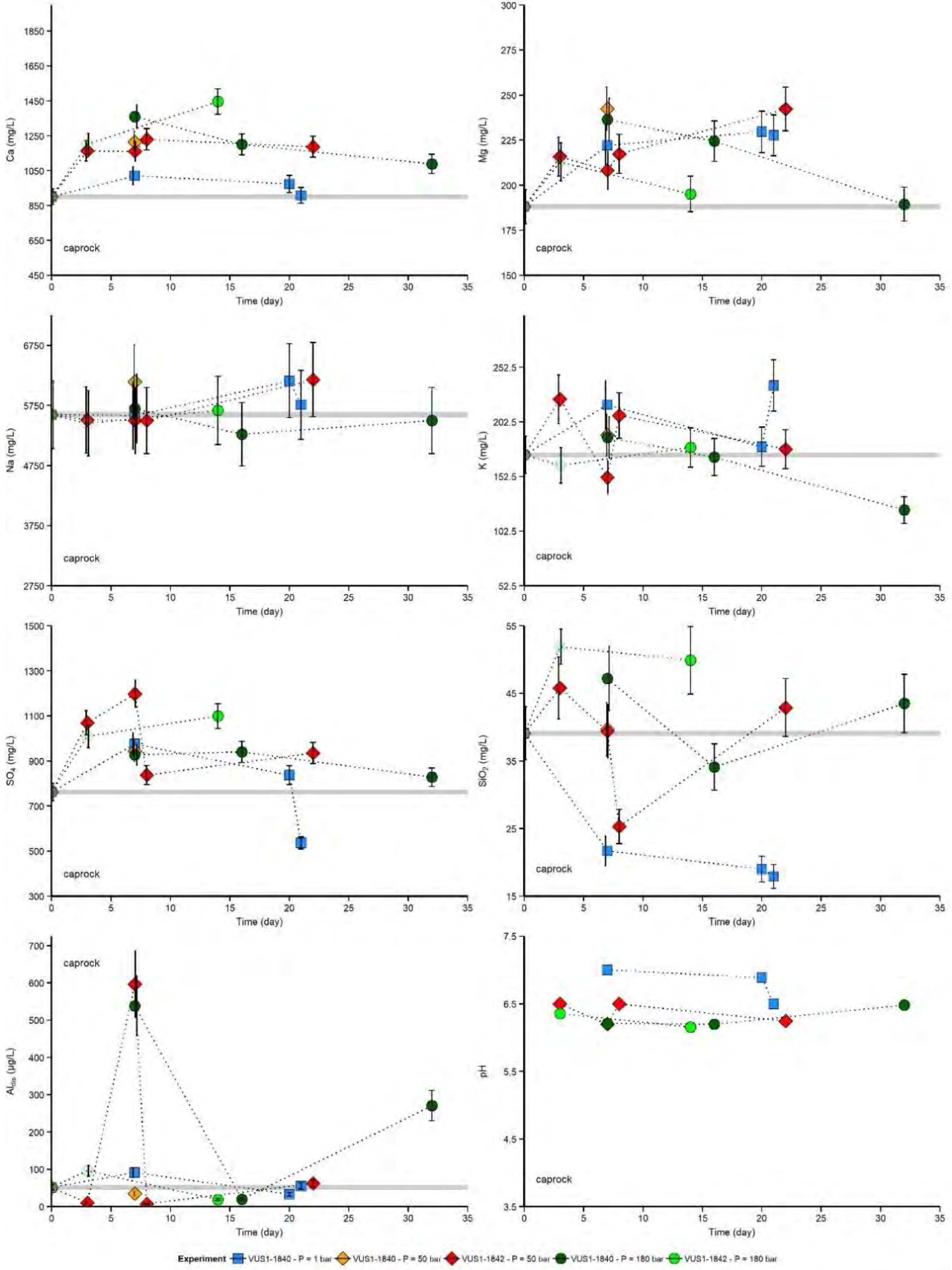

Figure 4-32. Concentration of selected dissolved elements, pH and Eh of the solution in contact with powder samples of the Callovian mudstone (transitional caprock) in batch experiments over different time steps of reaction with different CO2 gas partial pressure. Experimental runs occurred at a total pressure of 180 bar and 70 °C. Only fluid samples with coherent composition are plotted. The grey horizontal bar corresponds to the composition of the synthetic brine.

Potassium aluminosilicate minerals, i.e. K-feldspar and illite and/or mica, were expected to precipitate at an early stage of the experiment before reaching equilibrium according to the XRD-Rietveld results (Figure 4-31). However, the light rise of K concentration in the aqueous phase tends not to support this interpretation for pCO_2 at 1 and 50 bar (Figure 4-32). Based on calculated saturation indices, the aqueous solution is supersaturated with respect to microcline (K-feldspar), illite and muscovite (mica) for the experimental period of 20 days apart at early stage of the experiment (< 3 days), which excludes dissolution of any of these potassium aluminosilicate minerals. The source of the K enrichment in the aqueous solution remains unclear, which prevents an assessment of the reactivity of potassium aluminosilicate minerals by the batch experiments.

Among the other aluminosilicate minerals (mainly clay mineral), the aqueous solutions are supersaturated with respect to clinochlore (chlorite) and kaolinite, but reach equilibrium or near equilibrium with respect to montmorillonite – mainly for Mg-montmorillonite – independently of the pCO_2 conditions. The saturation indices suggest potential slow precipitation of chlorite and kaolinite mineral, likely driven by the potential slow dissolution of Mg rich montmorillonite, in line with the XRD-Rietveld results (Figure 4-31). The XRD-Rietveld results tend to also suggest a more extended dissolution of smectite and/or interstratified smectite/illite with conditions representative of pCO_2 at 50 and 180 bar.

Quartz dissolution may also occur as the aqueous solutions are at equilibrium with this mineral.

Taken together, these results define the main reactions involving the phases in the transitional caprock. Dissolution of calcite, gypsum and interstratified clays (likely Mg-rich montmorillonite) is enhanced with pCO_2 that are characteristic of CO_2 injection and storage (50 bars and 180 bars). Although difficult to quantify, dissolution of plagioclase and quartz attain thermodynamic equilibrium. The dissolution of other phases causes the precipitation of dolomite. The role of ankerite under conditions of pCO_2 at 180 bar remains unclear, as there are several Fe^{2+}-bearing minerals in the mineral assemblage. The precipitation of chlorite, kaolinite and/or illite are expected although the involvement of each of these aluminosilicate minerals could not be confirmed over the period simulated in the batch experiments. The decrease of SiO_2 concentration in the aqueous phase, only for pCO_2 at 1 bar, suggests higher precipitation of clay minerals with higher pCO_2 conditions (Figure 4-32).

These trends should be considered as first-order conceptual models for assessing geochemical reactions and understanding more generally the geochemical reactivity involved in the caprock. The conceptual model remains to be validated or adjusted by the geochemical modeling exercise aiming to numerically simulate the experimental results within the framework of the project.

5. Flow-through experiments

5.1 Introduction

Flow-through experiments were carried out on a number of core plugs representative of the reservoir and caprock of interest (i.e. drilled on deep cores or analogous outcrop rock). Applied to all sites, these tests were designed: (i) to test the gas and water relative permeability of the material during CO_2/water flow, and (ii) characterize the rock reactivity in contact with supercritical CO_2 and/or CO_2-enriched fluid.

5.2 Experiments on Material from France

5.2.1 Introduction

Percolation experiments were conducted to study geochemical processes under the dynamic conditions prevailing during CO_2 injection into the rock reservoir. Experiments were performed on rock samples from both the reservoir (Oolithe Blanche Formation) and the caprock. Two kinds of experiments were applied on rock samples from the French site:

- Cyclic Flow Tests: these tests, performed by UEDIN, were specifically designed to determine the relative permeability of water and supercritical CO_2 in the reservoir, and, to some extent, characterise rock reactivity in supercritical conditions. These tests can be considered representative of the environmental conditions that would occur near the well.

- Percolation of a CO_2-enriched brine tests: these tests, performed by BRGM, simulate a continuous flow of brine equilibrated with CO_2 percolating through the reservoir rock and the caprock. These tests are representative of conditions prevailing at the outer edge of the CO_2 plume, far from the injection well, where part of the injected supercritical CO_2 has already dissolved in the in-situ brine.

5.2.2 Rock sample selection and preparation

For the Paris Basin, four rock samples from the SEIF 1 core were used for the flow-through experiments. The selection of the core plugs was based on the reservoir knowledge and preliminary results of the batch experiments (*Table 5.1*). Detailed descriptions of the SEIF-1 cores – used for flow-through experiment –, and comparison with the samples from Vulaines-1 – used for batch experiment – are available in section 4.2.1.4 for the reservoir samples and in section 4.2.1.5 for the caprock sample.

Table 5.1. Rock core samples from the French site used for the flow-through experiments.

Rock type	Sample name	Depth (m)	Facies	Flow-through experiment
Caprock	SEIF 1 - 1841	1841.7		Geochemical reactivity assessment – *BRGM laboratory*
Reservoir	SEIF 1 - 1927	1927.62	Grainstone with ooids	Cyclic flow test – *UEDIN laboratory*
	SEIF 1 - 1952	1952	Packstone/Grainstone with oncoids and ooids	Cyclic flow test – *UEDIN laboratory*
	SEIF 1 - 1969	1969.03	Grainstone oolithic	Geochemical reactivity assessment – *BRGM laboratory*
		1969.1		Cyclic flow test – *UEDIN laboratory*

The permeability measurements, required for the final sample selection for the cyclic flow tests, focused mainly on the Oolithe Blanche Formation for the reservoir (SEIF 1 – 1927, SEIF 1 – 1952, and SEIF 1 – 1969). The geochemical reactivity assessment considered the caprock (SEIF 1 – 1841) and the most permeable selected core plug from the reservoir (SEIF 1 – 1969). The SEIF 1 – 1969 rock sample was taken in duplicate to perform both experiments. All core plugs were drilled perpendicular to the length of the SEIF 1 core (*Figure 5-1*). The resulting core plugs were trimmed to obtain parallel ends. The offcuts of the core plugs were used for rock analysis (see section 4.2.1.4).

Figure 5-1: Transverse drilling of the SEIF-1 core in the representative core section of the Oolithe Blanche Formation

5.2.3 Cyclic Flow Test

5.2.3.1 Cyclic flow methodology

To measure relative permeability, i.e. to assess the flow behaviour of supercritical CO_2 and brine during cyclic injection and withdrawal, an integrated experimental approach was adopted. This approach characterized the flow behaviour based on initial and residual fluid saturations, along with the relative permeability endpoints for each cycle. The following procedure was implemented to conduct the flow tests:

- The core samples were cleaned through cyclic injection of solvents after being loaded into the core holder. This process was continued until the differential pressure across the core sample stabilized and the effluent became transparent.

- The core samples were then dried at a temperature of 80°C in an air oven.
- Subsequently, the core was loaded into the core holder, wrapped in PTFE and aluminium foil and placed in a Viton jacket, with steel end-caps, to prevent any leakage of CO_2 into the overburden fluids, as minor leakages could introduce significant experimental artefacts.
- The porosity and permeability of each core sample were measured using the corresponding brine sample. The core was then flooded for at least one week at various injection rates to establish ionic equilibrium between the minerals and the brine ions.
- The first gas cycle was conducted on a vertically mounted core sample, injecting from top to bottom to minimize gravity instabilities. Both differential pressure across the core sample and the saturation profile were continuously and rigorously monitored to identify the onset of steady-state conditions. Following this, bump flooding was applied to overcome capillary end-effects and accurately determine residual saturation, continuing until no change in residual water saturation and differential pressure was observed.
- Water was subsequently injected from bottom to top to ensure gravitationally stable flooding, maintaining the same injection rate as the initial rate of the previous gas cycle. This cycle was sustained until steady-state conditions were reached.
- The test continued with cyclic injections of both gas and water for three additional cycles, following the procedure outlined above for each cycle.

Brine was pre-equilibrated with CO_2 before the start of the test to prevent any mass transfer during the experiment.

To assess the geochemical reactions during the cyclic flow experiments, effluent samples were taken at each cycle. The samples were collected once steady-state conditions were achieved, characterized by a constant differential pressure and saturation profile. The samples were then analysed using ICP-OES to track changes resulting from flow through the porous media. Samples were collected in glass vials and stored at room temperature prior to analysis. The porosity and permeability of the core samples were measured before and after the cyclic flow, based on the premise that geochemical reactions would cause variations in these properties.

Figure 5-2 illustrates the experimental setup, featuring an array of dual pump systems connected to high-pressure fluid transfer vessels, as well as overburden (OB) and back pressure regulators (BPR). These components are critical for injecting fluids into the core sample and precisely controlling the pressures of the OB and BPR. The fluids exiting the system are then routed through a BPR, where their pressure is reduced to atmospheric levels, and collected in a graduated cylinder for subsequent separation. The collected samples were further analysed using Inductively Coupled Plasma Mass Spectrometry (ICP-MS). An air fan oven was utilized to maintain a constant temperature throughout the system and during the experiments.

It is also important to note that the core was positioned vertically to mitigate any gravitational effects, such as overriding or underriding that could impact the results. Additionally, the overburden pressure was maintained at 500 psi above the pore pressure.

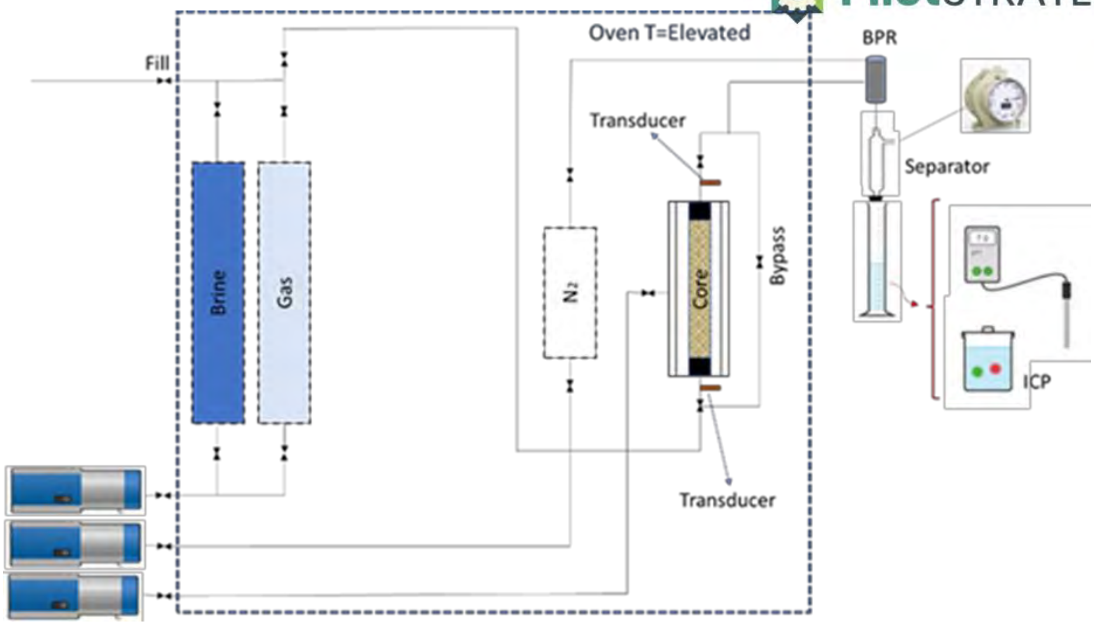

Figure 5-2: Schematic diagram of the core flooding system utilized for conducting the cyclic flow tests, with the core holder mounted vertically throughout all tests to ensure gravitationally stable displacement.

Research-grade carbon dioxide (CO_2) gas with a high purity of 99.9995 vol% was used, along with sodium chloride (NaCl), calcium chloride hexahydrate ($CaCl_2 \cdot 6H_2O$), magnesium chloride hexahydrate ($MgCl_2 \cdot 6H_2O$), potassium chloride (KCl), and sodium sulfate (Na_2SO_4), each with a verified purity of 99.5%. Deionized water required for the experiments was obtained using an ELGA DV 25 water purification system.

5.2.3.2 Cyclic Flow Results

BRGM provided three different core samples to UEDIN (*Table 5.1),* after which the rock characterization process, including porosity and permeability measurements as well as heterogeneity analysis using tracer tests, was conducted on these samples. Based on the technical discussions, tests were conducted on samples SEIF 1 – 1927, SEIF 1 – 1952, and SEIF 1 – 1969, the dimensions of which are shown in Table 5.*2*. Fluid samples were collected from the runs using Samples SEIF 1 – 1927 and SEIF 1 - 1969 in order to characterise any geochemical changes. It is believed that the core jacket used for sample SEIF 1 – 1927 punctured during testing, such that the test was abandoned after obtaining initial permeability and porosity data.

Table 5.2. Dimension of the core samples from the French site.

Sample Number	D (cm)	L (cm)
SEIF 1 - 1927	4.905	3.79
SEIF 1 - 1952	3.789	4.318
SEIF 1 - 1969	3.784	3.915

A synthetic brine was used, with a target chemical composition representative of the groundwater prevailing in the reservoir (Figure 4-7).

The PilotSTRATEGY project has received funding from the European Union’s Horizon 2020 research and innovation programme under grant agreement No. 101022664

Table 5.*3*, Figure 5-3, Figure 5-4 show the permeability and porosity measurements made during the cyclic flow runs for samples SEIF 1 - 1969 and SEIF 1 - 1952. Both samples which underwent cyclic flow testing showed an overall increase in permeability and porosity. In the case of sample SEIF 1 - 1952 porosity increased by c.a. 14% over the course of the test, with permeability increasing c.a. 13%. The percentage rise for sample SEIF 1 - 1969 was larger, with porosity increasing by around 25% and permeability by around 28%.

#	Initial		Final	
Sample Number	Porosity	Permeability (mD)	Porosity	Permeability (mD)
SEIF 1 - 1927	9.94	0.19	NA	NA
SEIF 1 - 1952	14.38	34.68	16.43	39.18
SEIF 1 - 1969	21.35	132.01	26.75	168.25

Table 5.3. Calculated permeabilities and porosities for samples before and after cyclic CO2-water flow.

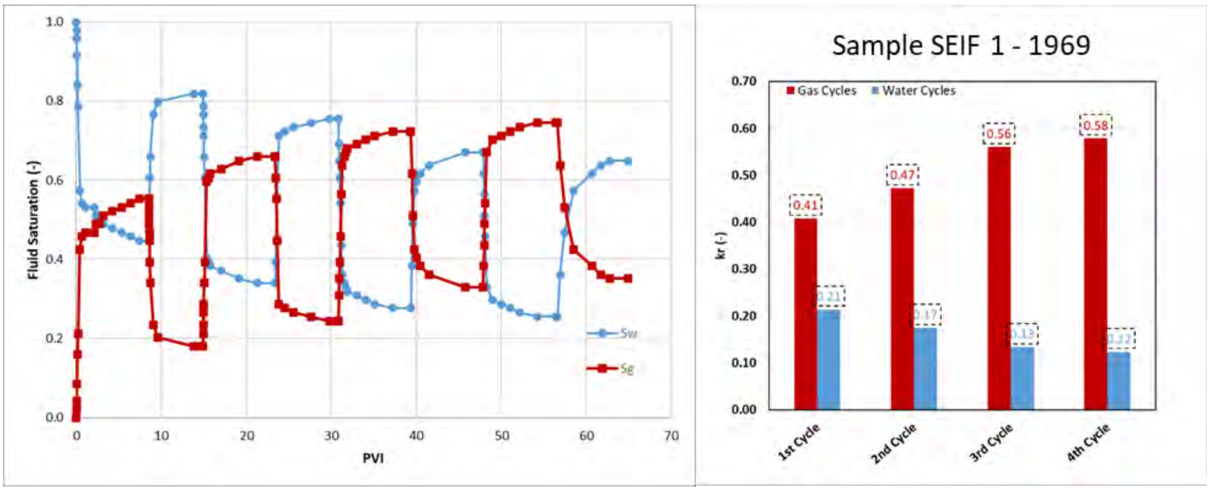

Figure 5-3: Fluid saturation and calculated gas-water relative permeabilities for sample SEIF 1 – 1969 during cyclic CO2-water flows.

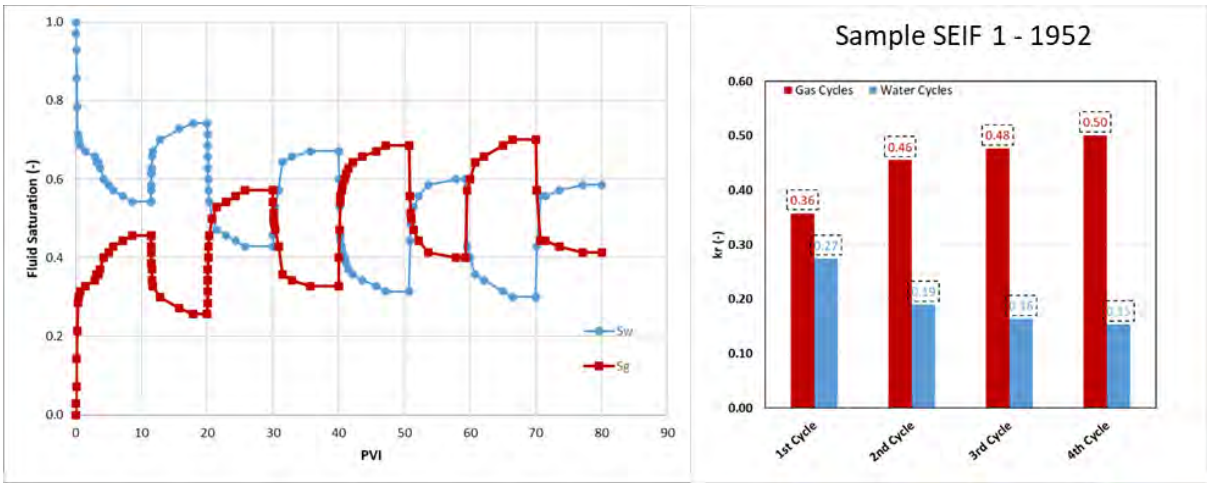

Figure 5-4: Fluid saturation and calculated gas-water relative permeabilities for sample SEIF 1 – 1952 during cyclic CO2-water flows.

The results indicate substantial dissolution of primary mineral assemblages in both samples. This corresponds with notable increases in effluent concentrations during the runs, particularly for Ca. Select effluent concentrations for the two runs are shown in Figure 5-5 and Figure 5-6.

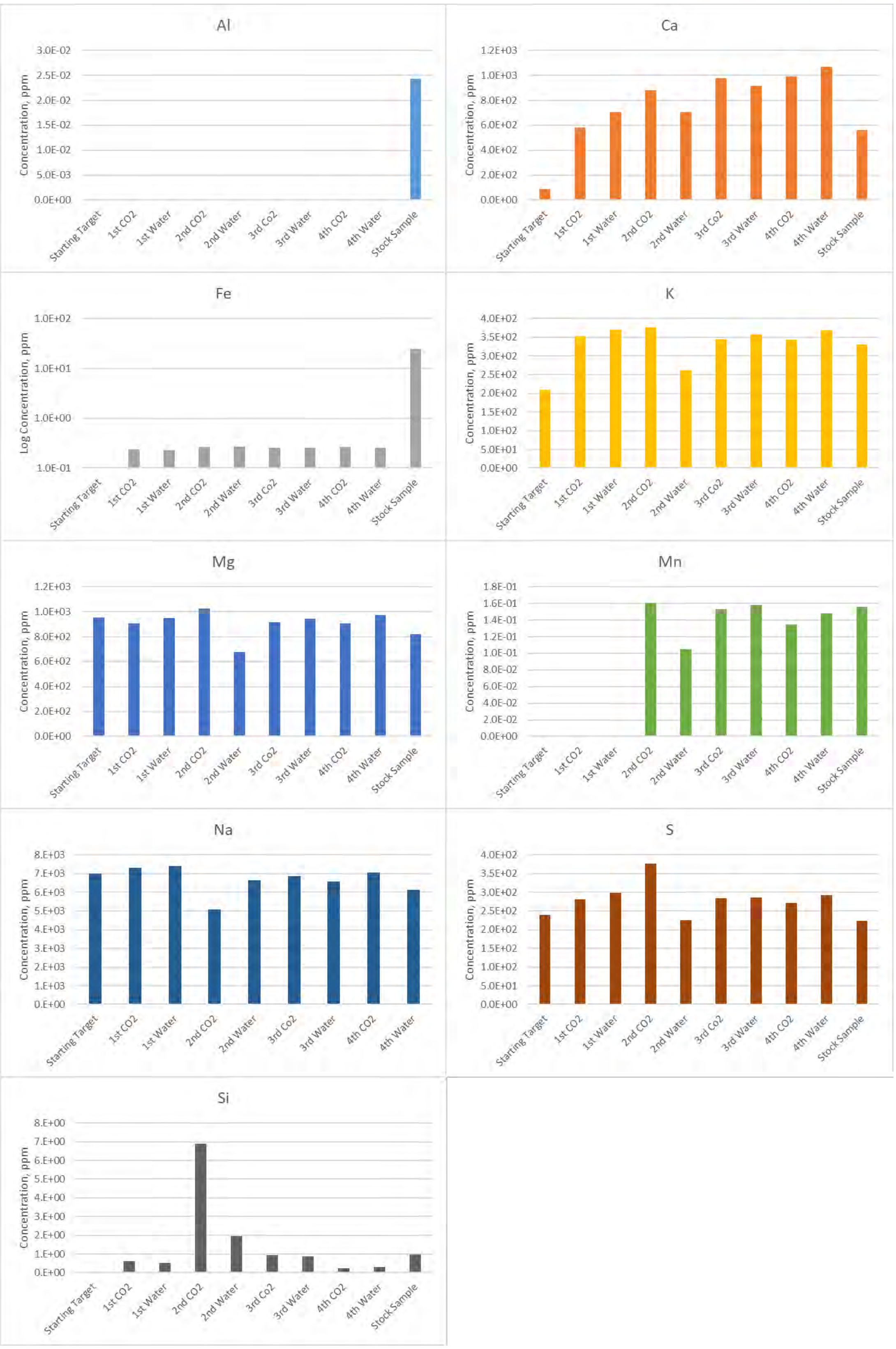

Figure 5-5: Selected elemental concentrations in effluent samples collected during CO2 and water flows for sample SEIF 1 – 1969.

The PilotSTRATEGY project has received funding from the European Union's Horizon 2020 research and innovation programme under grant agreement No. 101022664

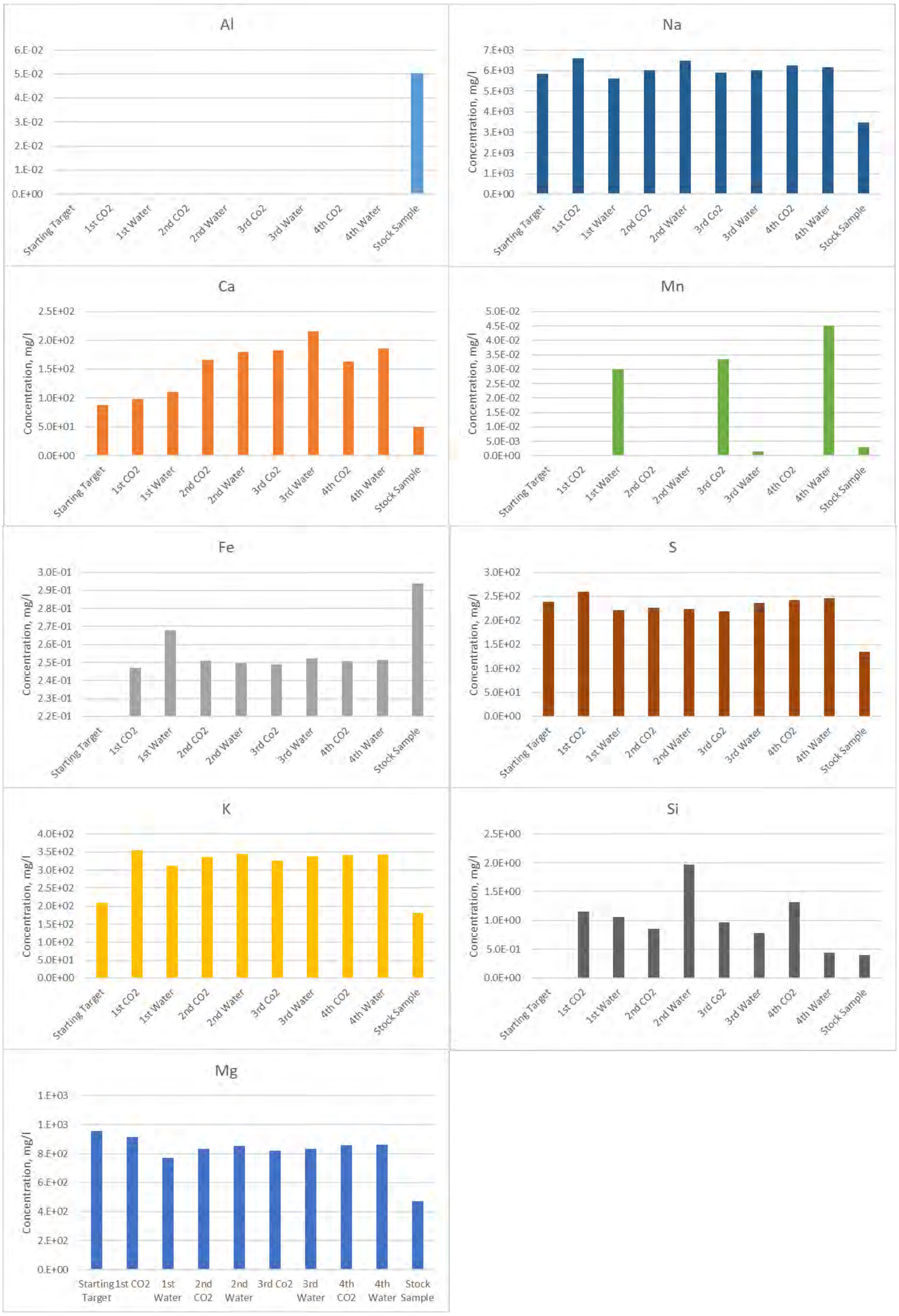

Figure 5-6: Selected elemental concentrations in effluent samples collected during CO2 and water flows for sample SEIF 1 – 1952.

For the run carried out using sample SEIF 1 – 1969, Ca concentrations are most notably elevated above the levels in the stock starting solutions. Ca concentrations are elevated in all effluent samples taken during this run and reach almost double that of the stock solution in the final sample collected. K, Mg, and S are also generally elevated in the effluent samples, relative to the stock solution, though not to the same extent as for Ca. Fe and Al, meanwhile, are depressed in the effluent samples compared to the stock solution. Si shows no clear trend, being relatively elevated for some samples and depressed for others.

For sample SEIF 1 – 1952, Ca concentrations were, likewise, notably elevated in the effluent samples collected. K and Si are also notably and consistently elevated in the effluent.

The cyclic flow test, with injection of supercritical CO_2, provides geochemical results in line with those of the batch experiment. The results from the two runs suggest large scale dissolution of a Ca bearing primary mineral. According to the conceptual geochemical model established from the batch experiment, the elevated Ca concentration result mostly from calcite dissolution and to some extent from dolomite dissolution. There is also some evidence for, more minor, dissolution of other phases, particularly for sample SEIF 1 – 1952, where elevated Si would confirm the assumed dissolution of primary quartz. Precipitation of aluminosilicate minerals may occur to explain the identified decrease in Fe and Al concentration.

5.2.4 Percolation of a CO_2-enriched brine

5.2.4.1 Experimental design

Continuous flow-through tests were conducted to assess and characterize ongoing geochemical processes under dynamic conditions with a CO_2-enriched brine. These tests were complementary to the 'cyclic flow tests' as CO_2 was injected in a dissolved state rather than a supercritical free-phase. These tests aimed to reproduce the flow of CO_2-enriched brine typically occurring at the outer edge of the CO_2 plume, far from the injection well, where some of the supercritical CO_2 injected has already dissolved in the *in-situ* brine.

High-pressure experiments were conducted on a dedicated experimental setup (Figure 5-7), which consisted of a high-pressure pump (to inject the synthetic brine), percolation cell (Hassler cell) and a second pressure pump to store the outlet water. The first high-pressure pump was used to pressurize the inlet water and maintain a semi-constant flow rate (i.e. flow periodically stopped to fill in the pump) through the rock, while the second pump was set to maintain a constant pressure at 180 bar. The Hassler cell was divided into two parts separated by a cylindrical silicon rubber membrane. The internal part contained the rock sample (twin sample to the one used for the 'cyclic flow tests'), enclosed by a cylindrical rubber membrane, while the external part was filled with compressed water to apply a 195 bar radial pressure on the rock sample. This radial pressure minimized the risk of generating preferential paths for the solution in the cell. Each part of the device was maintained at a temperature of 70°C with a heat-circulating bath, heater ribbons, and insulation with aluminium foil. Before the injection, the synthetic brine, with a chemical composition representative of the groundwater in reservoir (Table 4.4), was equilibrated with 50 bar of CO_2.

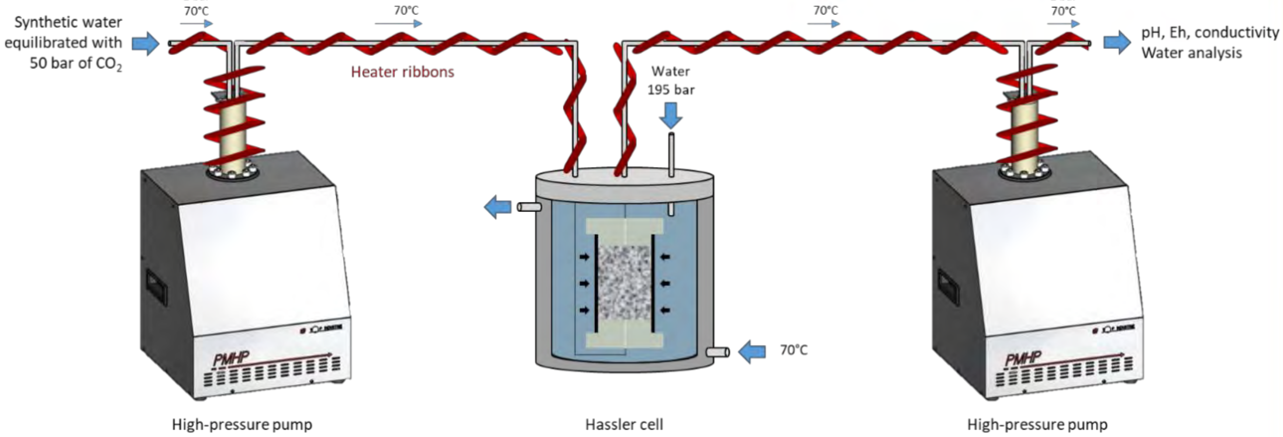

Figure 5-7: Illustration of the high-pressure setup used for percolation tests with a CO_2 enriched fluid.

Two tests were performed, one with the reservoir sample (core plug SEIF 1 – 1969) and one with the caprock sample (core plug SEIF 1 – 1841). The core plug has a diameter of 3.8 cm and a length of about 4.5 cm (Figure 5-8). For both experiments, the initial flow rate of the brine (enriched with CO_2) was fixed to 0.4 ml/min. This flow rate was occasionally decreased in case of clogging (mainly for the caprock sample) or short maintenance (e.g. refilling of the synthetic brine tank).

The SEIF 1 –1969 sample remained fully consolidated after the drilling of the core plug. The reactive flow-through experiment was run without any preliminary flow test considering the known permeability of the sample (Table 5.*3*).

Comparatively, the SEIF 1 –1841 sample presented many cracks after drilling of the core plug. The caprock formation was naturally very crumbly, mostly because of the storage conditions of the core. Despite these cracks, a significant portion (c.a. 60 %) of the sample remained as a consolidate sample. A first percolation test was performed with entire core plug sample to determine if brine could flow through the rock under these conditions. No outlet water was collected for 24 hours despite a 180 bars of pressure difference between the inlet and outlet. To overcome the lack of flow, the core plug was sawed vertically to simulate a vertical crack along the intact part of the sample (red line; Figure 5-8).

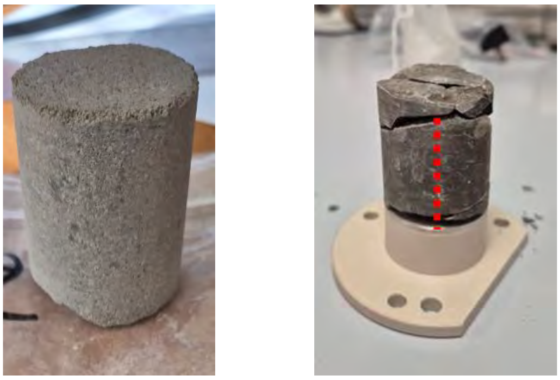

SEIF 1 – 1969 SEIF 1 - 1841

Figure 5-8: core plugs SEIF 1 – 1969 for the reservoir (left) and SEIF 1 – 1841 for the caprock (right) before use in the reactive flow-through experiments with CO2-enriched fluid. The red line (right) represent the cut-off line of the sample post experiment.

Water samples were collected throughout the experiments, in a similar way to the batch experiments (see section 4.2.2.4), with frequent sampling (every 2 hours) at the beginning of the experiment, followed by more intermittent sampling (1 to 4 days) thereafter. At the end of the experiments, 15 ml of ethanol was injected through the rock sample to remove the pore water and avoid salt precipitation during the sample drying. The resulting core plugs were divided into three parts, with horizontal sections at the top (inlet – up flow), middle and the bottom (outlet – down flow) of the sample to perform rock analyses.

5.2.4.2 Rock and water analyses

The mineralogical and geochemical characterisation of the core plug samples, both prior and after reactive flow-through experiments, relied on a combination of several analytical methods, previously presented in section 4.2.1.3, and summarised in Table 4.*3*. Additionally, the elemental composition (bulk chemistry) of the rock were determined before and after experimental test to attempt to better monitor the chemical evolution in the rock.

The elemental rock composition was measured by combining X-ray fluorescence (XRF) analysis for major elements and ICP-MS measurements after the rock dissolution in sodium peroxide and hydrochloric acid solution (33%) for trace elements. The sulfur content was determined by heating the sample and quantifying the SO_2 emitted by infrared spectroscopy. Chloride concentrations were determined by addition of silver nitrate to precipitate silver chloride, and titration of silver excess by ammonium thiocyanate. Fluoride content was obtained by alkaline sintering and quantified with a Fluoride Ion-Selective Electrode.

The composition of the water flowing through the core plug samples were analysed for all collected samples. The sampling method used for the batch experiment was applied to the reactive flow-through experiment (see section 4.2.2.5).

5.2.4.3 Results

5.2.4.3.1 Reservoir

The percolation test, conducted with the CO_2 enriched fluid and the SEIF 1 – 1969 rock sample was performed for 33 days. The pressure difference between the inlet and outlet remained low (< 1 bar) throughout the experiment, indicating a high rock permeability. This pressure difference gradually decreased over the course of the experiment, which suggested the rock sample was undergoing dissolution. The latter was confirmed by the observation of the core rock sample after the experiment, where the aqueous solution acidified by CO_2 had significantly increased the porosity of rock, forming a vertical wormhole through the entire core plug from the upper/inlet part to the bottom/outlet part (Figure 5-9).

The PilotSTRATEGY project has received funding from the
European Union's Horizon 2020 research and innovation
programme under grant agreement No. 101022664

Inlet Outlet Cross section

Figure 5-9. Photographs of the core plug SEIF 1 – 1969 after 33 days of flow-through experiment with CO2-enriched fluid: inlet / upper part of the sample (left), outlet/bottom part of the sample (middle), cross section of the core plug (right), after sawing of the sample along the red line

Despite the formation of the wormhole, the proportion of different mineral phase did not change significantly from the unreacted rock proportion (Figure 5-10). The same observation can be made for most of the elements quantified with elemental analyses of SEIF 1 – 1969 before and after the experiment (Figure 5-11; Figure 5-12), considering the analytical uncertainties. However, among the major elements, a slight decrease in sulfur concentrations can be highlighted. On the other hand, silicon dioxide concentration increased slightly (Figure 5-11). This result illustrates the heterogeneity of the mineral assemblage along the length of the core plug, where quartz can be only quantified – i.e. is above the limit of detection – in some parts (middle and outlet) of the rock sample after the experiment.

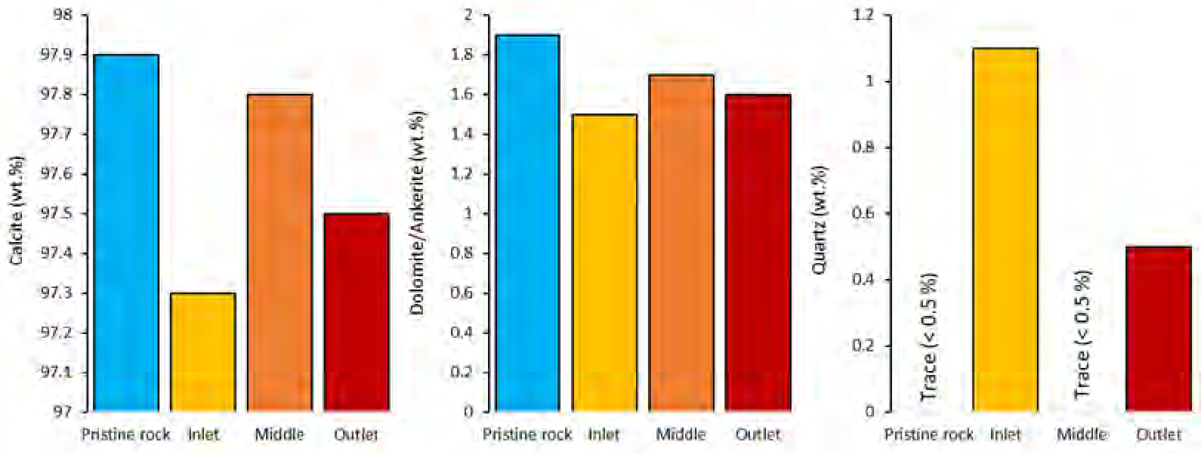

Figure 5-10: Semi-quantitative proportion of mineral phases (weight %) composing the core plug SEIF 1 – 1969 before (pristine rock; blue) and after formation of the wormhole from percolation of a CO2-enriched fluid in the porosity (XRD-Rietveld analyses; analytical uncertainty +/- 2%). After the end of the experiment, the rock core sample was divided in three parts (inlet, middle and outlet). Trace of siderite (middle part), muscovite (outlet) and kaolinite (all samples) were also detected after the 33-day experiment, but were too low to be quantified.

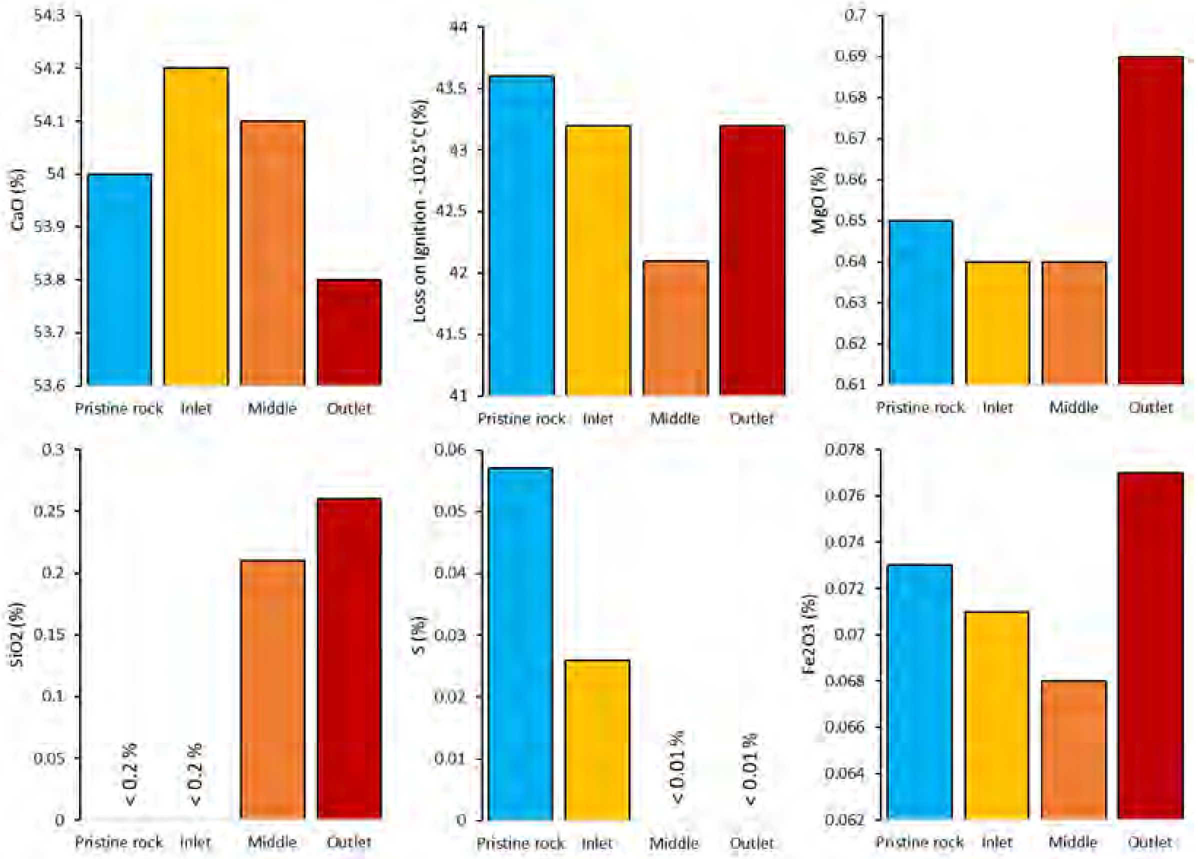

Figure 5-11: Concentration of major elements (bulk chemistry) in the SEIF 1 – 1969 core plug, before and after formation of the wormhole from percolation of a CO2-enriched fluid in the porosity. After the end of the experiment, the rock core sample was divided in three parts (inlet, middle and outlet).

Among the minor to trace elements (Figure 5-12), aluminium, manganese and barium concentrations decrease significantly in the inlet part, but the concentration progressively increase along the core plug. This suggest a preferential dissolution of aluminosilicate and Ba rich mineral in the inlet part, where CO_2 enriched solution is injected in the porosity of the core plug. The dissolution front of this mineral phases is progressive along the core plug, in line with the identified decrease in diameter of the wormhole along the core plug (Figure 5-9).

Analyses of the experimental brine from the outlet further support the idea of major dissolution involving the formation of a wormhole (Figure 5-13; Figure 5-14). The concentration of calcium, magnesium and potassium were significantly higher than that of the synthetic brine (up to twice the initial concentration). The concentration rise occurred mainly within the first 3 days of the experiment, reaching up to 42.5 mmol/l for Ca (synthetic brine: 22.7 mmol), 3.4 mmol/ for K (synthetic brine: 1.8 mmol), and 8.1 mmol/l for Mg (synthetic brine: 7.4 mmol) and inducing a pH increase (Figure 5-13). After this plateau, the concentrations decreased through time. Calcium and potassium concentration displayed a significant decrease respectively after 5 and 20 days of experiments. The drop in calcium concentration can be related to the pH evolution. The final potassium concentration reached values near the concentration of the synthetic brine. The stabilisation of the potassium concentration could be due to the depletion of the potassium stock in the rock, as potassium mineral was initially too low to be detected in the rock elemental analyses or XRD analysis. However, the formation of the wormhole induced a preferential flow, where the specific surface area is significantly reduced and thus contribute to minimise the rock reactivity in the hydrodynamic experimental system. This hypothesis could contribute to explain the stable concentrations observed after c.a. 20 days of experiment for many major dissolved elements, such as magnesium and potassium.

The initial drop in sodium concentration for the first 3 days of the experiment, before reaching a relatively stable concentration – equivalent to the concentration of the synthetic brine –, suggests ongoing cation-exchange processes at an early stage of the experience, in line with the occurrence of kaolinite and illite and/or mica. This would imply that part of the observed Ca, Mg and K rise might result from cation desorption from illite and kaolinite over this early period.

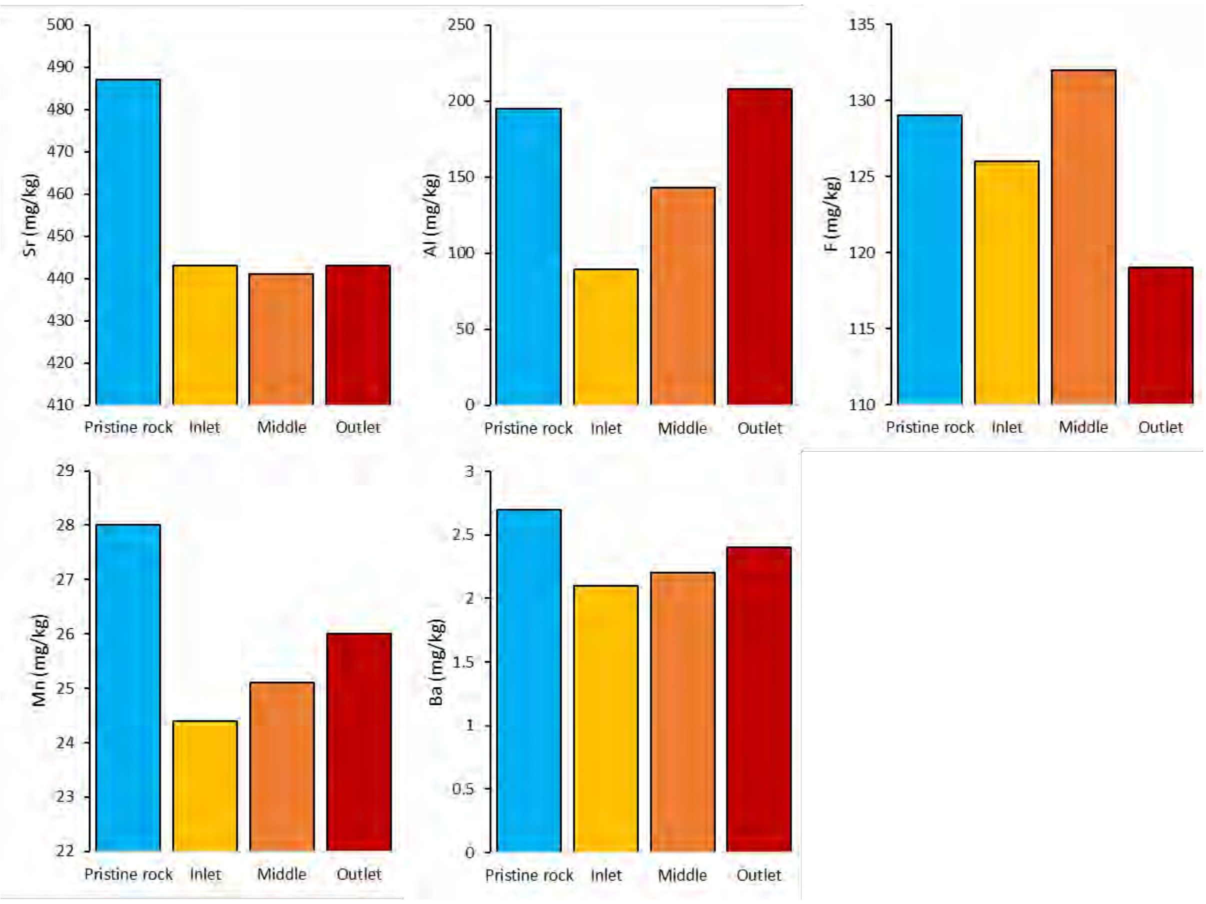

Figure 5-12: Concentration of minor elements (bulk chemistry) in the SEIF 1 – 1969 core plug, before and after formation of the wormhole from percolation of a CO2-enriched fluid in the porosity. After the end of the experiment, the rock core sample was divided in three parts (inlet, middle and outlet).

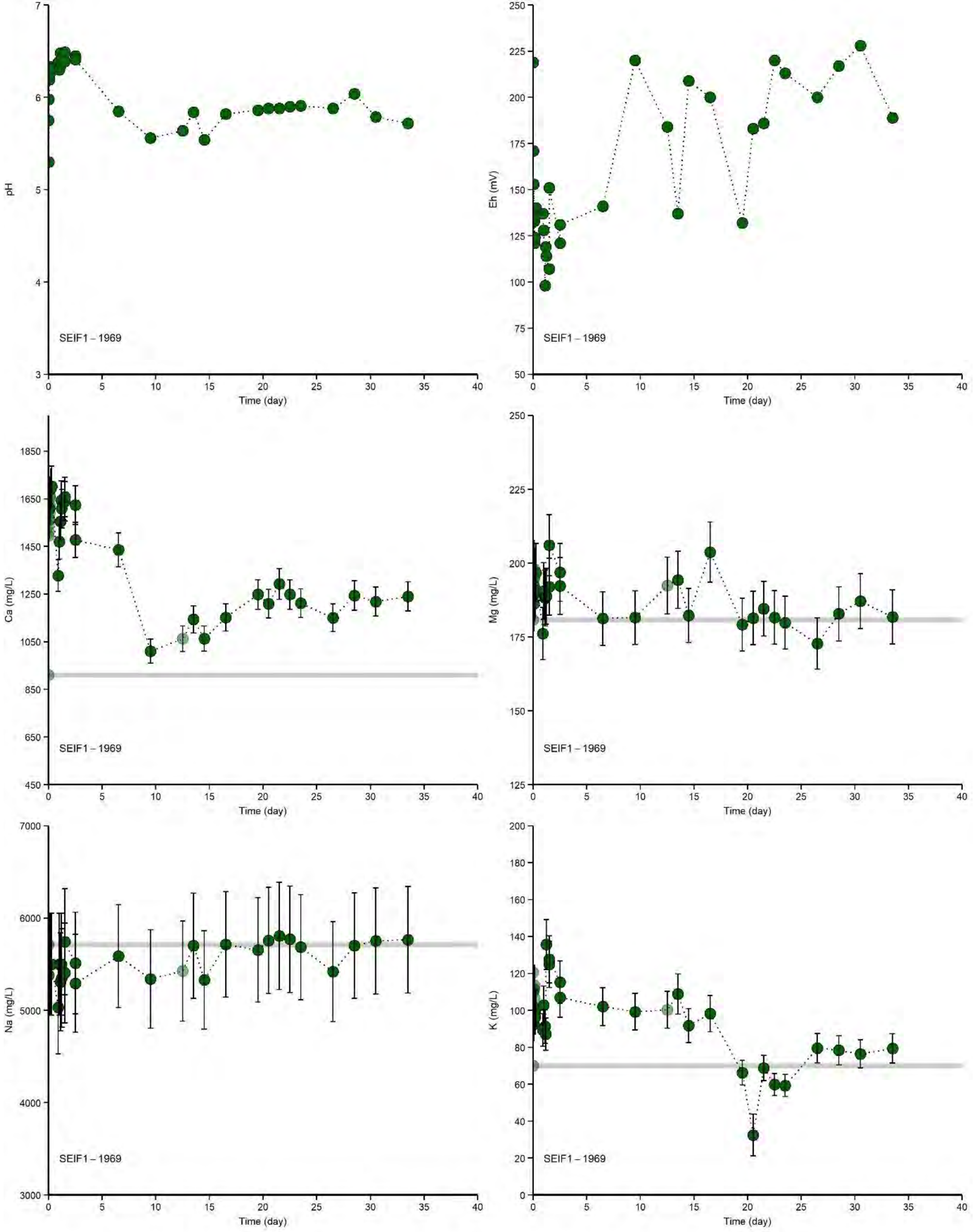

Figure 5-13: Evolution of pH, Eh values and concentrations of major cations through the experimental time of the reactive flow-through experiment with the sample SEIF 1 – 1969 and CO2-enriched fluid. The grey horizontal bar corresponds to the composition of the synthetic brine.

The PilotSTRATEGY project has received funding from the European Union's Horizon 2020 research and innovation programme under grant agreement No. 101022664

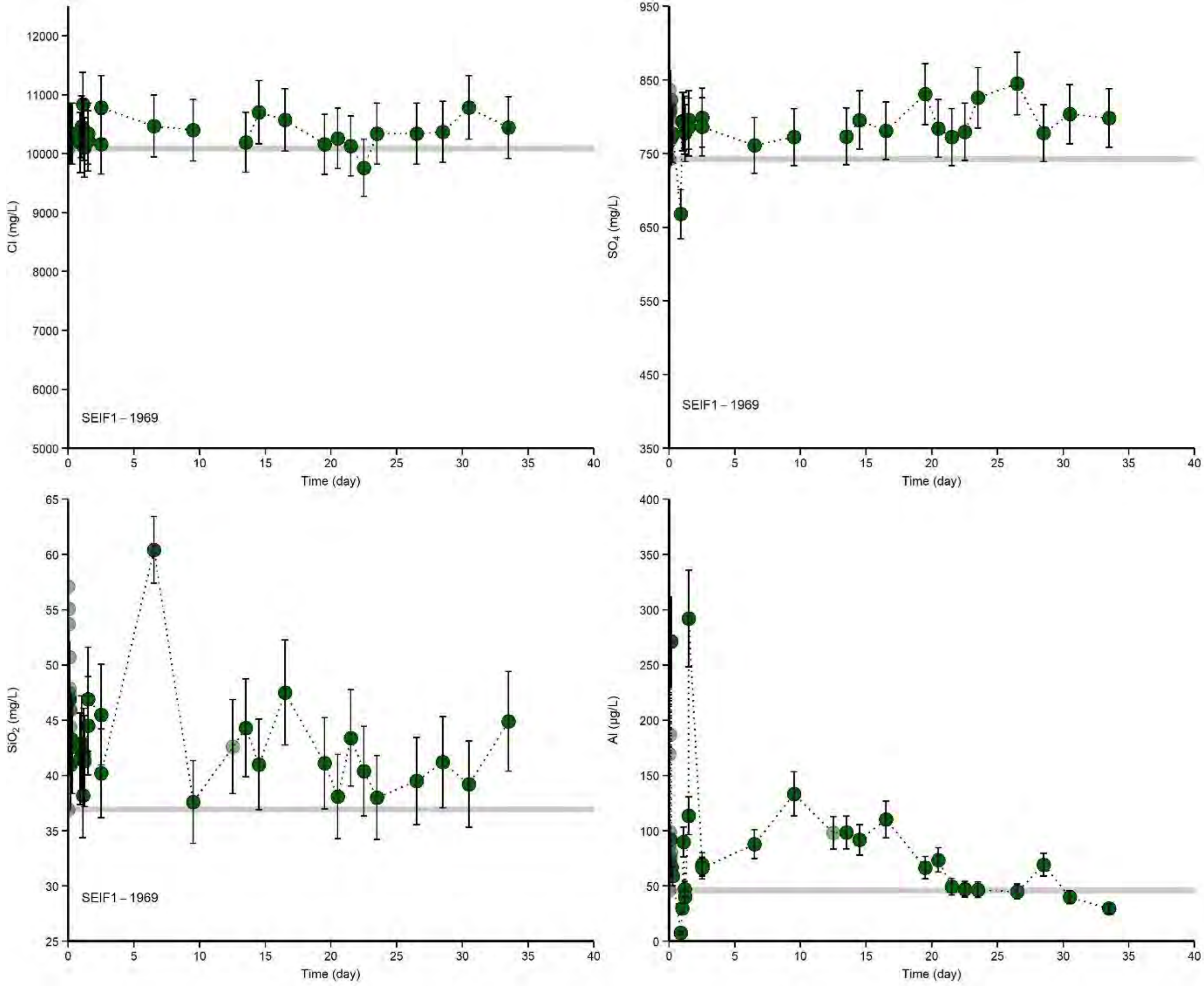

Figure 5-14: Evolution of concentrations of chloride, sulphate, silica and aluminium through the experimental time of the reactive flow-through experiment with the sample SEIF 1 – 1969 and CO2-enriched fluid. The grey horizontal bar corresponds to the composition of the synthetic brine.

Chloride, sulphate and silicon dioxide concentrations remained roughly constant throughout the test and were comparable or near to the initial concentrations of the synthetic brine (Figure 5-14). The aluminium concentration was more variable but tended to decrease over time.

Despite the hydrodynamic context, the saturation indices of the aqueous solution at the outlet flow were calculated using the PhreeqC software with the Thermoddem database. The aqueous solution was initially supersaturated with respect to most of the mineral phases identified within the mineralogical assemblage. The saturation indices of the carbonate minerals indicated supersaturation of the aqueous solution with respect to calcite, dolomite and ankerite over the first 3 days of experiment, after which the aqueous solution reached a near equilibrium with the carbonate minerals. This evolution further confirms a stabilisation of most reactive phase and thus the stabilisation of the rock sample reactivity. The initial supersaturation state (at the outlet flow) of the carbonate minerals suggests significant dissolution within the porous media near the inlet and the middle part of core plug, in line with the formation of the wormhole. The aqueous solution is also in equilibrium with gypsum/anhydrite and quartz all over the experimental time, in line with the relative stability of the sulphate and silica concentration. The dissolution of gypsum/ankerite and quartz may contribute only to a minor part to the formation of the wormhole.

5.2.4.3.2 Caprock

After the vertical sawing of the (dry) sample SEIF 1 – 1841 to initiate a flow of the CO_2-enriched fluid, the reactive flow-through experiments was run for a period of 28 days. Initially, the difference of pressure between the inlet and the outlet part of the sample was low (<1 bar). The difference of pressure progressively increased to reach up to 100 bar after 28 days, which inform of obvious clogging of the mudstone porosity. At the end of the experiment, the fractured and sawed core plug were partly unified, support the clogging process and the permeability decrease over time (Figure 5-15).

Figure 5-15: Photograph of the core plug SEIF 1 – 1841 after the end of the reactive flow-through experiment with CO2-enriched fluid (28 days).

The XRD-Rietveld analyses highlighted an evolution in the proportion of the mineral phases (Figure *5-16*). A decrease in proportion of calcite, kaolinite, smectite and/or interstratified illite/smectite, plagioclase and chlorite can be observed after the experiments, suggesting that dissolution may have occurred. On the other hand, the proportion of ankerite/dolomite, K-feldspar and anatase increased, probably due to the dissolution of the other minerals initially composing a major part of the mineral assemblage (e.g. carbonate minerals). The proportion of pyrite in the outlet part of the rock after the test was much higher than the unreacted rock and the other parts of the rock sample. This difference was also observed in the iron, sulphur content and the mass loss on ignition. This high concentration could be ascribed to the variability of the rock composition.

Elemental analyses of the rock sample (Figure 5-17; Figure 5-18) do not show significant variation for most of the analysed chemical species. Main changes are observed for Na_2O, P_2O_5 and Sr concentrations, which were slightly lower after the experiment. The barium concentrations also decreased through the experiment. However, the middle part of the rock sample presented similar concentrations than the pristine rock, probably because of the rock heterogeneity.

The PilotSTRATEGY project has received funding from the European Union's Horizon 2020 research and innovation programme under grant agreement No. 101022664

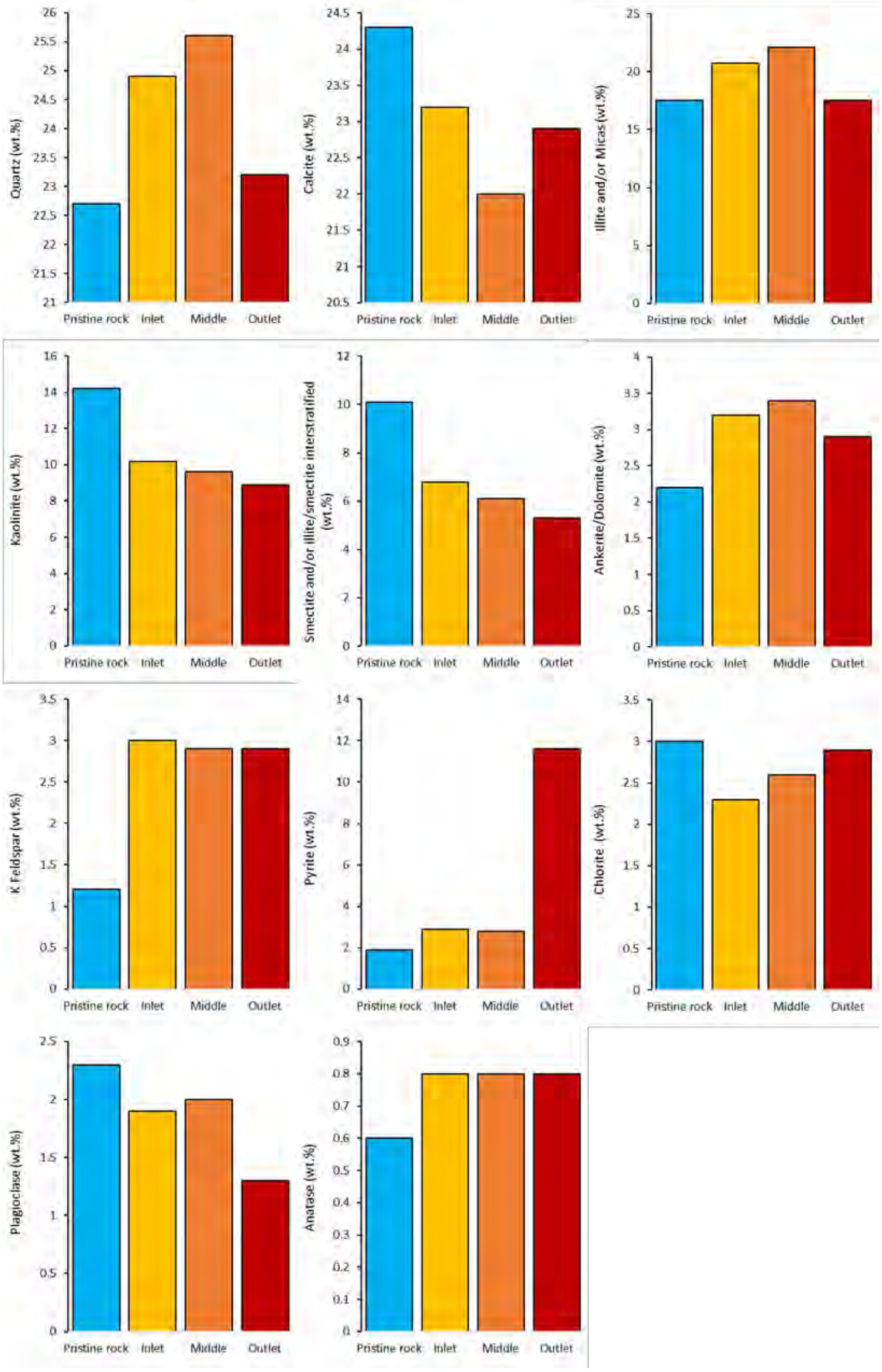

Figure 5-16: Semi-quantitative proportion of mineral phase (weight %) composing the sample SEIF 1 – 1841 before and after the reactive flow-through experiment with a CO2-enriched fluid (XRD-Rietveld analyses; analytical uncertainty +/- 2%). After the end of the experiment, the rock core sample was divided in three parts (inlet, middle and outlet).

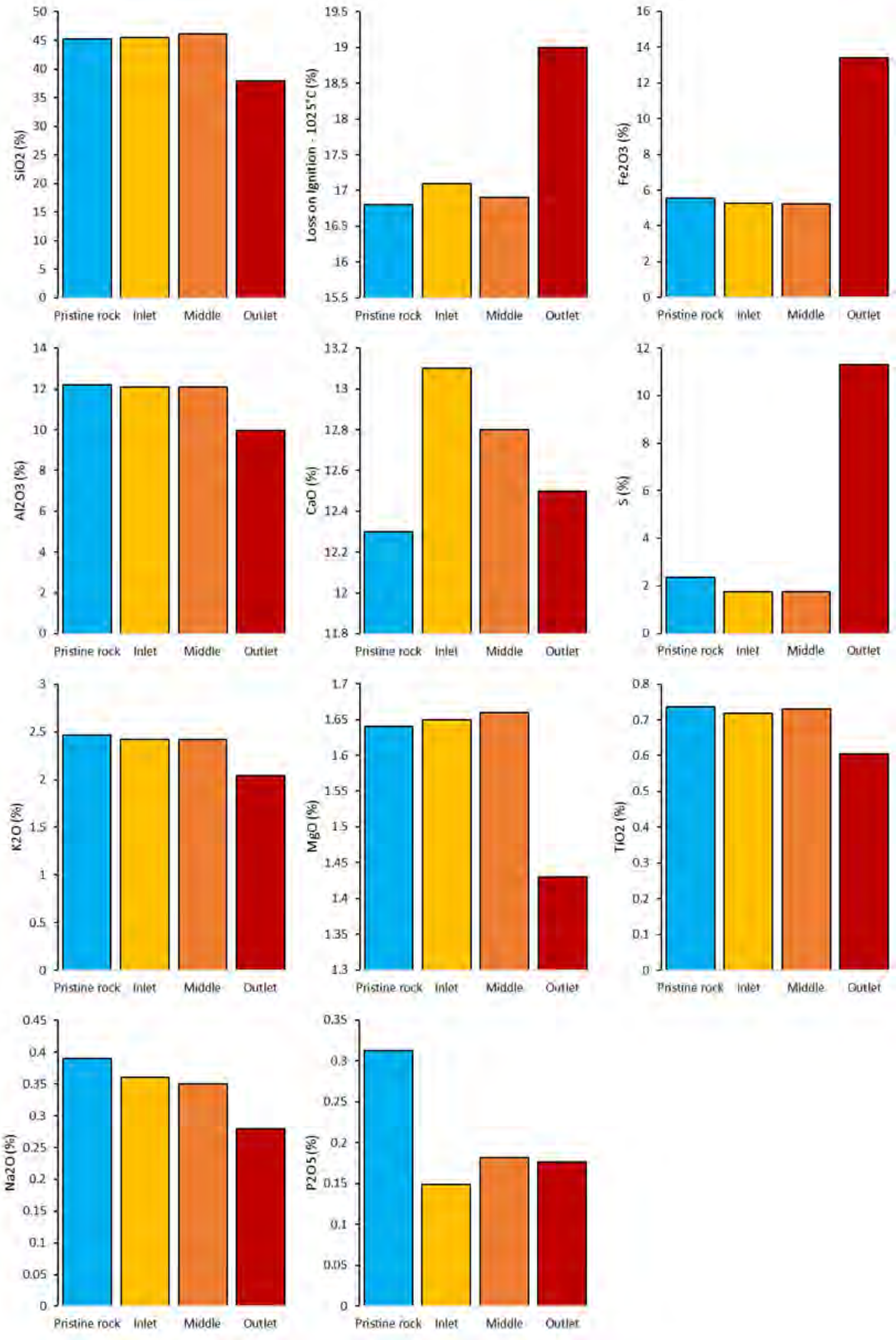

Figure 5-17: Concentration of major elements in the sample SEIF 1 – 1841.

The PilotSTRATEGY project has received funding from the European Union's Horizon 2020 research and innovation programme under grant agreement No. 101022664

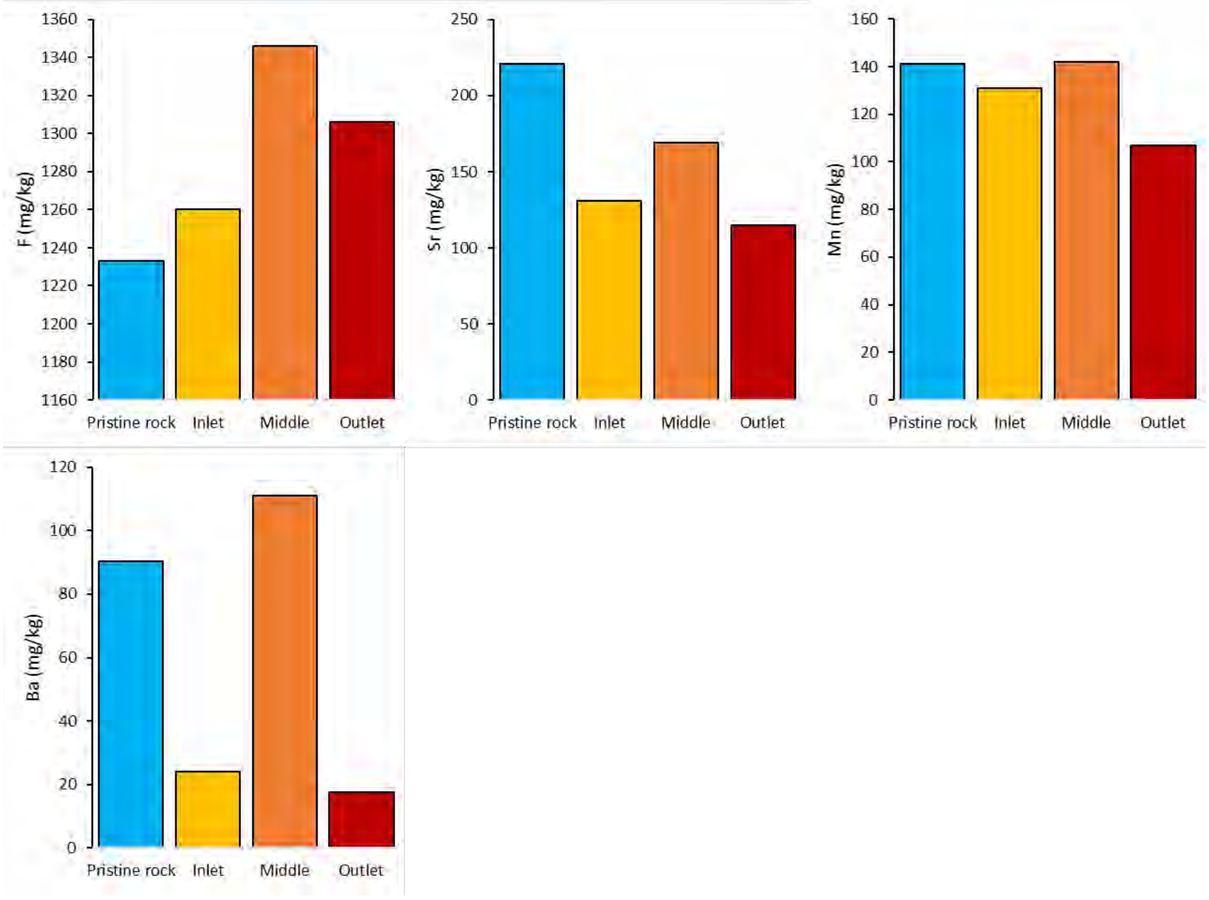

Figure 5-18: Concentration of minor elements in the sample SEIF 1 – 1841.

Chemical analyses of the outlet water highlight a high reactivity in the caprock during the first day, with a marked increase of pH and Ca, Mg, K, SO_4, SiO_2 and Al concentrations (Figure 5-19; Figure 5-20). Three main patterns are observed in the concentrations over time: (i) high Ca concentrations remained relatively constant over the entire experimental time, in line with the stabilisation of the pH value; (ii) an initial rise of Mg and SiO_2 concentration followed by a progressive decrease over the following days, before increasing again after 4-6 days; (iii) K, SO_4 and Al progressively decrease towards – but stay higher than – the initial concentration of the synthetic brine after a few days, in line with the trend of the redox potential.

Saturation indexes of most primary mineral highlight changes over the reaction time. The aqueous solution at the outlet flow was initially slightly supersaturated with respect to the carbonate minerals (calcite, dolomite) and sulphate minerals (gypsum / anhydrite), before reaching equilibrium after 6 and 2 days respectively. Accordingly, the flow of the CO_2-enriched brine induced substantial dissolution of carbonate and sulphate minerals in the porous media along the core-plug before reaching a relative steady state with respect to these mineral phases. Conversely, the aqueous solution was initially at equilibrium with respect to quartz but progressively become supersaturated to reach equilibrium with respect to chalcedony, suggesting the presence of this mineral.

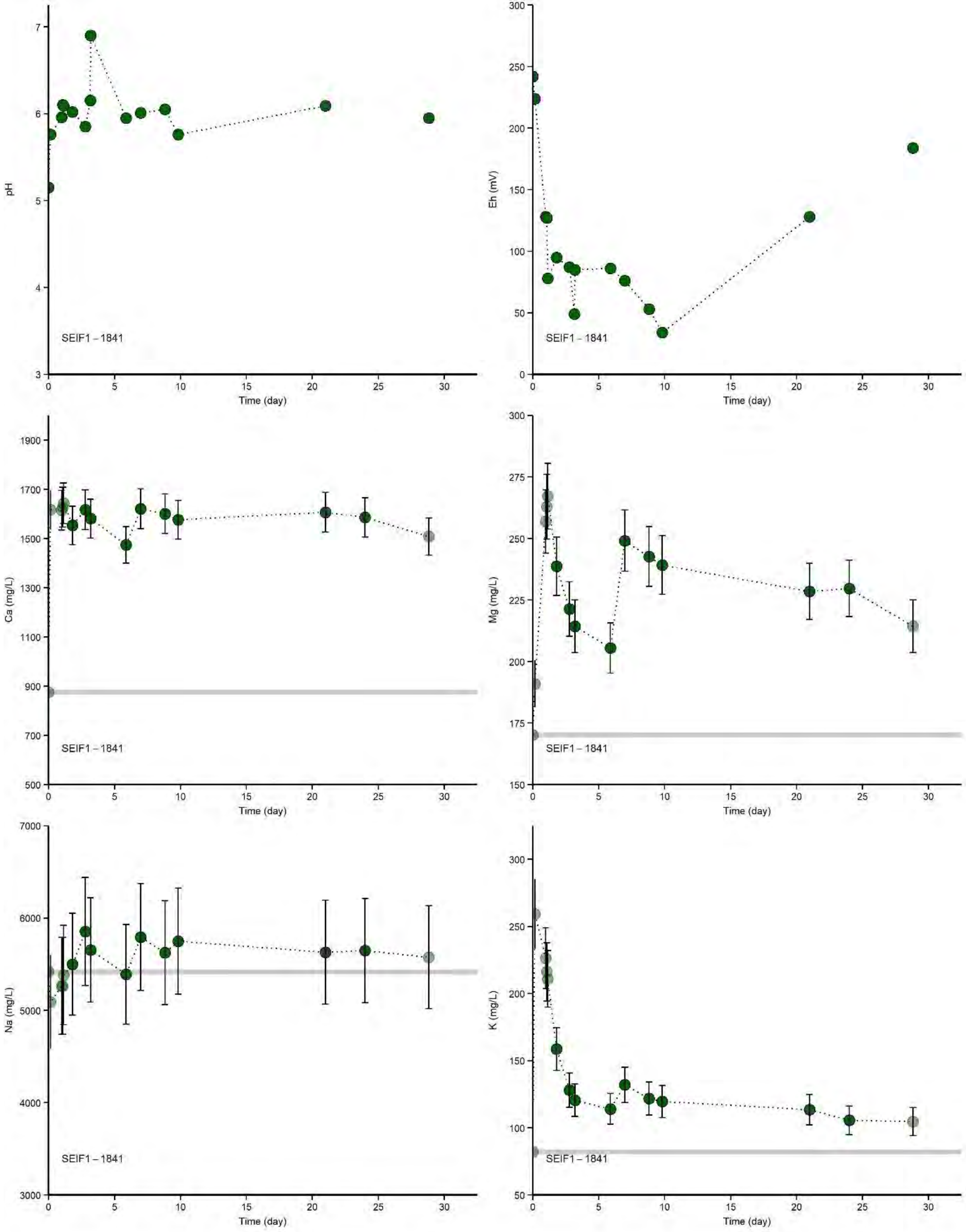

Erreur ! Source du renvoi introuvable.Erreur ! Source du renvoi introuvable.

Figure 5-19: Evolution of pH, Eh values and concentrations of major cations through the experimental time of the reactive flow-through experiment with the sample SEIF 1 – 1841 and CO2-enriched fluid. The grey horizontal bar corresponds to the composition of the synthetic brine.

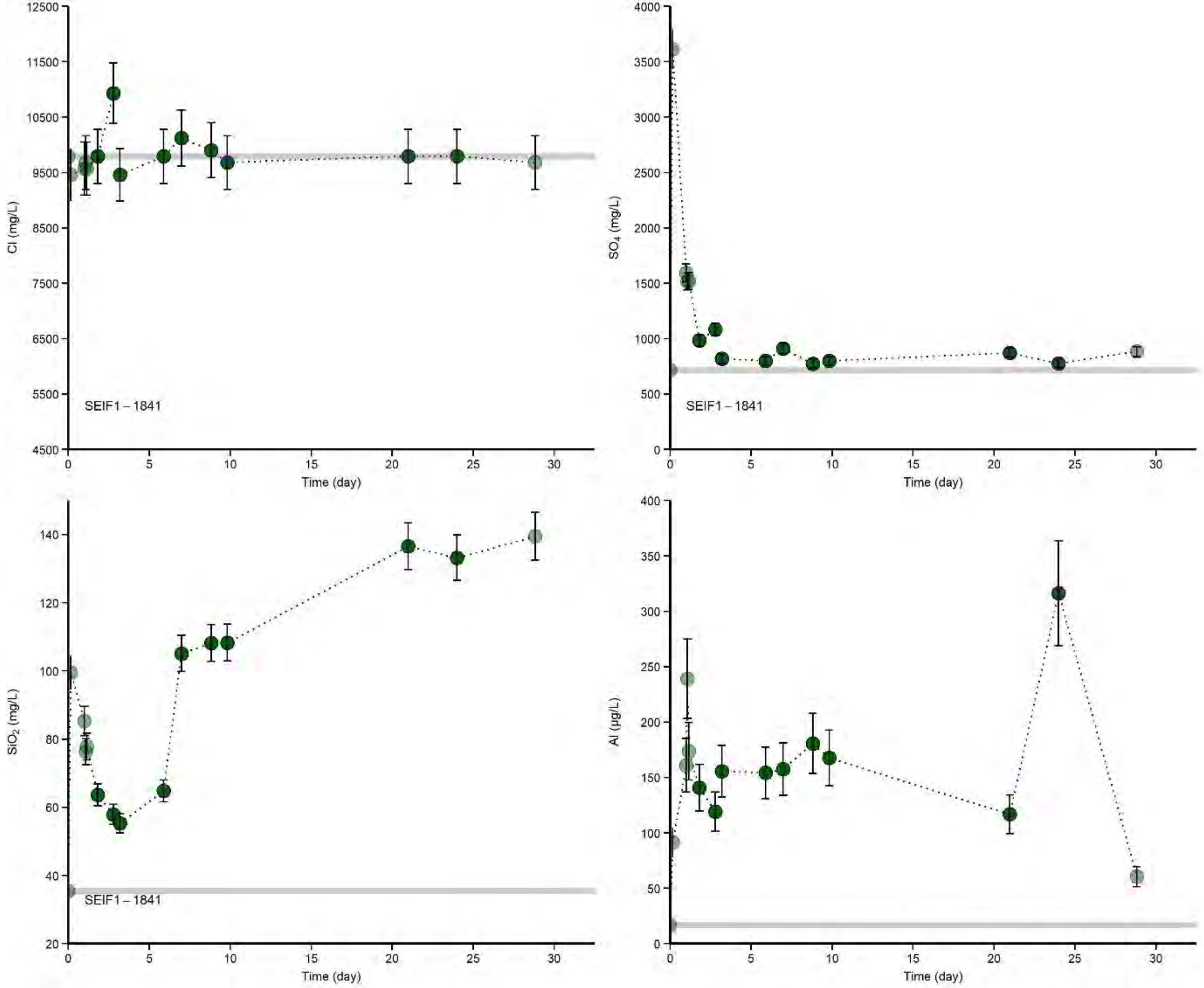

Figure 5-20: Evolution of concentrations of chloride, sulphate, silica and aluminium through the experimental time of the reactive flow-through experiment with the sample SEIF 1 – 1841 and CO2-enriched fluid. The grey horizontal bar corresponds to the composition of the synthetic brine.

5.2.5 Discussion and conclusion

Cyclic flow tests with supercritical CO_2 were performed to characterize the rock transport properties (i.e., total porosity and relative permeability) of the Oolithe Blanche Formation from the reservoir (SEIF 1 – 1969) under conditions of injection of CO_2 under supercritical state. The results confirmed the high permeability of the Oolithe formation. The tests also highlighted strong dissolution processes. This dissolution induced a progressive increase of the porosity, intrinsic permeability and the measured water and CO_2 (supercritical) relative permeability.

The reactive percolation experiments with a CO_2-enriched fluid (dissolved CO_2) and the sample SEIF 1 – 1969 highlighted the high intrinsic permeability and strong dissolution processes, particularly calcite dissolution, which is consistent with the results from the cyclic flow tests. Due to the very high calcite content in the sample (both before and after the experiments), rock analyses did not allow identifying other minerals (secondary precipitation). The formation of a wormhole, resulting from calcite dissolution, is one of the main findings of this test. While it is unclear when the wormhole was formed, its implementation within the core plug likely modified the specific surface area and thus the reactivity of the porous sample. Chemical analyses of aqueous solution from the outlet flow revealed three main periods: i) most element concentrations increased until day 3 of the experiments, ii) at day 10, the pH and Ca concentrations dropped, and iii) at day 20, the K concentration decreased, along with, to a lesser extent, the sulphate, magnesium and chloride concentrations. The aqueous solution, initially supersaturated with respect to most identified minerals (as expected in a reactive hydrodynamic system), equilibrium tended to be reached with respect to calcite, dolomite and quartz after 3 days of experimentation. The initial supersaturation state (at the outlet flow) of the carbonate minerals suggested significant dissolution within the porous media near the inlet and the middle part of core plug, in line with the formation of the wormhole. Geochemical modelling of the reactive flow-through experiment shall further clarify the impact of the dissolution (wormhole formation) on the flux of dissolved elements from the outlet flow and define the potential of mineral phases able to (re-precipitate) under hydrodynamic conditions.

The reactive flow-through test with a CO_2-enriched fluid was performed with the sample SEIF 1 – 1841 from the caprock formation. Due to the very low permeability of the core plug, no brine could circulate through the rock despite a pressure difference of 180 bar. The core was thus artificially fractured (sawed) to allow brine percolation and characterize the induced geochemical processes. The experiment was conducted for 28 days before the (progressive and) complete clogging of the porosity. Rock analyses did not reveal specific changes in the relative mineral proportions, probably due to the low rock permeability. Chemical analyses of the outlet brines highlighted a quick increase in concentrations, which were consistent with the rock's mineral composition. The flow of the CO_2-enriched brine in the porous media induced a substantial dissolution of carbonate (calcite, dolomite) and sulphate minerals (gypsum/anhydrite) in the porous media along the core-plug (geochemical transient state), before to reach a relative geochemical steady state with respect to these mineral phases. Due to the large set of aluminosilicate minerals composing the mineral assemblage, the interpretation of the reactive process from the composition of the brine solution require use of geochemical modelling to build a robust geochemical conceptual model taking into account the evolving hydrodynamic system simulated experimentally.

5.3 Experiments on Material from Spain and Portugal - Steady State Flooding Experiments

5.3.1 Steady state methodology

Steady-state core flooding tests are employed to acquire relative permeability functions, which are crucial for assessing fluid flow through porous media during geological gas storage. These tests are conducted under high-pressure and high-temperature conditions to simulate reservoir conditions accurately. This experimental program is specifically designed to obtain relative permeability functions for CO_2-Brine under a real reservoir condition. The resulting data will serve as input for reservoir simulators and enhance the understanding of fluid behaviour in the subsurface.

Initially, a representative core sample was taken from the provided rock sample. Then, to conduct each test, the taken core sample was first subject to preparation and cleaning procedures. Subsequently, the core sample was characterized by measuring its basic properties, including porosity and permeability, as well as tracer test to assess its heterogeneity.

Following this, a steady-state core flooding test was conducted at various fractional flows (Fg) – different injection rate ratios of gas and water - using the corresponding gas and brine.

Research-grade carbon dioxide (CO_2) (purity 99.9995 vol %) and Sodium Chloride (NaCl) of certified purity (99.5%) were supplied by BOC Ltd. and Fisher Scientific, respectively. Deionized water generated by an integral water purification system (ELGA DV 25) was used exclusively throughout the experiments.

The high-pressure core flood rig that was used for the steady-state experiments is as used for the cyclic flow experiments shown in Figure 5-2. It consists of several dual pump systems connected to high-pressure fluid transfer vessels, back pressure regulator (BPR) and overburden (OB), which are used to deliver the fluids into the core and maintain the OB and BPR pressures constant during the injection. The core effluent is carried through a backpressure regulator (BPR) where the pressure drops to atmospheric pressure, and hence any dissolved gas would be liberated. Then, the separated liquids are collected in a graduated cylinder.

The core orientation can be adjusted during experiments. While performing a test, the pressure and temperature at the inlet and outlet of the core holder are recorded and displayed continuously on a computer monitor, which has a built-in data acquisition system. The experiments are performed under constant, and well-controlled temperature maintained at the test temperature by keeping the apparatus inside a heated air oven.

The following procedures were employed to conduct each steady-state core flooding test. The selected core sample was subjected to loading, and subsequently, liquid porosity measurements were performed under experimental pressure. These measurements were conducted using synthetic brine containing both monovalent and divalent ions. Once the liquid porosity had been measured with the brine, the core was subjected to flooding with the same brine at a slow rate. This step was crucial to establish surface charge equilibrium between the brine and the core sample's mineral. Following that, the core underwent flooding at various rates, and the differential pressure across the core sample was recorded at each injection rate. Each injection rate was maintained until the differential pressure across the core sample stabilized. The absolute permeability of the core sample was then determined using Darcy's Equation.

To prevent mass transfer during the experiments, the brine sample was initially fully saturated with the corresponding gas (CO_2) and was pre-equilibrated with the crushed rock under experimental conditions, referred to as 'live brine'. Subsequently, the core was subjected to continuous flooding with this live brine at both low and high rates over an extended duration of 20 pore volumes of injection. Afterward, the absolute permeability of the core was measured again. This process was repeated until the absolute permeability value matched the previously measured one.

To measure the drainage relative permeabilities, both gas and brine were simultaneously injected into the core sample using different ratios known as fractional flows ($Fg=Qg/Qt$). The gas fractional flow values employed were 0.01, 0.05, 0.15, 0.5, 0.85, 0.95, 0.99 and 1. The total injection rate was equal to 60 cc/hr.

During each fractional flow (Fg) stage, the average saturation of fluids was determined using the volumetric method, while the differential pressure across the core was continuously monitored using two highly accurate pressure transducers. These transducers, connected to the core's inlet and outlet, have a precision of 0.001 psi. Progression to the next step was determined based on obtaining stable saturation and pressure profiles. Additionally, each step was extended until 1 pore volume (PV) of the fluid with a lower ratio had been injected, allowing ample time for any potential changes.

After completing the final fractional flow (Fg) stage, a bump flooding technique was implemented to overcome the capillary end-effects and assess the end-point saturations more accurately. It is worth noting that the total flow rate of the experiments was 40 cc/hr, and at the later stages of the tests the bump flooding was conducted with injection rates of 60, and 90 cc/hr.

Following this, for measuring the subsequent imbibition relative permeabilities and also to investigate the impact hysteresis on relative permeability functions, after the bump flooding, the test continued with another stage. In this stage, the gas fractional flows began decreasing, attempting to return to the ratios encountered during the drainage process. The gas fractional flows for these two tests at this stage were: 1, 0.99, 0.95, 0.85, 0.5, 0.15, 0.05, 0.01, and 0. An Fg of 0 means that only water was injected at a rate of 40 cc/hr. After completing this stage, bump flooding was also conducted at injection rates of 60, and 90 cc/hr. Once this stage had been completed, cleaning was conducted and the permeability of the core sample was measured again.

5.3.2 Results (Spain)

The samples supplied for relative permeability testing proved to be too unconsolidated for core plugs to be made, so one analogue reservoir sample (a sample from the Bunter Sandstone, cored in the Southern North Sea) was tested as an analogue. The experiment was carried out using a synthetic 150,000 ppm NaCl brine. The initial sample properties and experimental conditions are summarised in Table 5*.4: Summary of sample properties and experimental conditions for Spanish samples*.

For the analogue reservoir sample the first step of the test involved measuring the gas and water relative permeability values at different saturation levels in a drainage scenario for the CO_2-brine system using steady-state displacement. Subsequently, the relative permeability functions for the imbibition scenario were measured to replicate the phenomena occurring during geological gas storage and assess the hysteresis in this system.

Following the core saturation process using CO_2-saturated brine, the test commenced with a total flow rate of 40 cc/hr and a gas fractional flow rate (Fg) of 0.01. During the test, both the saturation profile and differential pressure across the core sample were rigorously monitored. Each ratio was maintained until both measurements reached a plateau. These steady-state values were then used to determine the relative permeabilities. The gas fractional flow rates used for this test, as well as for all tests, were 0.01, 0.05, 0.15, 0.5, 0.85, 0.95, 0.99, and 1. Once all ratios had been tested, bump flooding was performed at total rates of 60 and 90 cc/hr to overcome capillary end effects and more accurately assess the irreducible water saturation (Swir).

Sample	**Bunter (reservoir analogue)**
Length, cm	*6.93*
Diameter, cm	*3.78*
Porosity, %	*20.42*
Permeability, mD	*1.63*
Pressure, bar	*215*
Temperature, C	*69*

Table 5.4: Summary of sample properties and experimental conditions for Spanish samples

The PilotSTRATEGY project has received funding from the European Union's Horizon 2020 research and innovation programme under grant agreement No. 101022664

After reaching Swir, the test continued with another stage to measure the relative permeabilities of the sample as the gas ratio decreased, reversing the sequence used in the drainage stage. Therefore, the order of performing gas fractional flows was: 1, 0.99, 0.95, 0.85, 0.50, 0.15, 0.05, 0.01, and 0. Each ratio was maintained until both measurements reached a plateau. Additionally, the injection rate was increased to 60, and 90 cc/hr to surpass the capillary end-effects and assess the endpoints more accurately.

Figure 5-21 displays the water and gas relative permeabilities at different water saturation values for this test during the drainage scenario on a linear scale. The results indicate that the irreducible water saturation before bump flooding was 35% and reached 29% at the final stages of the test after bump flooding. It can also be inferred that the endpoints for this test are Swir= 0.29 and krg at Swir=0.14.

Figure 5-21 and Figure ***5-22**: CO2-water relative permeability values vs. water saturation levels during both drainage and imbibition scenarios. Linear (left) and semi-log (right) scales.* display the relative permeability functions for this test; the water relative permeability curve is shown in blue, while the gas one is shown in red. As can be observed, the test began at Sw=0.29, and as the water fractional flow increased, both the water saturation and water relative permeability also increased. Conversely, the gas relative permeability began decreasing until it reached zero at the latest stages of the experiment. The results indicate that the maximum water saturation is 67%, showing the residual gas saturation here is 33% of the saturation unit. Additionally, the water relative permeability endpoint is equal to 0.11. Such a low water relative permeability endpoint in the imbibition cycle might be attributed to the water-wetness of the core sample, as the core had not been in contact with any polar components of hydrocarbons to alter its wettability.

Figure Figure ***5-22**: CO2-water relative permeability values vs. water saturation levels during both drainage and imbibition scenarios. Linear (left) and semi-log (right) scales.* displays the relative permeability functions for both gas and water under both drainage and imbibition scenarios in the CO_2 - brine system in both linear and semi-log scale. The test began with the drainage scenario and was followed by an imbibition cycle. The filled square with solid line in blue represents the water relative permeability in the drainage cycle, while the dashed blue line with empty squares indicates the water relative permeability curve during the imbibition cycle. The filled circle with the solid line in red shows the gas relative permeability during the drainage process, and the dashed line with empty circles relates to the gas relative permeability curve during the imbibition cycle. Several important features should be highlighted here:

- There appears to be hysteresis between both gas and water relative permeability curves under the drainage and imbibition cycles, as the relative permeability curves during the subsequent imbibition cycle do not follow those obtained during the initial drainage.
- The hysteresis is more pronounced in the gas phase, or better said, the non-wetting phase, and for the water phase, the hysteresis decreases as the water saturation increases.
- The water relative permeability values during the imbibition process are higher compared to the drainage process. Conversely, the gas relative permeability values during the drainage process are higher than those during the imbibition process.

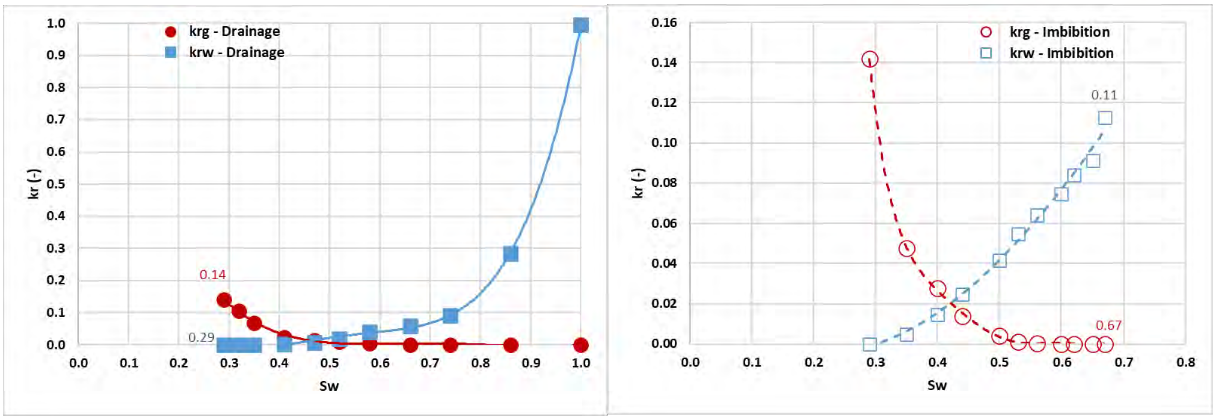

Figure 5-21: CO2-water relative permeabilities for Bunter Sandstone (analogous to the Spanish reservoir) sample during drainage (left) and imbibition (right).

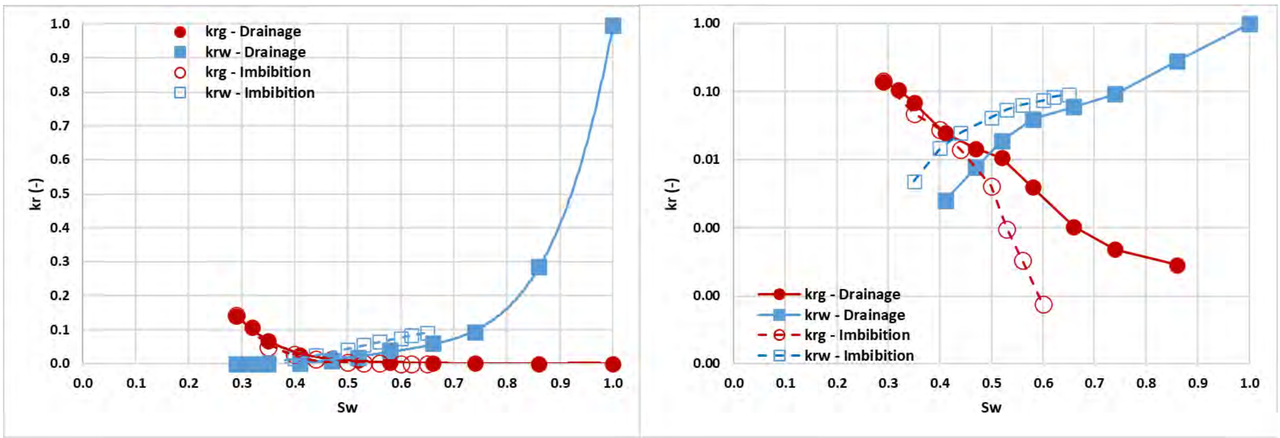

Figure 5-22: CO2-water relative permeability values vs. water saturation levels during both drainage and imbibition scenarios. Linear (left) and semi-log (right) scales.

5.3.3 Results (Portugal)

5.3.3.1 Permeability test

One sample of the target reservoir material from Portugal was tested, with dimensions and properties shown in *Table 5.5*. Fluid sampling for geochemical changes was not carried out for this run. The test was carried out at 100 bar pore pressure and 50°C. As for the Spanish samples tested, cyclic injection was not carried out, rather relative permeability was measured at varying water saturations during drainage and imbibition.

The first step of the permeability test involved measuring the gas and water relative permeability values at different saturation levels in a drainage scenario for the CO_2-brine system using steady-state displacement. Subsequently, the relative permeability functions for the imbibition scenario were measured to replicate the phenomena occurring during geological gas storage and assess the hysteresis in this system.

Following the core saturation process using CO_2-saturated brine, the test commenced with a total flow rate of 40 cm^3/hr and a gas fractional flow rate (Fg) of 0.01. During the test, both the saturation profile and differential pressure across the core sample were rigorously monitored. Each ratio was maintained until both measurements reached a plateau. These steady-state values were then used to determine the relative permeabilities. The gas fractional flow rates used for this test, as well as for all tests, were 0.01, 0.05, 0.15, 0.5, 0.85, 0.95, 0.99, and 1. Once all ratios had been tested, bump flooding was performed at total rates of 60 and 90 cc/hr to overcome capillary end effects and more accurately assess the irreducible water saturation (Swir).

After reaching Swir, the test continued with another stage to measure the relative permeabilities of the sample as the gas ratio decreased, reversing the sequence used in the drainage stage. Therefore, the order of performing gas fractional flows was: 1, 0.99, 0.95, 0.85, 0.50, 0.15, 0.05, 0.01, and 0. Each ratio was maintained until both measurements reached a plateau. Additionally, the injection rate was increased to 60, and 90 cc/hr to surpass the capillary end-effects and assess the endpoints more accurately.

Sample	*S69.8.3*
Length, cm	*3.79*
Diameter, cm	*5.861*
Porosity, %	*13.22*
Permeability, mD	*32.28*
Pressure, bar	*100*
Temperature, C	*50*

Table 5.5: Sample properties for Portuguese reservoir sample

Figure 5-23 displays the water and gas relative permeabilities at different water saturation values for this test during the drainage scenario on a linear scale. The results indicate that the irreducible water saturation before bump flooding was 57% and reached 45% at the final stages of the test after bump flooding. It can also be inferred that the endpoints for this test are Swir= 0.45 and krg at Swir=0.39.

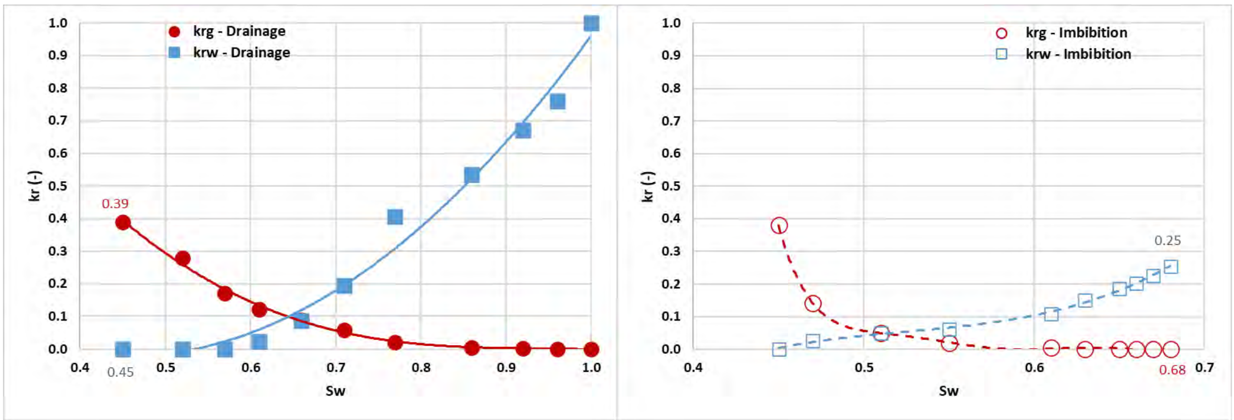

Figure 5-23: Gas-water relative permeabilities for Portuguese reservoir sample during drainage and imbibition

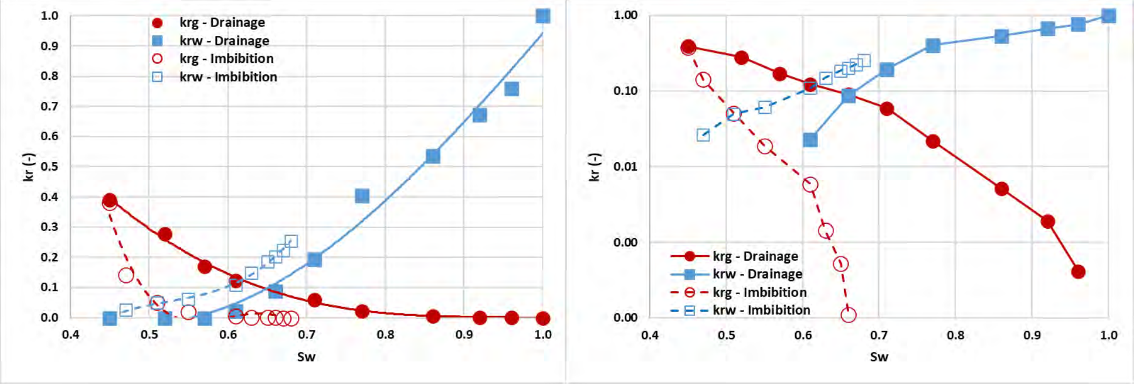

Figure 5-24: Gas-water relative permeability values vs. water saturation levels during both drainage and imbibition scenarios. Linear (left) and semi-log (right) scales

Figure 5-23 displays the relative permeability functions for this test; the water relative permeability curve is shown in blue, while the gas one is shown in red. As can be observed, the test began at Sw=0.45, and as the water fractional flow increased, both the water saturation and water relative permeability also increased. Conversely, the gas relative permeability began decreasing until it reached zero at the latest stages of the experiment. The results indicate that the maximum water saturation is 68%, showing the residual gas saturation here is 32% of the saturation unit. Additionally, the water relative permeability endpoint is equal to 0.25. Such a low water relative permeability endpoint in the imbibition cycle might be attributed to the water-wetness of the core sample, as the core had not been in contact with any polar components of hydrocarbons to alter its wettability.

Figure 5-24 displays the relative permeability functions for both gas and water under both drainage and imbibition scenarios in the CO_2 - brine system in both linear and semi-log scale. The test began with the drainage scenario and was followed by an imbibition cycle. The filled square with solid line in blue represents the water relative permeability in the drainage cycle, while the dashed blue line with empty squares indicates the water relative permeability curve during the imbibition cycle. The filled circle with the solid line in red shows the gas relative permeability during the drainage process, and the dashed line with empty circles relates to the gas relative permeability curve during the imbibition cycle. Several important features should be highlighted here:

- There appears to be hysteresis between both gas and water relative permeability curves under the drainage and imbibition cycles, as the relative permeability curves during the subsequent imbibition cycle do not follow those obtained during the initial drainage.
- The hysteresis is more pronounced in the gas phase, or better said, the non-wetting phase, and for the water phase, the hysteresis decreases as the water saturation increases.
- The water relative permeability values during the imbibition process are higher compared to the drainage process. Conversely, the gas relative permeability values during the drainage process are higher than those during the imbibition process.

5.3.3.2 Caprock reactivity test

In addition to the above, a caprock sample (CD-DARN15) was tested for reactivity under flowing conditions. The mineralogy of this sample is shown in *Table 5.6*. The reactivity test was carried out on a core artificially fractured longitudinally (using a chisel). Artificial brine (150,000 ppm NaCl) was

The PilotSTRATEGY project has received funding from the European Union's Horizon 2020 research and innovation programme under grant agreement No. 101022664

flowed through this at a temperature of 60°C and at a pressure of 69 bar for about 50 hours. CO_2 was then flowed for a period of around 20 hours, followed by a second flow of brine (*Figure 5-25*).

Table 5.6: XRD analysis of Portuguese caprock sample

CD-DARN15	
Phase	**%**
Quartz	*7*
Calcite	*89*
Kaolinite	*2*
K-Feldspar	*2*

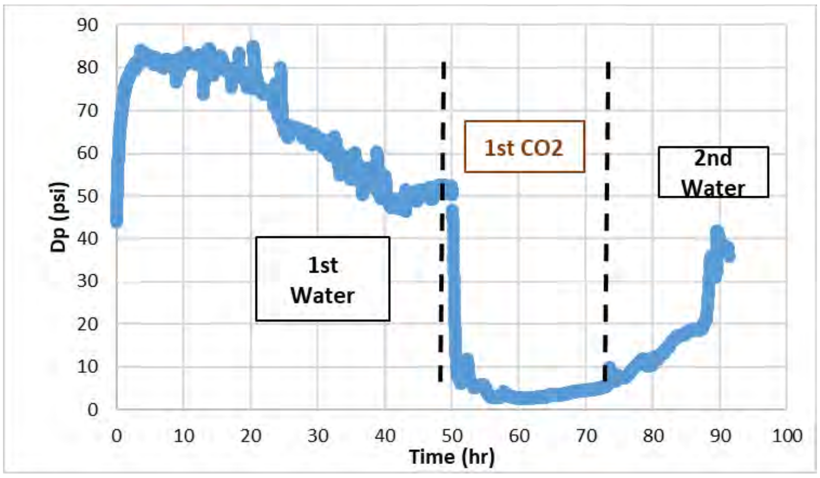

Figure 5-25: Timings of brine/CO2 flows and differential pressure observed during caprock reactivity test

For the reactivity test on the caprock effluent samples were collected during every stage of flow (i.e., two during initial brine flow, one during CO_2 flow, two during the final brine flow). Selected elemental concentrations are shown in **Erreur ! Source du renvoi introuvable.**.

The PilotSTRATEGY project has received funding from the European Union's Horizon 2020 research and innovation programme under grant agreement No. 101022664

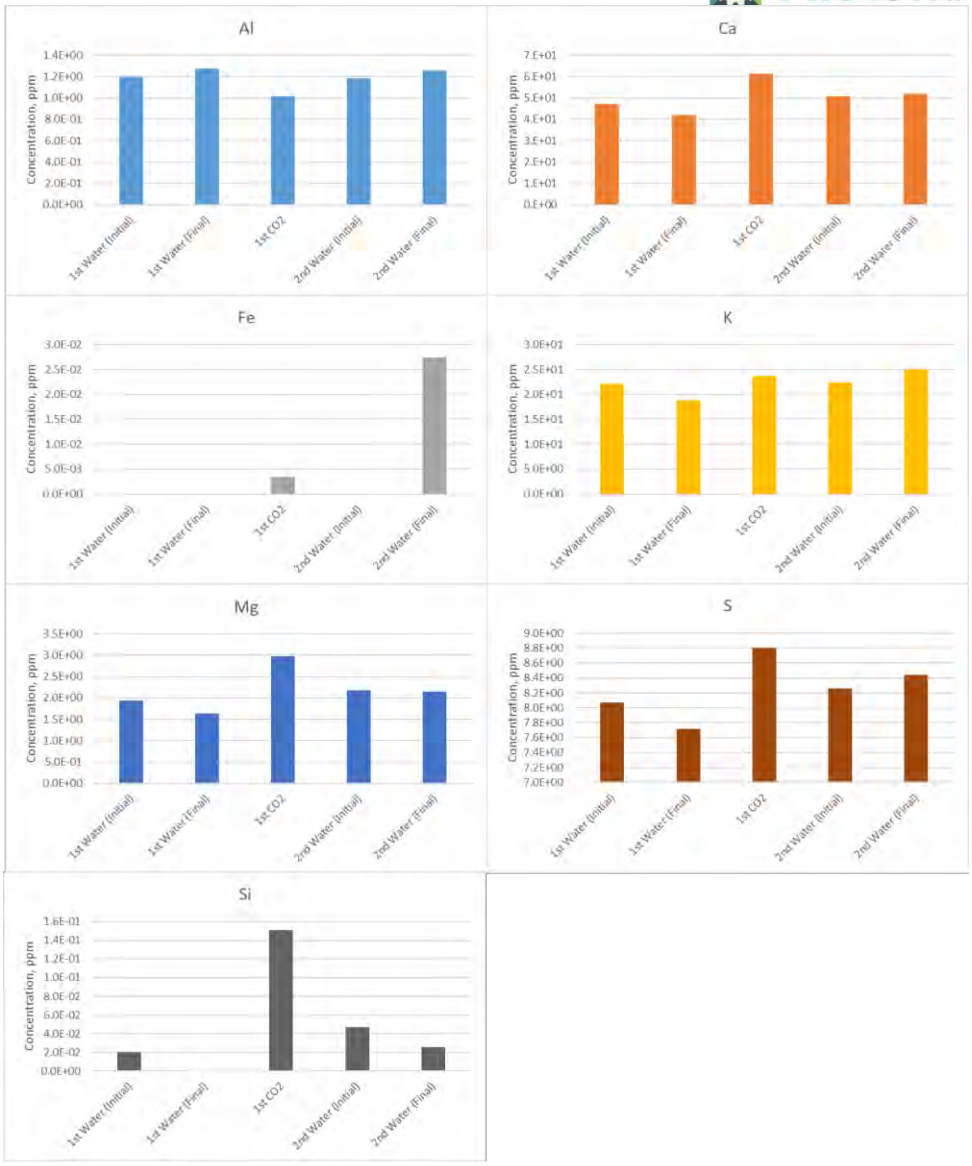

Figure 5-26: Selected elemental concentrations in effluent samples collected during CO2 and water flows for Portuguese caprock sample

No samples of the stock brine used for this experiment were analysed, meaning that there are uncertainties around the results which make interpretation difficult. However, as the starting brine was analytical grade NaCl solution (brine salinity = 150,000 ppm NaCl) the results indicate some dissolution of the primary mineral assemblage by action of the brine alone. Concentrations of Al, Mg, S and Si, while low, are all elevated in the effluent from the first brine flow. Ca and K concentrations are particularly elevated and while the K concentrations observed may have originated from impurities in the NaCl used to make the starting brine, the Ca concentrations (c. 40 – 50 ppm during the initial brine flow) are indicative of dissolution of primary calcite.

The majority of elements show a spike in concentration during the period when CO_2 was flowing through the sample. This may indicate enhanced dissolution of primary phases during this period. We would expect calcite to be particularly susceptible to dissolution during this period. The concentration of Ca, for example, rises by c. 50% and remains relatively elevated during the following brine flow. The largest relative increase was in Si concentrations which rose from below detection at the end of the first brine flow period to c. 0.15 ppm during CO_2 flow, likely reflecting enhanced (albeit very minor) dissolution of K-feldspar during this period.

Results indicate some enhanced dissolution of primary caprock material during exposure to CO_2. The results, however, are notably more subtle than those observed for the same material exposed to CO_2 in the batch experiments. This likely reflects the relative tightness of the intact sample used in the flow-through experiment, thereby limiting the surface area available for reactions (compared to the powdered material used in the batch experiment).

6. Conclusions

A site-specific approach has been adopted to assess the reactivity of the rocks present at each of the proposed pilot sites.

For the Paris Basin (France), the reservoir rocks are overwhelmingly calcite, and the proportions of most of the minor mineral phases are near or below the limit of quantification or the limit of detection. Unsurprisingly, the minerals most susceptible to dissolution in all experiments are calcite. Apart from gypsum / anhydrite, changes in the apparent abundances of other minerals are difficult to quantify, as the detection limit and analytical precision of X-ray diffraction are too low to be confident that genuine changes are occurring. The dissolution of calcite, ankerite/dolomite and quartz and the precipitation of one or more aluminosilicates, such as kaolinite or illite, are the main reactive process in the Dogger reservoir when CO_2 is added. However, the sulphate minerals (gypsum/anhydrite) appeared to dissolve in the Dalle Nacrée Formation, but precipitate in the Comblanchian and Oolithe Blanche formations. For the Callovian mudstone (transitional caprock) the main reactions enhanced by the addition of CO_2 are the dissolution of calcite and gypsum, and possibly interstratified clays. Plagioclase and quartz attain equilibrium and dolomite precipitates.

For the Ebro Basin (Spain) reservoir, an arkosic ‘red bed’ sandstone, batch reaction experiments indicate some very minor dissolution of K-feldspar, along with some dissolution of or ion-exchange with some of the minor components present with only Fe reaching concentrations significantly above sub-ppm levels. There is no reason to suspect that this would interfere with the injection of CO_2 into the reservoir. There is no strong evidence for secondary precipitation (of carbonates, for example). Any precipitation which did occur is likely to be very minor and unlikely to be of concern at the reservoir scale.

For the Ebro Basin caprock (Spain) which contains more primary calcite than the reservoir, batch reaction experiments reflect a system where reaction is dominated by dissolution of primary calcite, possibly with some minor secondary precipitation and minor dissolution of quartz and minor aluminosilicate phases. pH is buffered by calcite dissolution, likely making the dissolution of any silicate or aluminosilicate (which would only be present at concentrations <1%) phases present relatively slow. It is difficult to extrapolate this result to the scale of the storage site.

For the Paris Basin (France), cyclic flow experiments using reservoir samples highlighted strong dissolution and a progressive increase of the porosity, intrinsic permeability, and water and CO_2 relative permeability. The flow through experiments with CO_2-enriched brine on an oolitic grainstone from the Oolithe Blanche Formation generated a so-called ‘worm-hole’, which is probably not representative of subsurface processes. The test confirmed the high permeability of this formation and that carbonate minerals (mostly calcite) account, by far, the largest part of system’s reactivity after the addition of CO_2.

The caprock sample (a carbonate-rich mudstone) from the Paris Basin recorded no flow over 24 hours with 180 bars of pressure differential, despite the sample being cracked. The sample was sawn to produce an artificial ‘fracture’ to enable the experiment to proceed when almost total clogging of the porosity occurred during the experiment.

For Spain, the samples supplied for relative permeability testing proved to be too unconsolidated for core plugs to be made, so one reservoir sample (a sample from the Bunter Sandstone, cored in the

Southern North Sea) was tested as an analogue. For both Portugal and Spain, relative permeability curves were successfully measured, with hysteresis between both gas and water relative permeability curves under the drainage and imbibition cycles. The hysteresis is more pronounced in the gas phase. The water relative permeability values during the imbibition process are higher compared to the drainage process. Conversely, the gas relative permeability values during the drainage process are higher than those during the imbibition process.

For Portugal, a caprock sample was tested for reactivity under flowing conditions along an induced fracture. Results indicate some enhanced dissolution of primary caprock material during exposure to CO_2. The results, however, are notably more subtle than those observed for the same material exposed to CO_2 in the batch experiments. This likely reflects the relative tightness of the intact sample used in the flow-through experiment, thereby limiting the surface area available for reactions (compared to the powdered material used in the batch experiment).

For both Spain and Portugal, the caprocks both contain significant calcite (13% of the sample in the Spanish case, 87% in the Portuguese case), which exhibited significant dissolution when exposed to CO_2 saturated brine. Calcite dissolution removed 6% of the original rock mass in the case of the Spanish sample and 11% in the Portuguese case. In both cases fluids likely became saturated with respect to calcium carbonate, leading to some secondary precipitation.

Overall, the results confirm that calcite-rich sediments are subject to at least some dissolution under the acidic conditions associated with CO_2 injection. Direct extrapolation of these results to the scale of a reservoir and/or caprock is difficult. Calcite-poor sandstones undergo little reaction on laboratory time scales, as expected. The identified trends should be considered as first-order conceptual models for assessing geochemical reactions and understanding more generally the geochemical reactivity involved. The conceptual model remains to be validated or adjusted by the geochemical modelling exercise aiming to numerically simulate the experimental results within the framework of the project.

7. References

Allan, M.M., A. Turner, and B.W.D. Yardley. 2011. "Relation between the Dissolution Rates of Single Minerals and Reservoir Rocks in Acidified Pore Waters." *Applied Geochemistry: Journal of the International Association of Geochemistry and Cosmochemistry* 26 (8): 1289–1301.

Baines, S. J., and R. H. Worden. 2004. "Geological Storage of Carbon Dioxide." *Geological Society, London, Special Publications* 233 (1): 1–6.

Bateman, Keith, C. Rochelle, A. Lacinska, and D. Wagner. 2011. "CO2-Porewater-Rock Reactions - Large-Scale Column Experiment (Big Rig II)." *Energy Procedia* 4: 4937–44.

Blanc P., Lassin A., Piantone P., Azaroual M., Jacquemet N., Fabbri A. and Gaucher E. C. (2012) Thermoddem: A geochemical database focused on low temperature water/rock interactions and waste materials. *Applied Geochemistry* **27**, 2107–2116.

Bordenave A. and Issautier B. (2023) *Geological Conceptual Model of Paris Basin, Grandpuits area, France. Deliverable 2.7. PilotSTRATEGY project (grant agreement: 101022664)*.

Celia, M., and J. M. Nordbotten. 2009. "Practical Modeling Approaches for Geological Storage of Carbon Dioxide." *Ground Water* 47 (5): 627–38.

Fleury M., Barradas J., Canteli P., Carneiro J., Correia A., Fernandez de Arévalo E., García Crespo J., García D., Valderrama F., Koukouzas N., Manrique C., Martinez J., Mediato J., Moita P., Pangaro 0Bedoya F., Tyrologou P., Ribeiro C., Rousseau N. and Wilkinson M. (2023) *Petrophysics report of all regions*.

Gaus, I., P. Audigane, L. André, J. Lions, N. Jacquemet, P. Durst, I. Czernichowski-Lauriol, and M. Azaroual. 2008. "Geochemical and Solute Transport Modelling for CO2 Storage, What to Expect from It?" In *International Journal of Greenhouse Gas Control*, 2:605–25. Trondheim, NORWAY: Elsevier Sci Ltd.

Gunter, W. D., S. Bachu, and S. Benson. 2004. "The Role of Hydrogeological and Geochemical Trapping in Sedimentary Basins for Secure Geological Storage of Carbon Dioxide." *Geological Society, London, Special Publications* 233 (1): 129–45.

Hill A. E., 1937, The Transition Temperature of Gypsum to Anhydrite. *J. Am. Chem. Soc.* **59**, 2242–2244.

Houel P., 2008, Description géologique et hydraulique préparatoire à l'interprétation de la zone PICOREF (SE du bassin de Paris). Project PICOREF., Rapport IFP n°60269.

Kaszuba, J., B. Yardley, and M. Andreani. 2013. "Experimental Perspectives of Mineral Dissolution and Precipitation Due to Carbon Dioxide-Water-Rock Interactions." *Reviews in Mineralogy and Geochemistry* 77: 153–88.

Mathurin F., Carneiro J., López-Gutiérrez J., Matos C., Moreno I. and Wilkinson M., 2023, *Report on the regional hydrogeology of the three study areas: Paris Basin (France), Lusitanian Basin (Portugal) and Ebro Basin (Spain)*.

Ordõnez, B., J. Mediato, T. Kovacs, J. Martínez-Martínez, P. Fernández-Canteli, L. González-Menéndez, S. Roces, J. Caicedo-Potosí, B. del Moral, and E. Berrezueta, 2024, Experimental geochemical assessment of a seal-reservoir system exposed to supercritical CO_2: A case study from the Ebro Basin, Spain. International Journal of Greenhouse Gas Control, 137, 104233.

Parkhurst D. L. and Appelo C. A. J. (2013) Description of Input and Examples for PHREEQC Version 3—A Computer Program for Speciation, Batch-Reaction, One-Dimensional Transport, and Inverse Geochemical Calculations. In *Techniques and Methods 6–A43* U.S. Geological Survey, Denver, Colorado.

Portier, S., and C. Rochelle, 2005. “Modelling CO2 Solubility in Pure Water and NaCl-Type Waters from 0 to 300 °C and from 1 to 300 Bar. Application to the Utsira Formation at Sleipner.” *Chemical Geology* 217 (3–4): 187–99.

Rochelle, C., I. Czernichowski-Lauriol, and A. E. Milodowski. 2004. “The Impact of Chemical Reactions on CO2 Storage in Geological Formations: A Brief Review.” *Geological Society, London, Special Publications* 233 (1): 87–106.

Rosenqvist, J., A. D. Kilpatrick, and B.W.D. Yardley. 2012. “Solubility of Carbon Dioxide in Aqueous Fluids and Mineral Suspensions at 294K and Subcritical Pressures.” *Applied Geochemistry: Journal of the International Association of Geochemistry and Cosmochemistry* 27 (8): 1610–14.